2018-07-01

Design and Characterization of a Plunge-Capable Friction Stir Welding Temperature Feedback Controller

Jonathan David Erickson
Brigham Young University

Design and Characterization of a Plunge-Capable Friction Stir Welding Temperature Feedback Controller

Jonathan David Erickson

A thesis submitted to the faculty of
Brigham Young University
in partial fulfillment of the requirements for the degree of

Master of Science

Carl D. Sorensen, Chair
Tracy W. Nelson
Marc D. Killpack

Department of Mechanical Engineering

Brigham Young University

ABSTRACT

Design and Characterization of a Plunge-Capable Friction Stir Welding
Temperature Feedback Controller

Jonathan David Erickson
Department of Mechanical Engineering, BYU
Master of Science

Temperature control in friction stir welding (FSW) is of interest because of the potential to improve the mechanical and microstructure characteristics of a weld. Two types of active temperature control have been previously implemented for steady-state friction stir welding conditions: PID Feedback Control and Model Predictive Control. The start-up portion of a weld is an obstacle for these types of active control.

To date, only minimal exploratory research has been done to develop an active temperature controller for the start-up portion of the weld. The FSW temperature controller presented in this thesis, a Position-Velocity-Acceleration (PVA) controller implemented with gain-scheduling, is capable of active control during the start-up portion of a weld. The objectives of the controller are (1) to facilitate fully-automated active temperature control during the entire welding process, (2) to minimize the rise time, the settling time, the percentage maximum post-rise error (overshoot calculated as a percentage of the settling band half-width), and the post-settled root-mean-square (RMS) of the temperature error, and (3) to maintain the steady state performance of previous control methods.

For welds performed in 6.35 mm plates of 7075-T651 Aluminum with controller gains identified through a manual tuning process, the mean controller performance is a rise time of 10.82 seconds, a settling time of 11.35 seconds, a percentage maximum post-rise error of 69.86% (as a percentage of the 3°C settling band half-width), and a post-settled RMS error of 0.92°C.

Tuning of the start-up controller for operator-specified behavior can be guided through construction of regression models of the weld settling time, rise time, percent maximum post-rise error, and post-settled RMS error. Characterization of the tuning design space is performed through regression modeling. The effects of the primary controller tuning parameters and their interactions are included. With the exception of the post-settled RMS error model, these models are inadequate to provide useful guidance of the controller tuning, as significant curvature is present in the design space. Exploration of higher-order models is performed and suggests that regression models including quadratic terms can adequately characterize the design space to guide controller tuning for operator-specified behavior.

Keywords: friction stir welding, feedback control, temperature control

ACKNOWLEDGMENTS

My time at BYU has been a remarkable opportunity to form worthwhile and formative relationships. The associations I have had with professors and fellow students during my enrollment in the BYU Mechanical Engineering Master's program have inspired me to strive for engineering, personal, and spiritual excellence.

Aid from my committee members has been fundamental to my success. In particular, Dr. Carl Sorensen has been a invaluable and engaging mentor.

I would like to especially acknowledge support from my wife and family who have encouraged and enabled me to achieve my academic goals.

CONTENTS

LIST OF TABLES

LIST OF FIGURES

NOMENCLATURE

α	Gain-scheduling continuous interval weighting parameter
β	Regression model constant
C	Weighting function constant
E	Temperature error, defined as $T_{set} - T(t)$
$\frac{dE}{dt}$	Derivative of temperature error
$\frac{d^2E}{dt^2}$	2^{nd} derivative, acceleration, or curvature of temperature error
K_P	PID/PVA controller proportional gain
K_I	PID integral gain
K_D	PID derivative gain
K_V	PVA velocity gain
K_A	PVA acceleration gain
$PMPE$	Percent Maximum Post-rise Error
$RMSE$	Root mean square error, calculated post-settling-time
σ	Standard deviation of a sample
σ^2	Variance of a sample
t	Time
t_{rise}	Rise time
t_{settle}	Settling time
T	Temperature
T_{set}	Temperature set-point
u	Controller output
W_{tran}	Half-width of the continuous interval
$W_{settled}$	Half-width of the settled band about T_{set}
$\bar{x}$	Mean of a sample
$\tilde{x}$	Median of a sample
X	Regression model explanatory variable
Y	Regression model dependent variable

Subscripts, superscripts, and other indicators

$[\,](t)$	indicates $[\,]$ is a function of time
$[\,]_k$	indicates $[\,]$ is the k^{th} time-step
$[\,]_n$	indicates $[\,]$ is the n^{th} value
$[\,]_o$	indicates $[\,]$ is the initial value
$[\,]_f$	indicates $[\,]$ is the final value
$[\,]_{max}$	indicates $[\,]$ is the maximum value
$[\,]_{min}$	indicates $[\,]$ is the minimum value

CHAPTER 1. INTRODUCTION

1.1 Overview of Friction Stir Welding

Friction Stir Welding (FSW) is a solid state process in which material is joined by a rotating, non-consumable tool. While rotating, the tool is driven axially into the joint of two adjacent workpieces (the "plunge") and subsequently traversed along the specified weld path, as can be seen in Figure 1.1. Friction between the rotating tool and the workpiece heats the material to a plasticized state at which point the base material is stirred together.

FSW has gained popularity because of the advantages it offers over traditional fusion welding. Problems related to residual stresses, second phases, porosity, and embrittlement are significantly reduced or eliminated because the base material is not melted. In addition, FSW is capable of producing welds with excellent mechanical and metallurgical properties. Distortion of the base metal is greatly reduced and fatigue crack propagation is less problematic than with fusion welded joints [2].

1.2 FSW Temperature Control Rational

It has been found that weld properties are influenced by thermal input of the weld [1]. The investigation of temperature control methods for FSW is of interest because of the potential to improve the mechanical and microstructure characteristics of the weld [3] [4] [5]. Many of the advantages of FSW mentioned in Section 1.1 can be further enhanced through temperature control.

1.3 Previous Work

Previously implemented steady-state temperature control methods include model-predictive control and variations of PID control [6] [7] [8] [9] [10]. The steady-state portion of the weld is characterized by the absence of dynamically changing temperature gradients. The comparison by

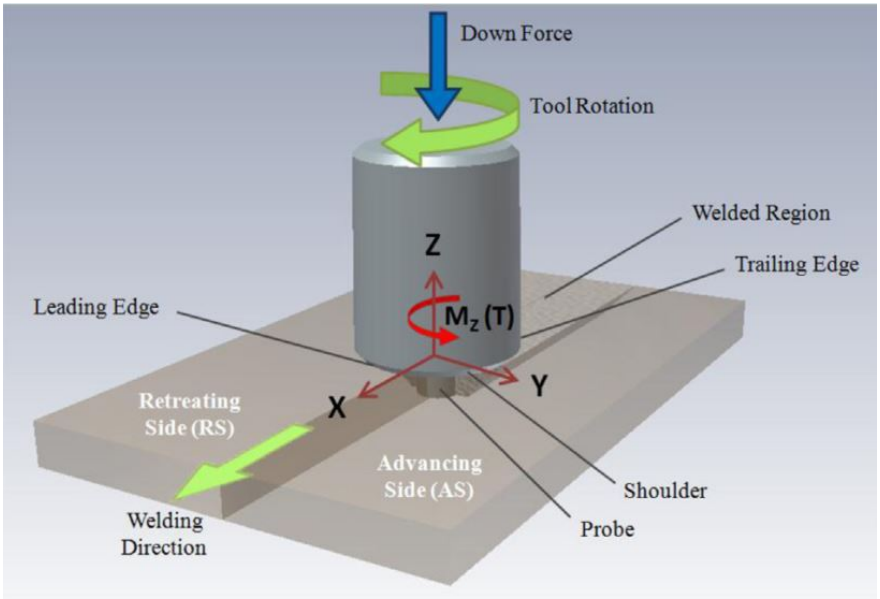

Figure 1.1: Diagram of friction stir welding [1]

Taysom et al. of model-predictive and PID control demonstrated that both methods are capable of maintaining the weld temperature within 2°C of the set-point during pseudo-steady-state conditions for welds performed with a CS4 tool (see Appendix A for geometry details) in 6.35 mm plates of 7075 Aluminum [11]. However, there are no previously implemented active temperature control methods designed specifically for use during start-up of the FSW process. The start-up portion of the weld is defined here to include the plunge and initial traverse of the weld.

1.4 Obstacles to Temperature Control During Start-up

Taysom et al. demonstrated that, during the initial traverse, the Hybrid Heat Source model predictive controller and the PID controller with regulator gains were both able to control temperature within 5°C of the set-point with an RPM-controlled plunge [11]. Active control during the plunge may improve this control performance. Model-predictive control as implemented by Taysom et al. operates on the assumption that the system is essentially non-transient, an assumption which is not valid during start-up. PID and PI control during start-up are inhibited by the integrator wind-up which occurs as a result of the time and large temperature change required to initially reach the temperature set-point. P and PD control also have drawbacks which are discussed in Section 2.1.

Previously implemented steady-state control methods must be manually activated at the operator's discretion. The lack of active control during start-up results in sub-optimal temperature profiles (e.g. long rise times and/or long settling times) which may be improved upon. In addition, the inability of steady-state methods to engage completely during start-up must be overcome to attain fully-automated FSW temperature control.

1.5 Research Contributions

This thesis presents an active feedback controller that is capable of rapidly and consistently reaching and subsequently maintaining the temperature set-point during start-up of the friction stir welding process. The temperature controller is capable of engaging the instant the weld begins, which facilitates complete automation of the FSW process.

To gauge the capability of the controller to rapidly reach the temperature set-point, the following performance metrics are utilized: settling time ($t_{settled}$), rise time (t_{rise}), and percentage maximum post-rise error (PMPE, the maximum overshoot as a percentage of the 3°C settling band half-width). To gauge the ability of the controller to maintain the temperature set-point, the post-settled root-mean-square error (RMSE) is reported. Minimization of the settling time is the primary tuning objective of the controller in this research, although the controller can be utilized to minimize any of the other performance metrics. In addition to measuring the performance of the controller, the coefficient of variation is utilized as a metric of performance consistency.

A statistical method for predictive tuning of the controller is explored. Experimental data is used to construct regression models for predicting the weld settling time, rise time, percentage maximum post-rise error, and the post-settled root-mean-squared error. The objective of constructing the regression models is to provide guidance and insight into how to effectively tune the start-up controller to obtain any desired controller behavior.

CHAPTER 2. CONTROL THEORY

This chapter describes the control theory necessary for implementation of the start-up FSW temperature controller. The derivation of controller equations and methods used for implementation of the controller are elucidated in the following sections.

2.1 Position-Velocity-Acceleration Control

Position-Velocity-Acceleration Control (PVA) is a variation of PID Control that offers advantages for control during start-up. The PVA controller form is the result of differentiating the PID controller equation with respect to time, t. Equations (2.1) and (2.2) show a compressed derivation of the analytical PVA controller form from the analytical PID controller form. With E as the temperature error, the PID controller takes the following form:

$$u(t) = K_P E + K_I \int_0^t E dt + K_D \frac{dE}{dt} \tag{2.1}$$

After taking the derivative, renaming K_P as K_V, K_I as K_P, and K_D as K_A, and rearranging terms, the PVA controller form results:

$$\frac{du(t)}{dt} = K_P E + K_V \frac{dE}{dt} + K_A \frac{d^2E}{dt^2} \tag{2.2}$$

The PVA controller form was selected for several reasons. First, it is immune to integrator wind-up because the integral is not calculated, as can be seen in Equation (2.2) [12]. Second, there is inherently no steady-state error. The P and PD controller forms were also considered for start-up control, but the steady-state error inherent in both forms inhibits the transition to a steady-state controller. Third, the PVA algorithm does not require any initialization of the output during control transitions (e.g. this is not the case with the PID controller form) [12]. This quality is utilized in the transition between the saturation and continuous control intervals discussed later in Section 2.2.

A discretized form of the PVA controller is needed for implementation. Below is the derivation of the discretized form of the PVA controller, beginning with the discretized PID controller form, Equation (2.3).

$$u_k = K_P E_k + K_I \sum_{j=1}^{k} E_j \Delta t + K_D \frac{(E_k - E_{k-1})}{\Delta t}, \tag{2.3}$$

Re-evaluating Equation (2.3) at the previous time-step, t_{k-1}, gives:

$$u_{k-1} = K_P E_{k-1} + K_I \sum_{j=1}^{k-1} E_j \Delta t + K_D \frac{(E_{k-1} - E_{k-2})}{\Delta t}, \tag{2.4}$$

Subtracting Equation (2.4) from Equation (2.3) results in:

$$u_k - u_{k-1} = K_P(E_k - E_{k-1}) + K_I \Delta t E_k + K_D \Delta t (E_k - 2E_{k-1} + E_{k-2}), \tag{2.5}$$

As previously done in Equation (2.2), the controller gains are renamed (K_P, K_I, and K_D as K_V, K_P, and K_A, respectively) and the terms are rearranged:

$$\Delta u_k = u_k - u_{k-1} = K_P \Delta t E_k + K_V(E_k - E_{k-1}) + K_A \Delta t (E_k - 2E_{k-1} + E_{k-2}), \tag{2.6}$$

Solving for u_k, the implementable PVA discretized form results:

$$u_k = u_{k-1} + K_P \Delta t E_k + K_V(E_k - E_{k-1}) + K_A \Delta t (E_k - 2E_{k-1} + E_{k-2}), \tag{2.7}$$

As stated previously, the controller output has units of RPM. The output of Equation (2.7), u_k, is the motor RPM commanded by the controller.

2.2 Gain Scheduling

As discussed in Section 1.4, a major obstacle to PID control during startup is integrator wind-up. The PVA controller is able to avoid integrator wind-up during start-up, but the issue of a transient plant requires further controller design. Gain scheduling is a technique used to improve

controller performance by utilizing more than a single set of controller gains. A common form of gain-scheduling varies controller gains as a function of the error signal [12]. For example, controller gains may be tuned for aggressive performance when error is "large" and tuned for tracking performance when the error is "small". Gain scheduling may be implemented as a piece-wise or continuous function of the error [12].

A piece-wise error-based gain scheduling scheme implemented with two intervals is used for control during start-up in FSW. The interval used for "large" absolute error is referred to as the saturation interval. The interval used for "small" absolute error is referred to as the continuous interval. The transition between these intervals occurs when the absolute value of the error is less than the continuous interval half-width, specified as when the criteria $|E| < W_{tran}$ is met.

2.2.1 Saturation Interval

Implementation of a saturation interval is intended to parallel the behavior of a hysteresis controller (a.k.a. a bang-bang controller). Hysteresis control operates on the simple assumption that if the input to the system is not fully saturated, additional controller input will stimulate an accelerated system response [13]. This approach is intended to minimize the rise time of the system. During the saturation interval, the motor RPM is held at the saturation value to reach the temperature set-point as quickly as possible. In terms of the controller notation, this is stated as $u_k = u_{sat}$ while $|E| \geq W_{tran}$.

2.2.2 Continuous Interval

The objectives of the continuous interval are to enable favorable conditions for hand-off to the steady-state interval and to minimize one of the four performance metrics. In this research, minimization of the settling time is the goal. The continuous interval is necessary because the saturation interval is not ideal for tunable controller performance.

It is important to note that the transition from the saturation interval to the continuous interval does not require supplementary calculations for a smooth hand-off, as the PVA controller does not require adjustment of the output for smooth transitions [12]. The PVA control algorithm utilized in this interval specifies a change in the process variable, so the transition between intervals

is straightforward. This is in contrast to the transition between the continuous and the steady-state intervals, as discussed in Section 2.3.

The controller output during the continuous interval is calculated with controller gains which are a function of the absolute value of the temperature error. To define the continuous interval controller gains, initial and final controller gains are selected. The initial controller gains ($K_{P,o}$, $K_{V,o}$, and $K_{A,o}$) correspond to when $|E| = W^{\circ}_{tran}$C and the final controller gains ($K_{P,f}$, $K_{V,f}$, and $K_{A,f}$) correspond to when $|E| = 0^{\circ}$C. A weighting function is used to vary the controller gains between the initial set and the final set. The weighting value, α, scales between 0 and 1 to vary the controller gains as shown in Equation 2.8.

$$K_I = \alpha * K_{I,f} + (1 - \alpha) * K_{I,o} \tag{2.8}$$

The subscript I can be P, V, or A. This relationship allows for the controller to be tuned for distinctive behavior at large and small error values. The weighting value is calculated as shown in Equation 2.9.

$$\alpha = C^{-|E|/W_{tran}} \tag{2.9}$$

The value of C in Equation 2.9 is selected to shape the gain schedule weighting function. α may be calculated in any number of ways, but this particular method results in the behavior of the initial controller gains dominating the transition. A linear weighting function was also considered to assign α, but the resulting control performance was sluggish. (2.9) maintains the aggressive behavior of the initial controller gains for longer than the linear weighting function.

The controller gains used for demonstrating the capabilities of the controller are shown in Section 3.7. The process of selecting those controller gains is described in Section 3.6.

2.3 Bumpless Transfer to a Steady-State PID Controller

The transition between any two controllers or control methods can be problematic due to differences in the controller output. It is highly unlikely that the output of any two control methods will be identical at the moment of transfer for a variety of reasons, such as differences in controller type or differences in controller gains. If precautions are not taken, this disparity will cause a

discontinuity, or "bump", in the process variable at the moment of transfer [14]. The "bump" is likely to inhibit performance, but may also cause damage to motors, valves, or other sensitive system components [12].

Bumpless transfer methods are generally utilized for manual-to-automatic or automatic-to-manual transitions, but the technique is utilized in this research to transition between the start-up (PVA) and steady-state (PID) controllers. Control is transferred to a PID controller once a set of predetermined transition criteria have been met (see Section 3.8). An example of the "bump" in the controller output can be seen in Figure 2.1. The intention of utilizing the bumpless transition method in this research is to enhance controller performance, as damage to the welding machinery is unlikely.

For transfer from PVA to PID control, the "bump" is avoided by artificially adjusting the integral term of the PID controller such that the output of the PID controller matches the output of the PVA controller at the moment of transfer. This allows the process variable to ramp towards its final value without the "bump". The value of the artificial integral is calculated by rearranging the PID controller equation, Equation (2.1), to solve for the integrated error term as shown in Equation (2.10):

$$\int_0^t E dt = \frac{K_P E + K_D \frac{dE}{dt} - u}{-K_I} \tag{2.10}$$

To achieve bumpless transfer, u is set to the previous PVA controller output. The value of the artificial integral is then inserted into the PID controller equation. Subsequent to the transfer, the integrated error term is updated normally. An example of an RPM profile where the "bump" has been eliminated is shown in Figure 2.2.

2.4 Relay Feedback Test

As stated in Section 1.3, PID control has been previously implemented and used for steady-state conditions. PID control is used for steady-state conditions in this research as several robust tuning methods are available. It may be possible to tune the PVA controller for acceptable set-point tracking, but the proven capability of PID control in FSW provides a straightforward method for

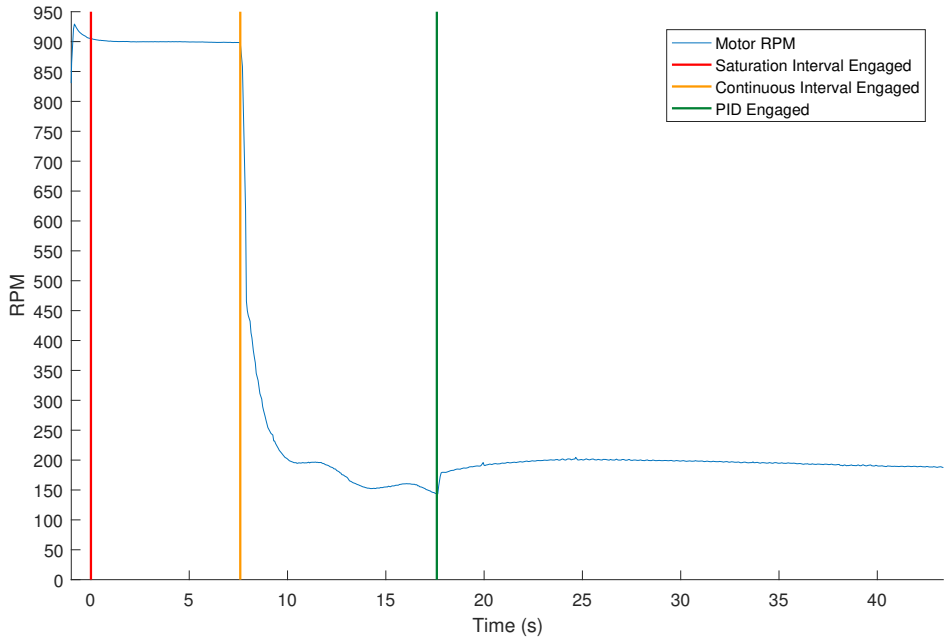

Figure 2.1: A C_0 discontinuity, or "bump", occurs in this example at the moment that the PID controller engages due to the difference in output of the PVA and PID controllers.

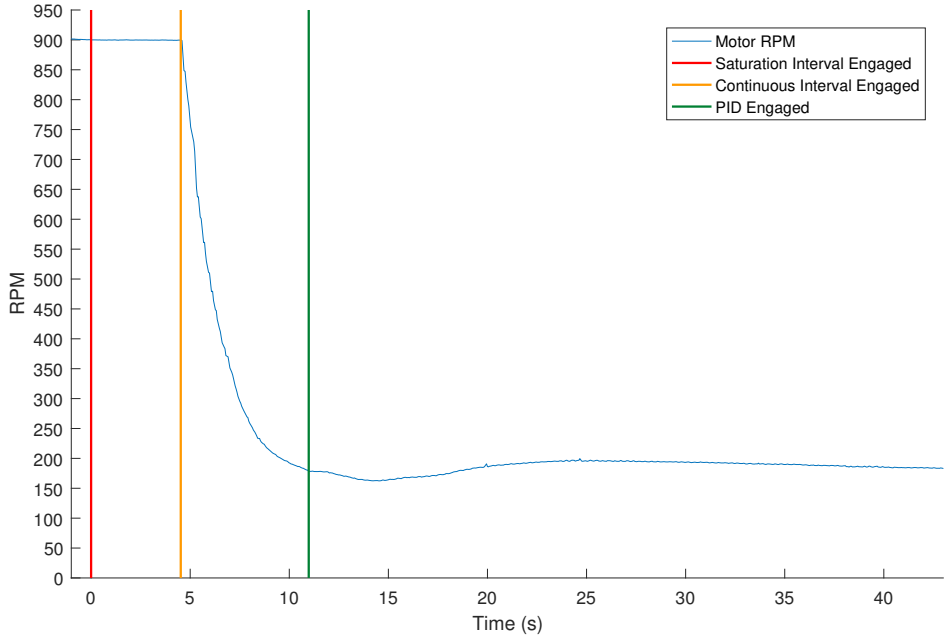

Figure 2.2: The "bump" which occurs at the moment of transfer between controllers can be eliminated through use of the bumpless transfer technique.

attaining excellent steady-state performance. The PID controller is tuned here with a variation of the tuning procedure implemented by Marshall [8].

A relay feedback test is performed during steady-state conditions, enabling estimation of key system parameters. The test relies on the assumption of a first-order-plus-dead-time system. The relay feedback test operates by alternating the input (motor RPM in this case) between high and low values, causing the output (the weld temperature) to oscillate. The input is set to the high value while the output is below the center-line of the oscillations, and vice versa. As shown in Figure 2.3, the time delay (θ), ultimate period (P_u), output amplitude (a), and input height (h) are measured from the resulting oscillations.

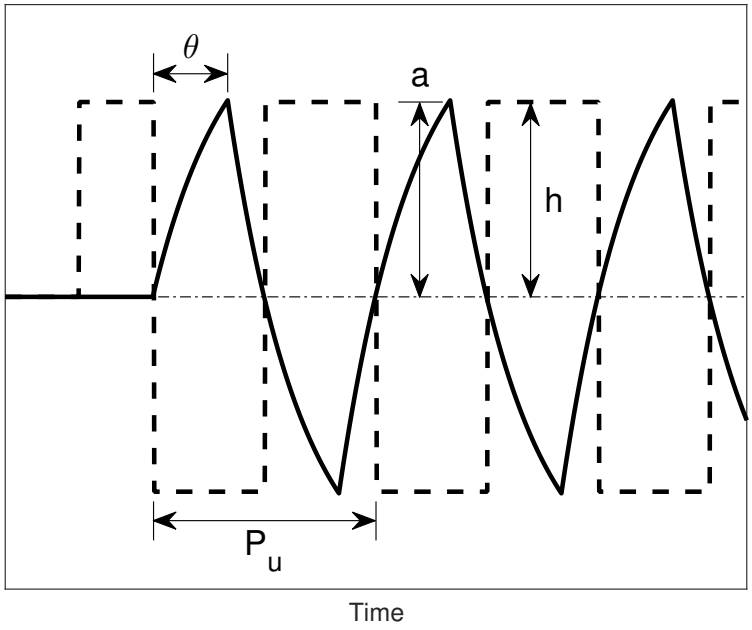

Figure 2.3: Diagram of the relay feedback test. The dashed and solid lines indicate the system input and output, respectively.

After measuring these parameters, the ultimate angular frequency (ω_u), ultimate gain (K_u), model gain (K_m), and time constant (τ) are approximated as shown in Equations 2.11, 2.12, 2.13, and 2.14, respectively.

$$\omega_u \approx \frac{2\pi}{P_u} \tag{2.11}$$

$$K_u \approx \frac{4h}{\pi a} \tag{2.12}$$

$$K_m = \int E(t)dt / u(t)dt \tag{2.13}$$

$$\tau = \frac{\sqrt{(K_u K_m)^2 - 1}}{\omega_u} \tag{2.14}$$

PID controller gains can be calculated for steady-state conditions given τ, θ, and K_m. Marshall [8] uses two tuning rules cited by O'Dwyer: 0% overshoot servo rules proposed by Chien and regulator rules proposed by Murrill [15]. The 0% overshoot servo gain rules are displayed in Equations 2.15 through 2.17.

$$K_{P,servo} = \frac{0.6\tau}{K_m \theta} \tag{2.15}$$

$$K_{I,servo} = \frac{K_P}{\tau} \tag{2.16}$$

$$K_{D,servo} = 0.5 K_P \theta \tag{2.17}$$

The regulator gain rules are displayed in Equations 2.18 through 2.20.

$$K_{P,regulator} = \frac{1.357}{K_m} \left(\frac{\tau}{\theta}\right)^{0.947} \tag{2.18}$$

$$K_{I,regulator} = \frac{K_P}{\frac{\tau}{0.842} \left(\frac{\theta}{\tau}\right)^{0.738}} \tag{2.19}$$

$$K_{D,regulator} = K_P \tau \left(\frac{\theta}{\tau}\right)^{0.995} \tag{2.20}$$

For the current setup, both sets of tuning rules exhibit unacceptable performance in the moments immediately after hand-off from the PVA controller. The servo gains are not adequately aggressive to maintain the temperature set-point within the settled band after hand-off. In con-

trast, the regulator gains exhibit semi-unstable oscillatory behavior. The performance of the servo and regulator PID gains necessitates a compromise which balances the servo and regulator performance. Equations 2.21 displays the weighted log mean relationship which was chosen to tune the controller, given servo and regulator gains.

$$K = (K_{servo}^2 * K_{regulator})^{\frac{1}{3}} \tag{2.21}$$

This relationship is intended to result in controller performance which tends towards servo gain performance for high stability while incorporating some of the responsive nature of the regulator gains.

2.5 Summary of the start-up controller

To summarize and contextualize the concepts presented in this chapter, Figure 2.4 displays a sample RPM profile commanded by the controller with indicators of the major weld and control events. The saturation interval is engaged from the moment the plunge begins at $t = 0$. Once $|E| < W_{tran}$, the continuous interval is engaged. $W_{tran} = 100°\text{C}$ in this example. PID control is engaged via the bumpless transfer technique once the transfer criteria are satisfied (Section 3.8). Figure 2.5 displays the resulting temperature profile for the controller input shown in Figure 2.4 with the same weld event indicators.

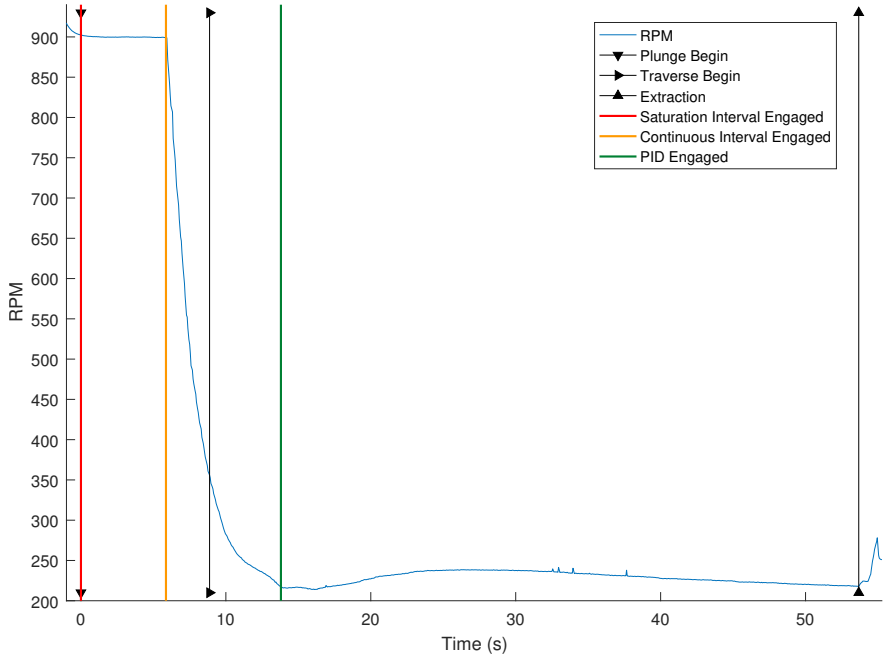

Figure 2.4: Tool RPM vs. Time with indicators of major control events.

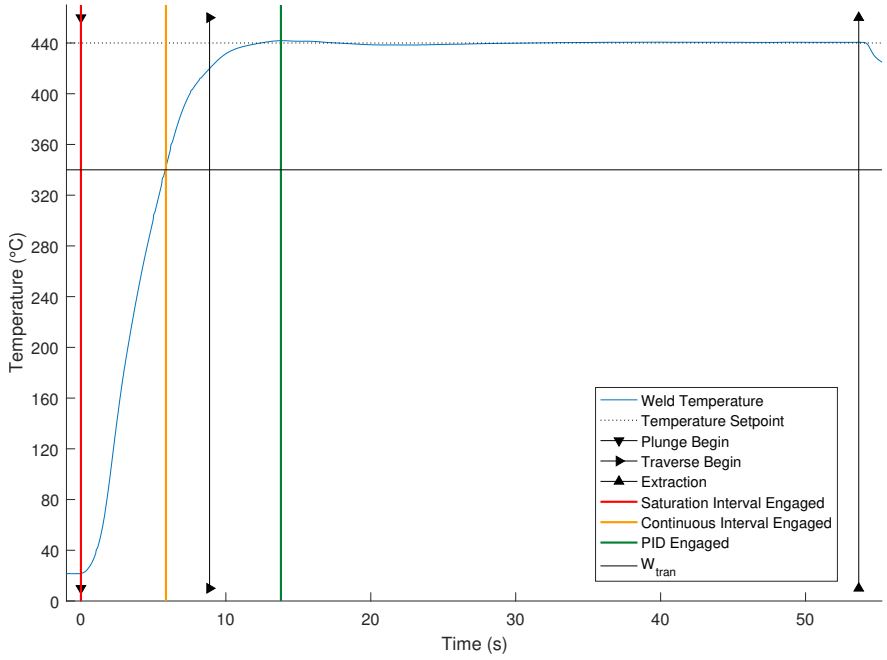

Figure 2.5: Weld temperature with indicators of major control events. W_{tran} is 100°C in this example, meaning the continuous interval engages at 340°C.

CHAPTER 3. IMPLEMENTATION OF THE TEMPERATURE CONTROLLER

3.1 Weld Configuration

All welds in this research are performed with the tool, work-piece, and geometry defined in this section. Welds are run with a CS4 tool in 6.35 mm plates of 7075-T651 Aluminum. The welding profile is 70 mm in length. The traverse feed-rate is 50 mm/min for the first 5 mm and increased to 100 mm/min for the remainder of the traverse. The plunge feed-rate is a constant 40 mm/min.

Details and dimensions of the tool geometry shown in Figure 3.1 can be seen in Appendix A. A thermocouple is threaded down the center hole of the tool to position the tip of the thermocouple in the center of the pin for measurement of the weld temperature. This thermocouple position has been determined to most closely represent the peak process temperature [16]. 32 gauge type K sheathed thermocouples are used.

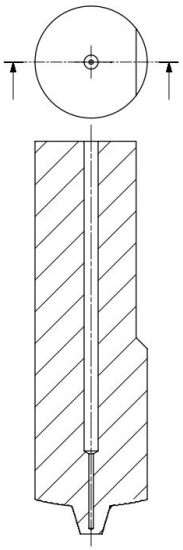

Figure 3.1: General geometry of a FSW tool. An EDM hole for threading a thermocouple to the center of the pin is shown.

3.2 Temperature Control via RPM

Temperature control can be implemented using motor torque [17], motor RPM [6], or motor power [7] as the controller output variable. Despite a correlation between motor power and thermal input to the weld [7], RPM is selected as the control variable because of the control stability it offers. Temperature control via RPM is stable because it is inherently able to prevent runaway motor output and motor stall. Torque and power control could be problematic due to the small and changing contact area of the tool with the workpiece which occurs during the plunge.

3.3 Implementation of Gain Scheduling

$W_{tran} = 100°\text{C}$ was selected as the point of transition between the saturation and continuous control intervals. With this value of W_{tran}, the saturation interval is engaged while $E \geq 100°\text{C}$ and the continuous interval controller is engaged while $E < 100°\text{C}$.

3.4 Saturation Interval Tuning

The saturation RPM, u_{sat}, is determined by performing constant-RPM welds, with each successive weld performed at a higher RPM than the last. Welds must be performed with sufficient temporal separation to prevent residual heat from influencing the subsequent results. In addition, the weld profile must be held constant for all welds (plunge rate, traverse rate, etc.). By observation, a saturation value can be identified in the data and implemented into the controller. Selection of the saturation RPM value for this research is described in Section 3.5. The resulting saturation value may be unique for different weld scenarios (geometries, materials, etc.).

8 welds were run with constant RPM through the plunge and traverse to identify a saturation RPM. Each subsequent weld was performed with an RPM 100 higher than the previous weld. The measured rise time to 440°C for each weld is displayed in Figure 3.2.

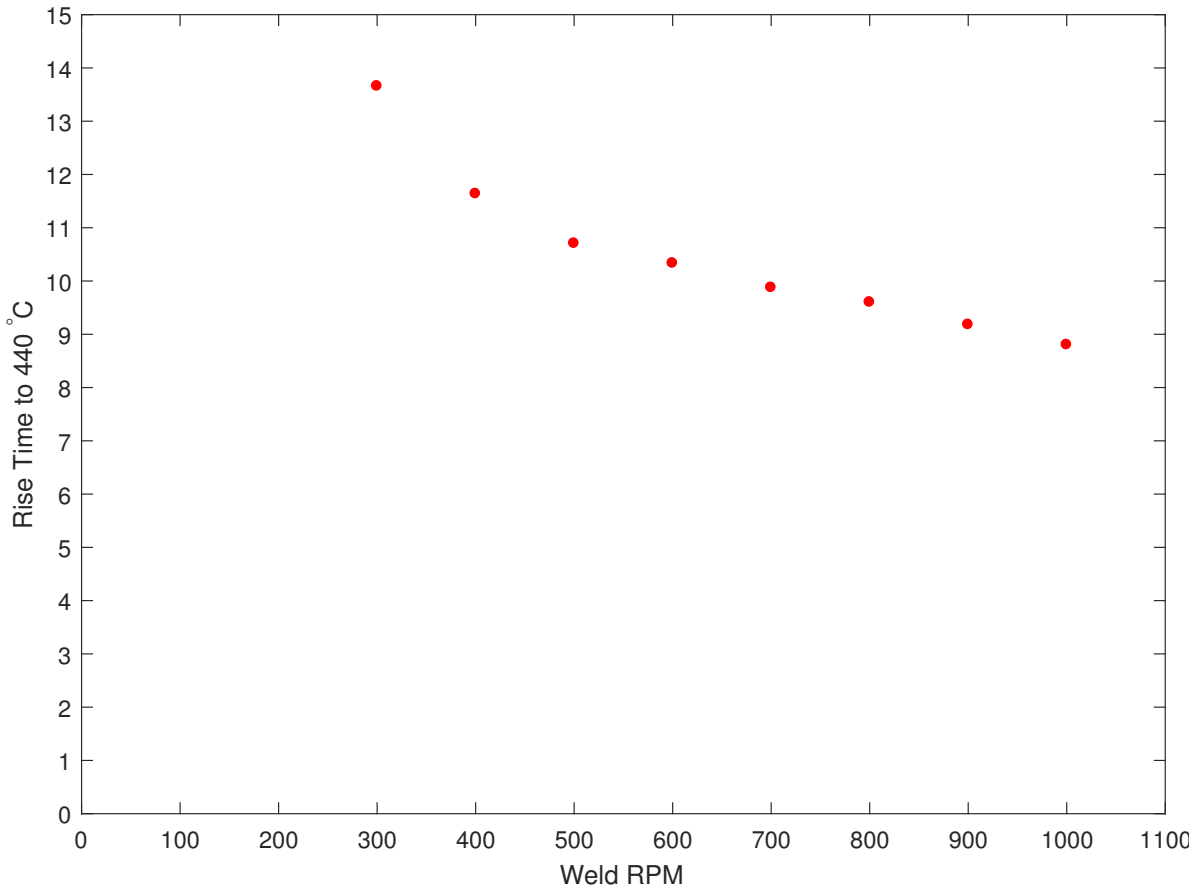

Figure 3.2: Rise time for welds run at constant RPM. The weld profile is identical for each weld.

3.5 Saturation Interval Implementation

The rise time decreases somewhat asymptotically as RPM increases. From the data displayed in Figure 3.2, an RPM of 900 was selected as the saturation value for the current weld setup.

Further decrease in rise time may be possible for higher RPM values, but a higher value is not selected. The reasoning for this selection is that the spindle RPM can exhibit a large, sudden decrease after the transition to the continuous interval, as seen in Figure 2.4. This spindle-braking event occasionally exceeded the machine limits with higher saturation RPM values, resulting in the cessation of active control during start-up. The spindle RPM commanded by the PVA controller was observed to consistently be within the machine limits with 900 RPM as the selected saturation

value. In other words, a saturation value of 900 RPM is deemed to be within a safe working range for the FSW machine used in this research.

3.6 Continuous Interval Tuning

For the welding configuration described in Section 3.1, non-zero values of K_A result in undesired or unstable controller behavior due to the behavior of the temperature acceleration signal, which can be seen in Figure 3.3. The extreme oscillatory behavior of the curvature signal renders it unusable for feedback control.

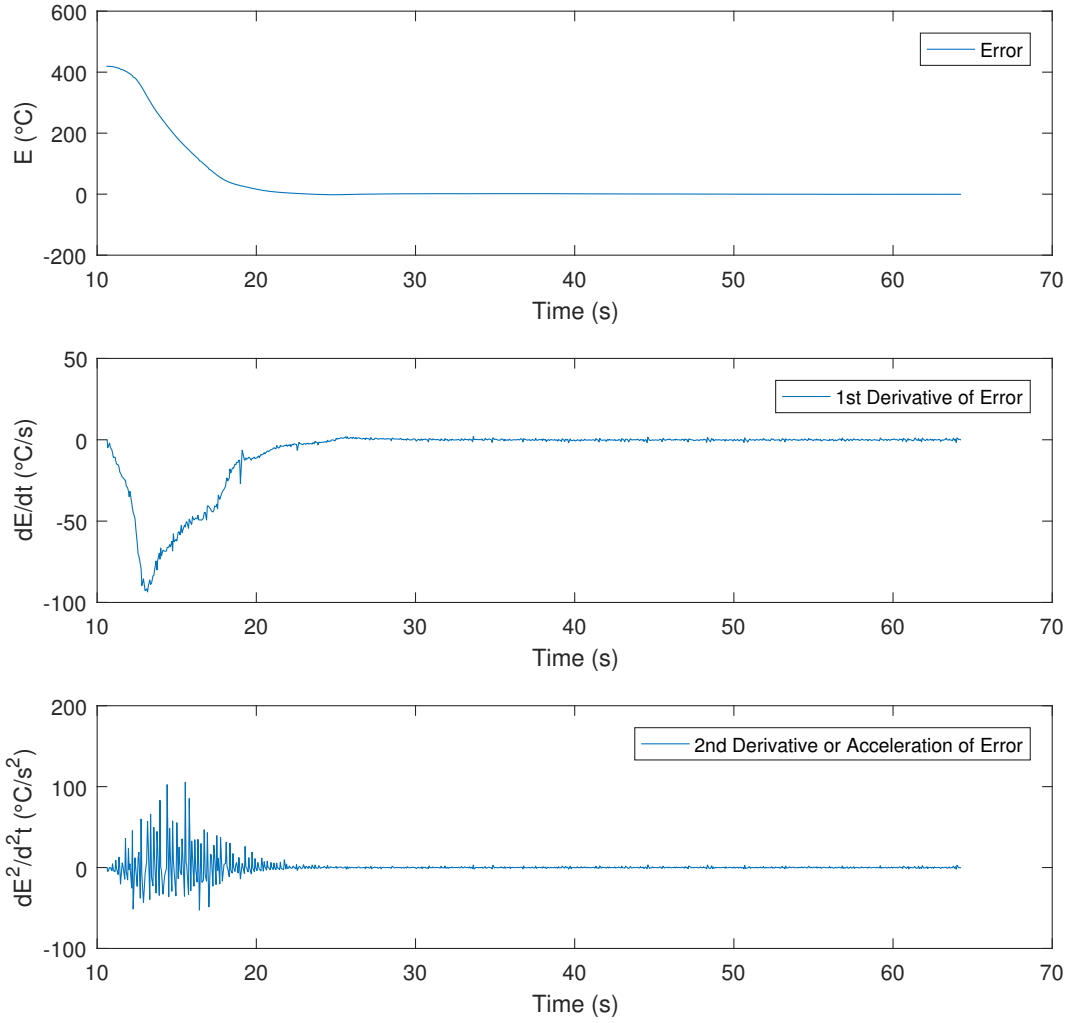

Figure 3.3: Typical example of temperature error, error 1^{st} derivative, and error 2^{nd} derivative.

The source of this behavior is not known, but is likely due to noise in the temperature signal. Regardless of the cause, the behavior necessitate $K_A = 0$. Filtering was considered as a solution, but only heavy filtering on the velocity and acceleration signals created a usable signal. The resulting lag in controller response was not adequate. Given a sufficiently smooth temperature signal, this segment of the PVA controller could be implemented with a non-zero gain. This is a common weakness of PVA controllers which could be addressed in future work through filtering of the temperature signal (or of its derivatives) [18].

Acceptable controller gains were selected through a manual tuning process. The controller gains used as a starting point for the tuning process are the steady-state PID controller gains calculated via the relay feedback test discussed in Section 2.4. These PID gains, K_P, K_I, and K_D, are used as the initial and final values of the PVA gains, K_V, K_P, and K_A, respectively. However, only K_P and K_V are non-zero due to the unusable temperature acceleration signal. The apparent restructuring of controller terms is the result of the renaming and rearranging of the controller terms which occurs in the PVA controller derivation (see Section 2.1 for clarification). The controller gains used in this research as a starting point for the tuning process are shown in Table 3.1.

Table 3.1: PVA Controller gains used as a starting-point for tuning the PVA controller.

Controller Gain	Initial Value, $\|E\| = 100°C$	Final Value, $\|E\| = 0°C$
K_P	1.65	1.65
K_V	6.02	6.02
K_A	0	0

Minimization of the settling time is the primary objective of the controller tuning process. The rise time and percentage maximum post-rise error (overshoot as percentage of the 3°C settling band half-width) are used as secondary metrics to provide insights into the achieved settling time values. The steps outlined below outline the procedure used to minimize the settling time.

1. **Select a controller gain to explore**: A total of 8 welds are performed in this step. Each weld is performed by individually increasing or decreasing each of the four PVA controller

gains ($K_{P,o}$, $K_{V,o}$, $K_{P,f}$, or $K_{V,f}$) by a selected step size. A step size of 1 or 2 sufficed for the current research, though this may be adjusted if deemed necessary. The measured settling time data from the 8 welds is used to identify a controller gain for further exploration. The gain change associated with the largest decrease in settling time is selected as the controller gain to explore. For example, if an increase in $K_{V,o}$ from 6 to 8 produces the largest decrease in settling time, $K_{V,o}$ is selected for further exploration.

2. **Continue exploration of the selected controller gain**: The objective of this step is to minimize the settling time by varying only the selected controller gain. Continuing with the previous example, if $K_{V,o}$ were the selected gain, the gain might be changed from 8 to 10, then from 10 to 12, and so on until the settling time begins to increase or no longer decreases. Any change which produce a decrease in settling time is incorporated into the updated set of "best" gains.

   Step sizes ranging from 0.5 to 5 were used for the current research, but as with identifying a search direction, a step size of 2 was frequently sufficient. If large changes to the selected gain produce an increase in settling time, smaller step sizes are taken to locate a settling time minimum along the search direction.

3. **Determine new search direction and continue exploration**: After changes to the selected gain greater than or equal to 0.5 no longer produce decreases in settling time, steps 1 and 2 are repeated.

4. **Identify acceptable controller gains**: If changes to any of the controller gains no longer produce a noticeable decrease in settling time, the identified gains are deemed acceptable and the manual tuning process is concluded.

Many optimization processes involve identifying a new search direction after each successive exploratory step within the design space. This custom minimization process seeks to reduce the number of welds needed to identify acceptable controller gains by ignoring possible interaction effects. It is not intended to be an exhaustive optimization routine. The controller gains resulting from the manual tuning process for the current research are shown in Table 3.2.

Table 3.2: PVA controller gains resulting from the manual tuning process. Minimization of the settling time is the objective of these controller gains.

Controller Gain	Initial Value, $\|E\| = 100°C$	Final Value, $\|E\| = 0°C$
K_P	3	5
K_V	20	4.5
K_A	0	0

3.6.1 Tuning Verification

After identifying acceptable controller gains, a coarse, non-statistical verification of the selected controller gains is performed. The purpose of the verification is to provide insight into whether other settling time minima exist in the surrounding design space. If the controller gains found during the manual optimization process are deemed sufficiently acceptable, this verification process may not be necessary.

18 welds are performed in the verification process. For 16 of the welds, a single controller gain is increased or decreased by a factor of two. Each variation is performed twice. This amount of variation in the controller gain values is intentionally large to allow for discovery of other possible minima in the design space. Two additional welds are performed with the controller gains found through the manual optimization process (shown in Table 3.4) as a point of comparison. The queue of 18 welds is randomized and carried out. In addition to settling time, rise time and maximum overshoot are measured to allow for a more complete comparison of the controller performance during start-up.

The randomized queue and results of this verification process for the current research is shown in Table 3.3. The results are displayed graphically in Figures 3.4, 3.5, 3.6, and 3.7. As can be observed, none of these results suggest that other settling time minima exist in the nearby design space, verifying the gains found through the manual optimization process. However, as interaction effects may play an important role in the process of selecting controller gains, a statistical

characterization of these tuning parameters (including significant interaction effects) is described and discussed in Chapter 5.

Table 3.3: Manual tuning verification results. The center-point welds are highlighted in blue, which corresponds to the blue markers in Figures 3.4, 3.5, 3.6, and 3.7.

	Controller Gain Values				Metrics		
Weld Number	Po	Vo	Pf	Vf	$t_{settled}$	t_{rise}	PMPE
1	3	10	5	4.5	22.63	8.66	1149 %
2	3	20	5	2.25	14.52	10.95	139 %
3	3	20	5	4.5	12.49	12.59	61 %
4	6	20	5	4.5	13.37	9.92	196 %
5	3	20	5	4.5	11.98	12.06	51 %
6	6	20	5	4.5	13.51	9.56	2893 %
7	3	20	5	9	12.59	12.7	749 %
8	3	20	2.5	4.5	16	13.09	120 %
9	3	10	5	4.5	24.38	8.81	1043 %
10	3	20	10	4.5	13.37	10.48	123 %
11	3	20	10	4.5	16.73	10.15	199 %
12	3	40	5	4.5	26.61	26.71	33 %
13	1.5	20	5	4.5	15.15	15.23	24 %
14	1.5	20	5	4.5	18.03	18.08	21 %
15	3	20	5	9	16.21	12.18	121 %
16	3	40	5	4.5	24.9	24.94	27 %
17	3	20	5	2.25	14.55	10.78	158 %
18	3	20	2.5	4.5	14.73	14.82	45 %

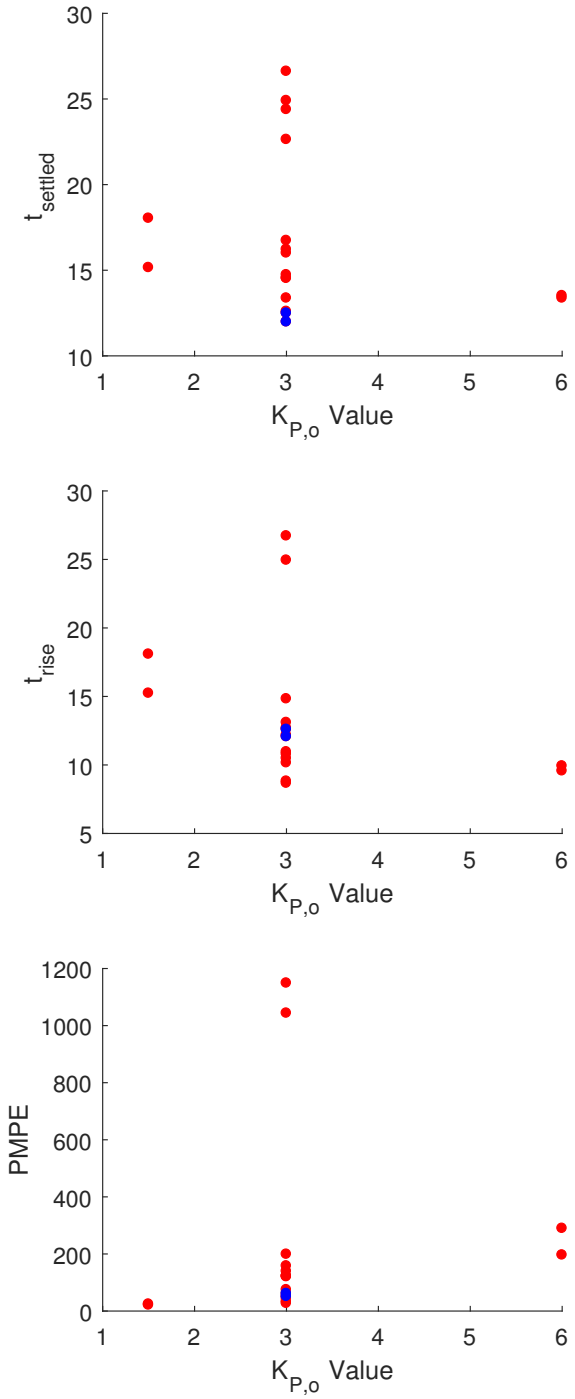

Figure 3.4: Demonstration of the effect of $K_{P,o}$ on rise time, settling time, and percentage maximum post-rise error.

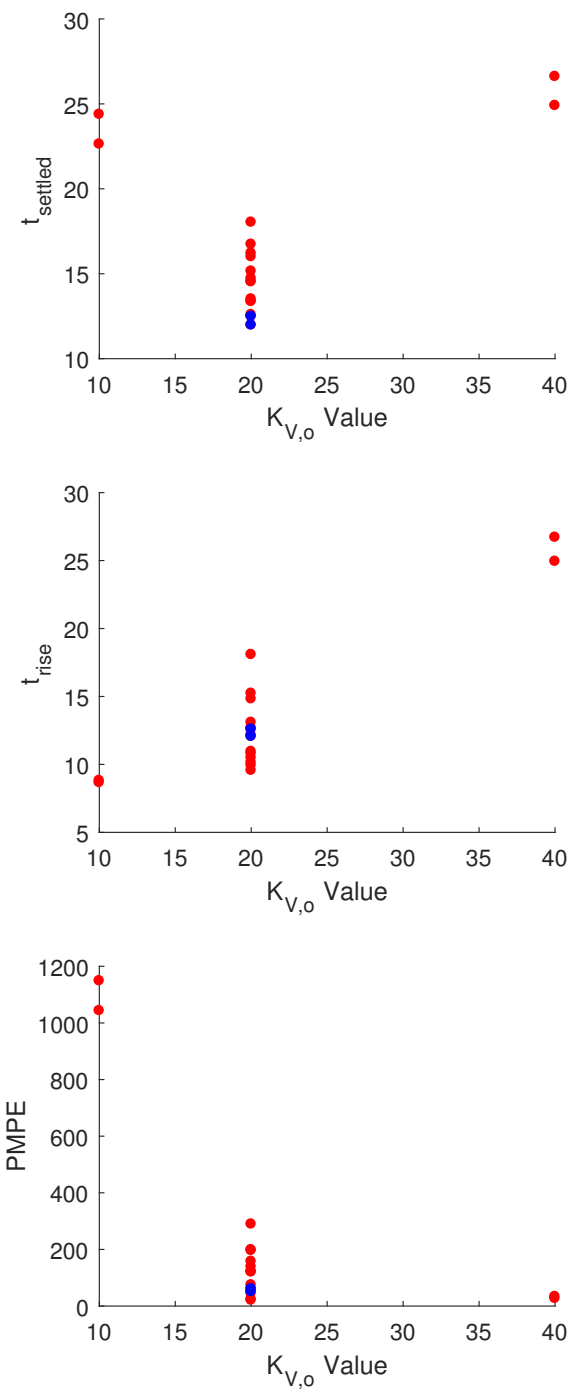

Figure 3.5: Demonstration of the effect of $K_{V,o}$ on rise time, settling time, and percentage maximum post-rise error.

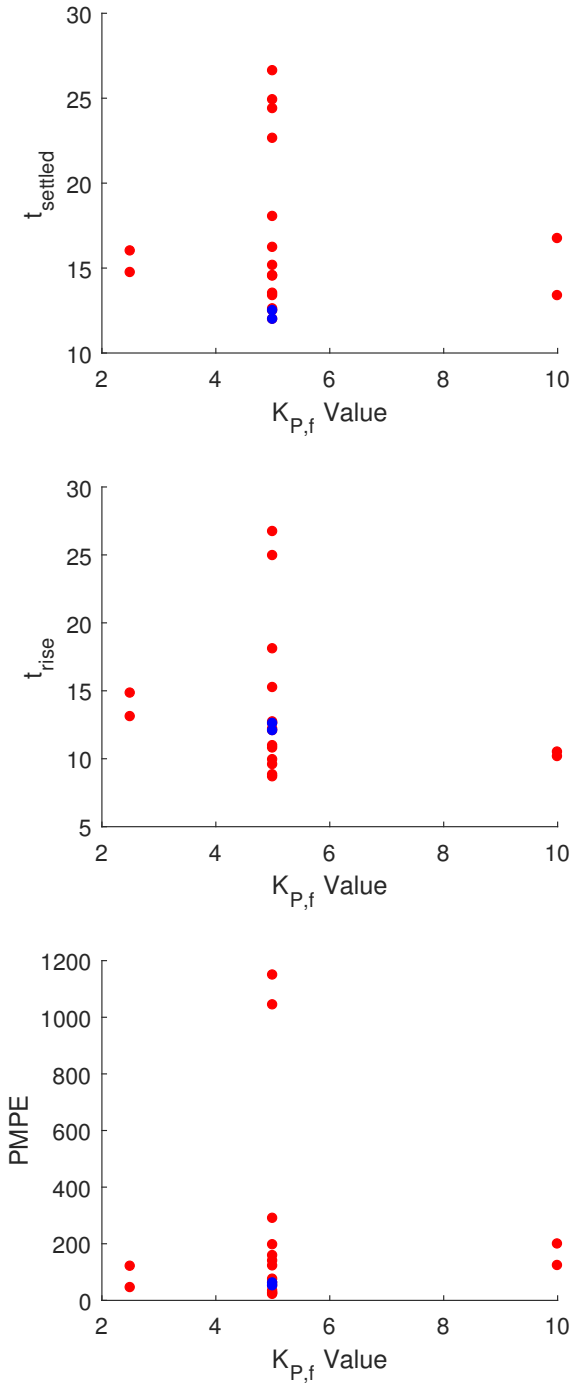

Figure 3.6: Demonstration of the effect of $K_{P,f}$ on rise time, settling time, and percentage maximum post-rise error.

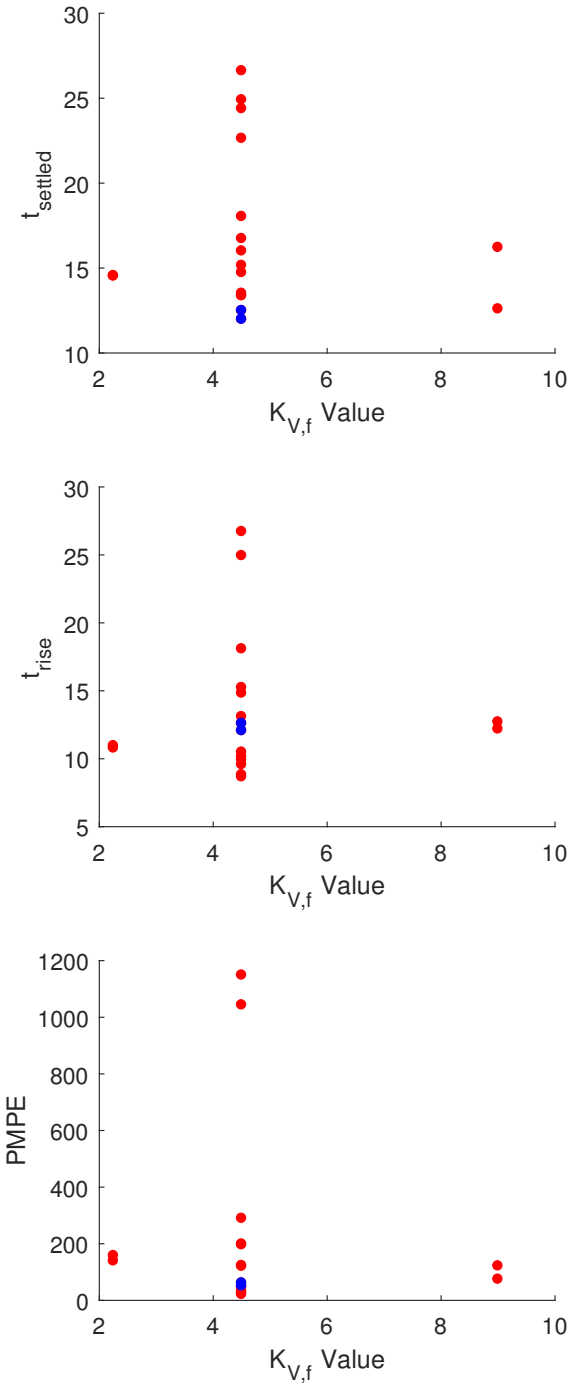

Figure 3.7: Demonstration of the effect of $K_{V,f}$ on rise time, settling time, and percentage maximum post-rise error.

3.7 Continuous Interval Implementation

The controller gains found through the manual tuning process (shown in Table 3.4) are used to demonstrate the performance of the controller in Chapter 4. A weighting constant of $C = 100$ is used to vary the controller gains as a function of $|E|$ (as shown in Equation 2.9) between the initial and final gains. W_{tran} is implemented as 100°C. The resulting controller gains are shown in Figure 3.8.

Table 3.4: PVA controller gains used during the continuous interval.

Controller Gain	Initial Value, $\|E\| = 100°C$	Final Value, $\|E\| = 0°C$
K_P	3	5
K_V	20	4.5
K_A	0	0

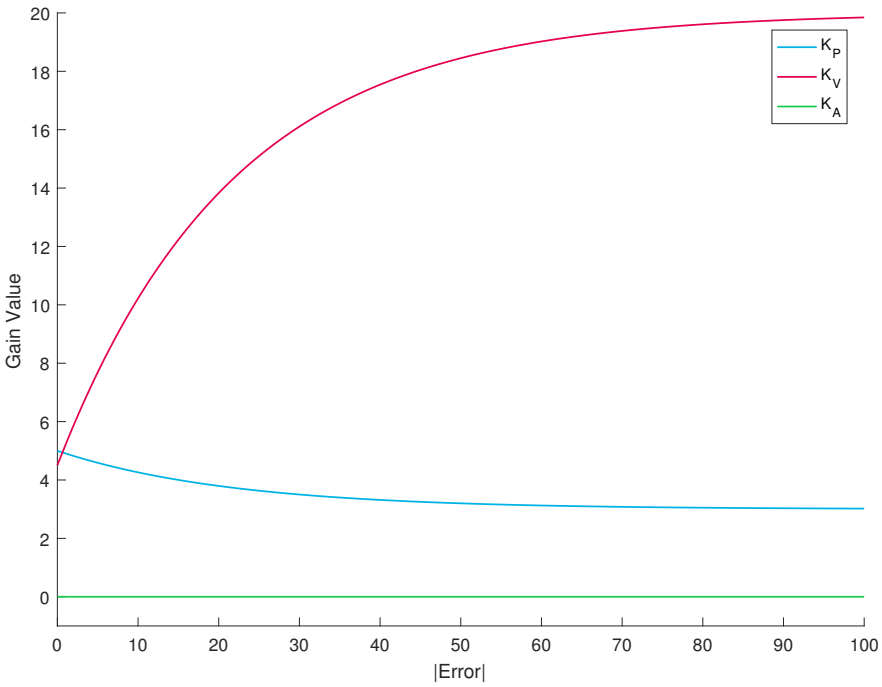

Figure 3.8: Continuous interval PVA controller gains associated with the values displayed in Table 3.4.

3.8 Criteria for Transfer to Steady-State Control

To ensure that favorable conditions exist at the moment of transfer from the PVA controller to the PID controller, a set of transition criteria is embedded in the controller algorithm. Qualitatively, the criteria are stated as the following:

1. The weld temperature must be near the set-point.
2. The derivative of the weld temperature must be small.
3. The weld temperature must be approaching the set-point (from either above or below).

The third statement of the transfer criteria determines the sign of the temperature derivative criteria. The sign of the temperature derivative criteria mirrors the sign of the current temperature error. This ensures that the weld temperature is approaching the temperature set-point at the moment of transfer. For example, in the case of positive error (the weld temperature is below the set-point), transfer to the PID controller may only occur when the temperature derivative is positive and sufficiently small. The quantitative implementation of the transfer criteria is chosen as follows:

1. Transfer may only occur while $|E| \leq 5°\text{C}$.

2a. If $E > 0$, transfer may only occur while $\frac{dT}{dt} < 0.2°\text{C/s}$.

2b. If $E < 0$, transfer may only occur while $\frac{dT}{dt} > -0.2°\text{C/s}$.

The instant that these criteria are met, control is transferred to the PID controller. The bumpless transition method discussed in Section 2.3 is used to eliminate C_0 discontinuities in the controller output at hand-off.

3.9 Steady State Control

Data collected from the relay feedback test, the calculated system parameters, and the resultant servo and regulator PID gains can be seen in Appendix C. Table 3.5 displays the PID controller gains used for steady-state control for the controller results shown in Chapter 4.

Table 3.5: PID controller gains used during steady-state conditions.

Controller Gain	Value
K_P	6.02
K_I	1.65
K_D	1.83

CHAPTER 4. TEMPERATURE CONTROLLER PERFORMANCE

4.1 Performance Metrics

The metrics used to measure important characteristics of the controller performance are enumerated in Table 4.1. For clarification, the quantities necessary for calculation of the performance metrics are graphically displayed in Figure 4.1. The performance of the controller for each weld is reported in terms of the performance metrics.

Table 4.1: Controller performance metrics used to quantify the behavior of the controller.

Performance Characteristic	Associated Metric	Notation	Definition
Reach the temperature set-point as quickly as possible	Rise Time	t_{rise}	Time from beginning of the plunge to the time the weld temperature first intersects the settled band.
Settle to the weld temperature as quickly as possible	Settling Time	$t_{settled}$	Time after which all temperature error satisfies $\|E\| < 3°$C.
Avoid overheating the weld	Percentage Maximum Post-rise Error	PMPE	$\frac{T_{max}-T_{set}}{W_{settled}}$ where $W_{settled}$ is the half-width of the settled band, 3°C.
Track closely to the temperature set-point	Post-Settled Root Mean Square Error	RMSE	Calculated as $\sqrt{\frac{1}{n}\sum_{k=0}^{n} E_k^2}$. $k = 0$ corresponds to $t_{settled}$, n is the number of data points from $t_{settled}$ and $t_{extraction}$.

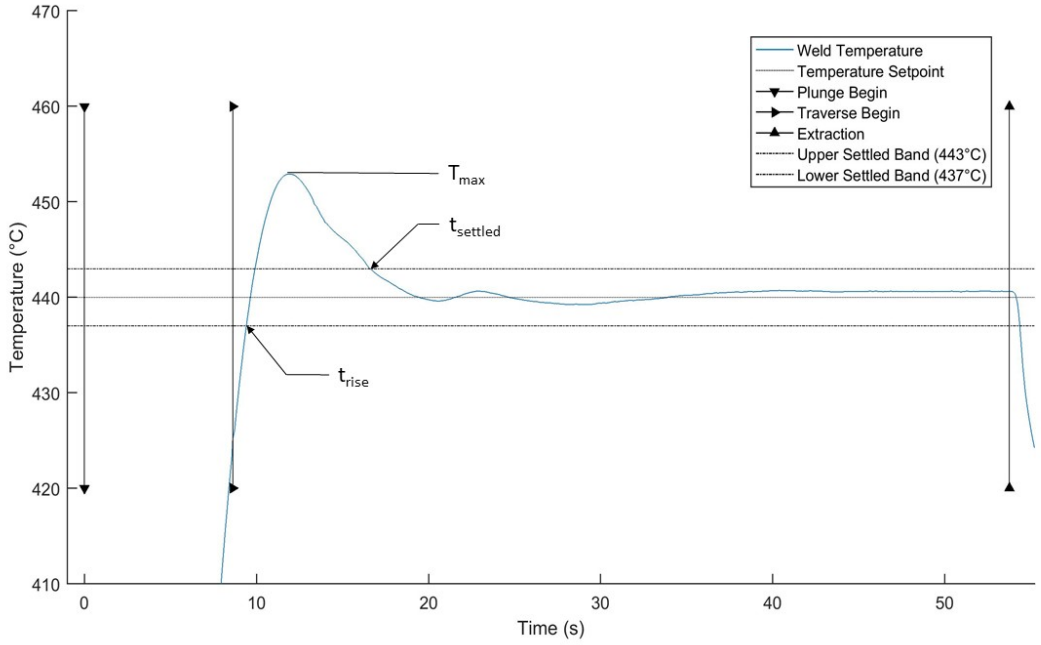

Figure 4.1: A graphical representation of the quantities needed for calculating the performance metrics described in Table 4.1.

4.2 Temperature Controller Performance

9 welds were run with the weld and tuning parameters described in Chapter 3 with a temperature set-point of 440°C. The measured performance metrics are reported in Table 4.2. For a more intuitive visualization, Figure 4.2 displays the controller performance metrics in a radar plot.

From the 9 welds, Weld 1 is shown in greater detail. This weld temperature profile is graphically displayed in its entirety in Figure 4.3. The same weld temperature profile is displayed in Figure 4.4 with the Temperature axis limited to $\pm 20^{\circ}C$ about the temperature set-point to emphasize the controller performance near the set-point. Figures displaying the weld temperature profiles of the remaining 8 welds are shown in Appendix D.

Controller Performance Discussion

As discussed in Section 1.4, FSW temperature controllers were previously limited by the need for a machine operator to manually engage the controller once the weld had reached steady-state. The performance of the 9 welds demonstrate that the temperature controller can successfully

Table 4.2: Performance metrics of the 9 demonstration welds performed with the PVA controller gains shown in Table 3.4 and the steady-state PID gains shown in Table 3.5.

Weld No.	$t_{settled}$	t_{rise}	PMPE	RMSE
1	11.79s	11.79s	63.8%	0.97°C
2	12.14s	12.14s	42.6%	0.95°C
3	11.12s	11.12s	62.1%	0.87°C
4	11.02s	11.02s	62.7%	0.79°C
5	10.24s	10.24s	85.0%	1.07°C
6	10.12s	10.12s	68.8%	0.84°C
7	10.51s	10.51s	43.4%	0.87°C
8	10.14s	10.14s	99.6%	1.06°C
9	15.16s	10.00s	100.7%	0.86°C

control the weld temperature during start-up without operator input, which is an enhancement over previous FSW temperature control methodologies.

The temperature profile of Weld 1 (shown in Figures 4.3 and 4.4) is a typical example of the performance of the temperature controller. While not a specific goal of the controller, it is significant that the majority of the weld traverse is within the settling band. The intended effects of the control intervals can be observed in the temperature profile of weld 1. First, the saturation interval causes the weld temperature to approach the set-point rapidly. Second, the behavior of the continuous interval influences the settling time and percentage maximum post-rise error while also facilitating favorable conditions for transition to the steady-state controller. The post-settled RMSE is influenced by the performance of the PVA controller continuous interval, but due to the design of the controller, this performance metric is dominated by the steady-state PID controller performance.

4.3 Consistency Metric

An additional metric is required to assess the ability of the temperature controller to perform from weld to weld consistently. The coefficient of variation, also known as the relative standard deviation, is a statistic used to quantitatively assess consistency. This statistic is calculated as shown in Equation 4.1 and is reported as the percent variation about the mean.

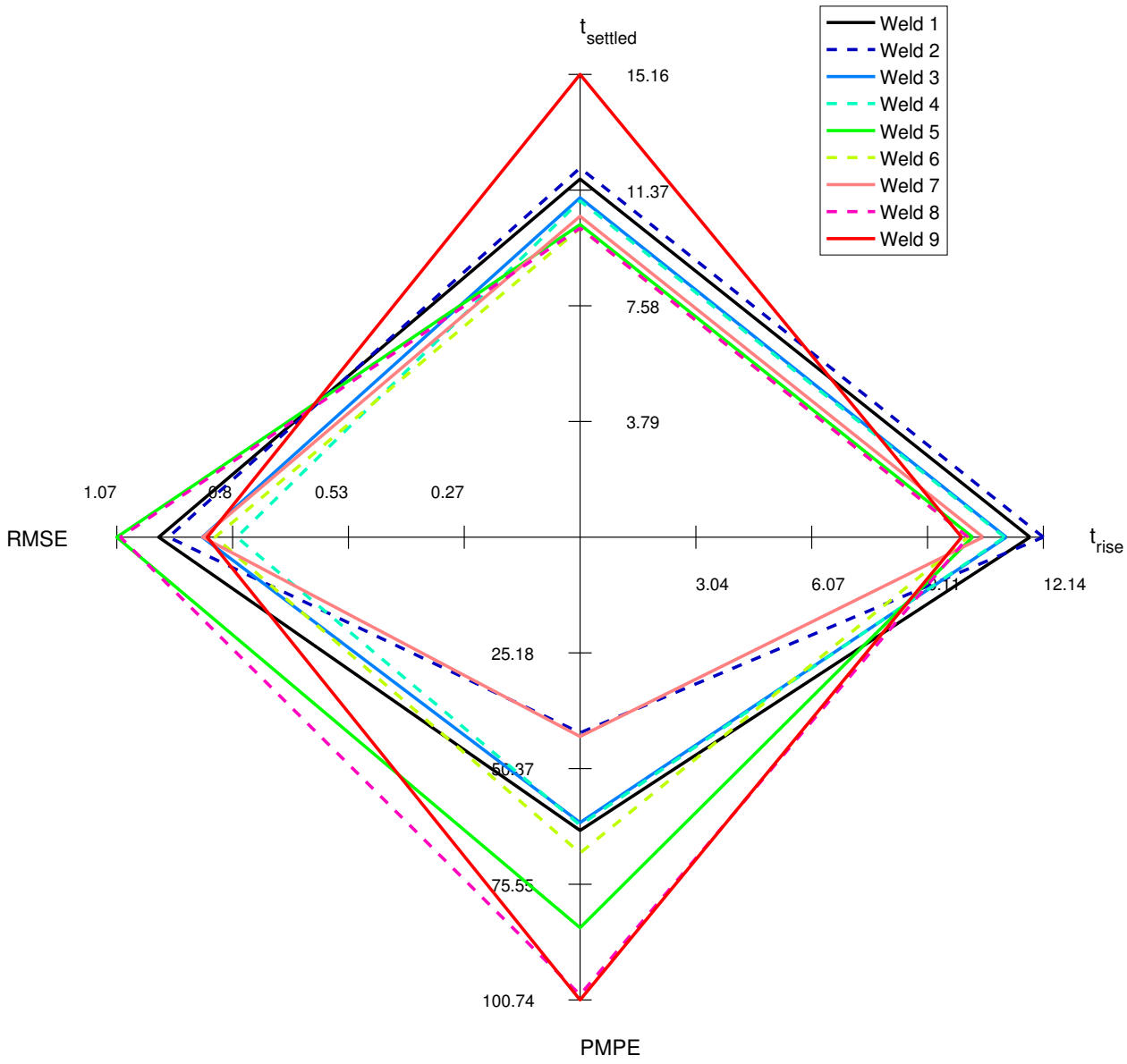

Figure 4.2: Radar plot of the 9 demonstration center-point welds shown in Table 4.2.

$$CV = \sigma/\bar{x} * 100\% \tag{4.1}$$

Traditional calculation of the standard deviation assume near-normal sample distributions. However, as can be observed in Figure 4.5, the distribution of the performance metrics cannot be assumed to be normal. A distribution-free estimation of the standard deviation is utilized to calculate coefficients of variation for each performance metric. Equations 4.2 and 4.3 are used to

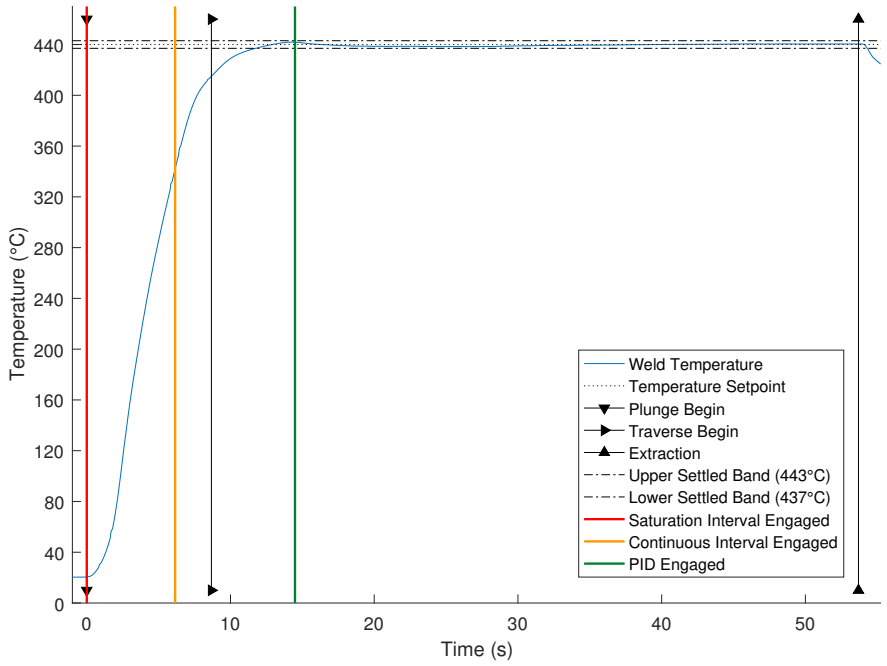

Figure 4.3: The weld temperature profile of Weld 1 in Table 4.2 with the Temperature axis shown in its entirety.

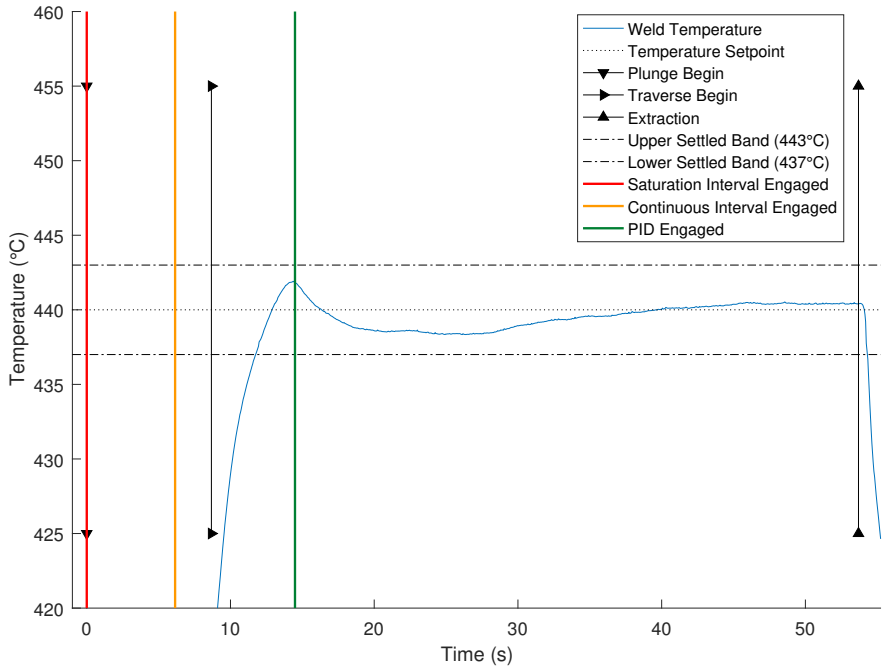

Figure 4.4: The weld temperature profile of Weld 1 from Table 4.2 with the Temperature axis limited to $\pm 20^{\circ}C$.

calculate the sample mean and estimate the sample standard deviation [19] from a set of measured performance metrics.

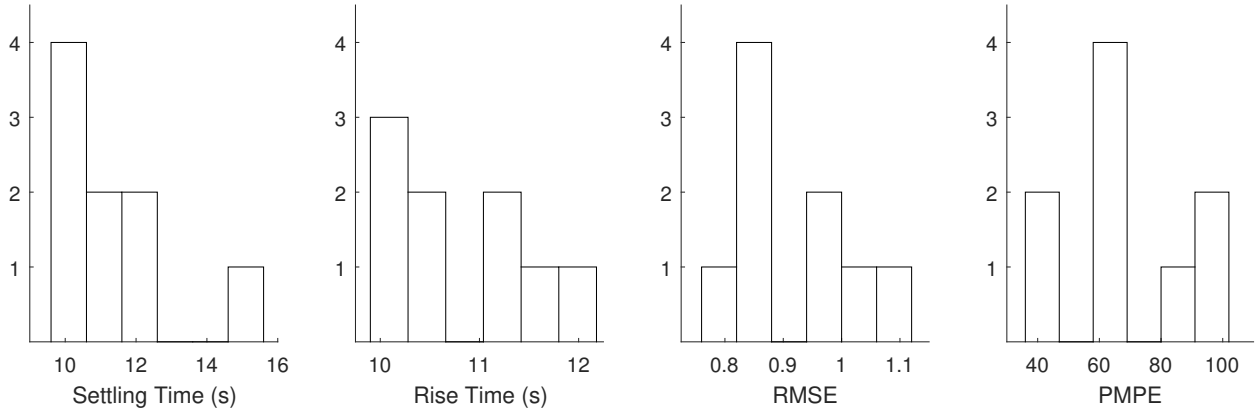

Figure 4.5: Histograms of the performance metrics for 9 welds with center-point PVA controller gains.

$$\bar{x} = \frac{1}{n}\sum_{i=1}^{n} x_i \tag{4.2}$$

$$\sigma \approx \sqrt{\frac{1}{12}\frac{(x_{min} - 2\tilde{x} + x_{max})^2}{4} + (x_{max} - x_{min})^2} \tag{4.3}$$

4.4 Temperature Controller Consistency

Histograms and boxplots of the performance metric data from the 9 demonstration welds are displayed in Figure 4.5 and 4.6, respectively. Table 4.3 displays the calculated mean, estimated standard deviation, and coefficient of variation of the performance metrics for the 9 welds.

Controller Consistency Discussion

The controller provides reliable and repeatable temperature control, as indicated by the coefficients of variation and box-plots of each performance metric, shown in Table 4.3 and Figure 4.6. The percentage maximum post-rise error has the highest coefficient of variation, but this is acceptable as the majority of values are less than 100%. The consistency of the settling time is

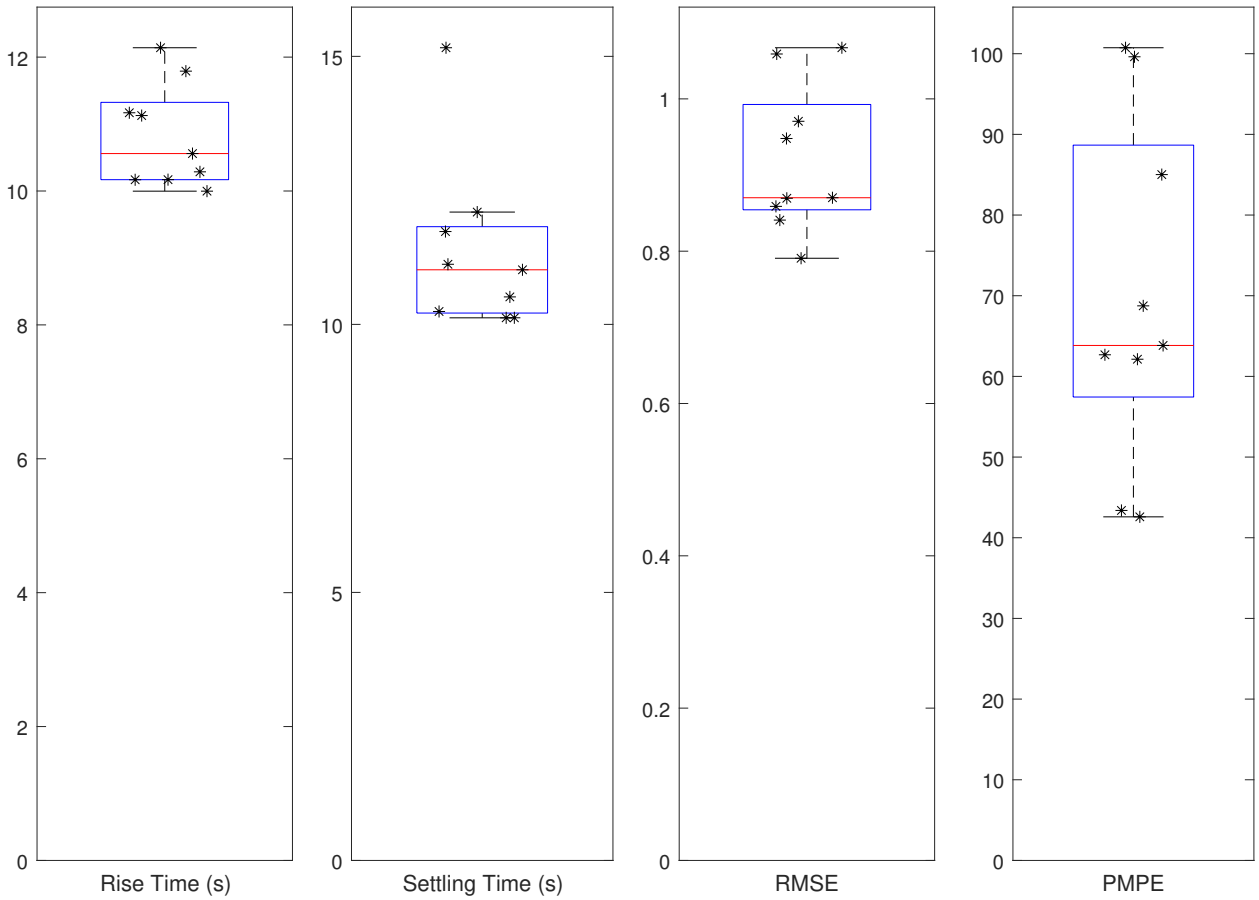

Figure 4.6: Box-plots of the performance metrics for 9 demonstration welds with center-point PVA controller gains.

Table 4.3: Mean, estimated standard deviation, and coefficient of variation of the performance metrics for the 9 demonstration welds with center-point PVA controller gains.

Performance Metric	$\bar{x}$	σ	CV
$t_{settled}$	11.35s	1.53s	13.5%
t_{rise}	10.82s	0.64s	5.9%
PMPE	69.86%	16.94%	24.2%
RMSE	0.92°C	0.08°C	8.9%

largely dependent on the PMPE: If the PMPE is greater than 100%, the settling time will be significantly longer. The temperature profile of Weld 9 is very similar to the other welds, but the settling time could be considered part of a separate population due to a corresponding percentage maximum post-rise error of 100.7%. The natural variation in the process causes this behavior. Due to the method for measuring the settling time, distinct populations exist depending on the oscillatory behavior of the weld temperature.

4.5 Comparison to Previous Work

The performance of the start-up controller is compared in this section to the performance of the steady-state PID control method developed by Taysom et al. In that work, the steady-state controller is engaged at the moment the weld traverse begins after a constant-RPM plunge. The PID controller (with regulator tuning) is able to maintain the temperature within 5°C of the temperature set-point during the initial traverse [6] [11].

Using this same methodology (but adapted to the weld profile described in Section 3.1), two welds are performed with constant 300 and 500 RPM plunges. The steady-state PID controller is engaged at the moment the traverse begins. For additional comparison, two welds are performed at 300 and 500 constant RPM with the steady-state PID controller engaged at the operator's discretion. The steady-state PID controller gains used for the four welds are the same controller gains used for the steady-state portion of the 9 demonstration welds (shown in Table 3.5).

The resultant temperature profiles of these four welds are displayed in Figure 4.7. The temperature profiles of the 9 demonstration centerpoint welds are shown for comparison. The performance metrics of the 4 comparative welds are displayed in Figure 4.8. The average performance metrics of the 9 demonstration welds is included for comparison.

The comparisons shown in Figures 4.7 and 4.8 highlight the superior performance of the start-up controller. The average PMPE is nearly half the PMPE of the best comparison weld. The start-up controller settles within the settled band nearly 5 seconds faster than the best comparison weld. The average post-settled RMSE performance and the average rise time are not diminished. Maintaining the RMSE performance is a significant achievement as it shows that the start-up controller does not negatively impact the steady-state tracking performance. Although it is not a direct comparison due to the difference in weld profiles, the start-up controller improves the set-point

tracking performance during the initial traverse to $\pm 3^{\circ}$C. In addition to these improvements, the start-up controller reduces inconsistencies introduced in the controller performance during welds in which the steady-state PID controller is engaged at the operator's discretion.

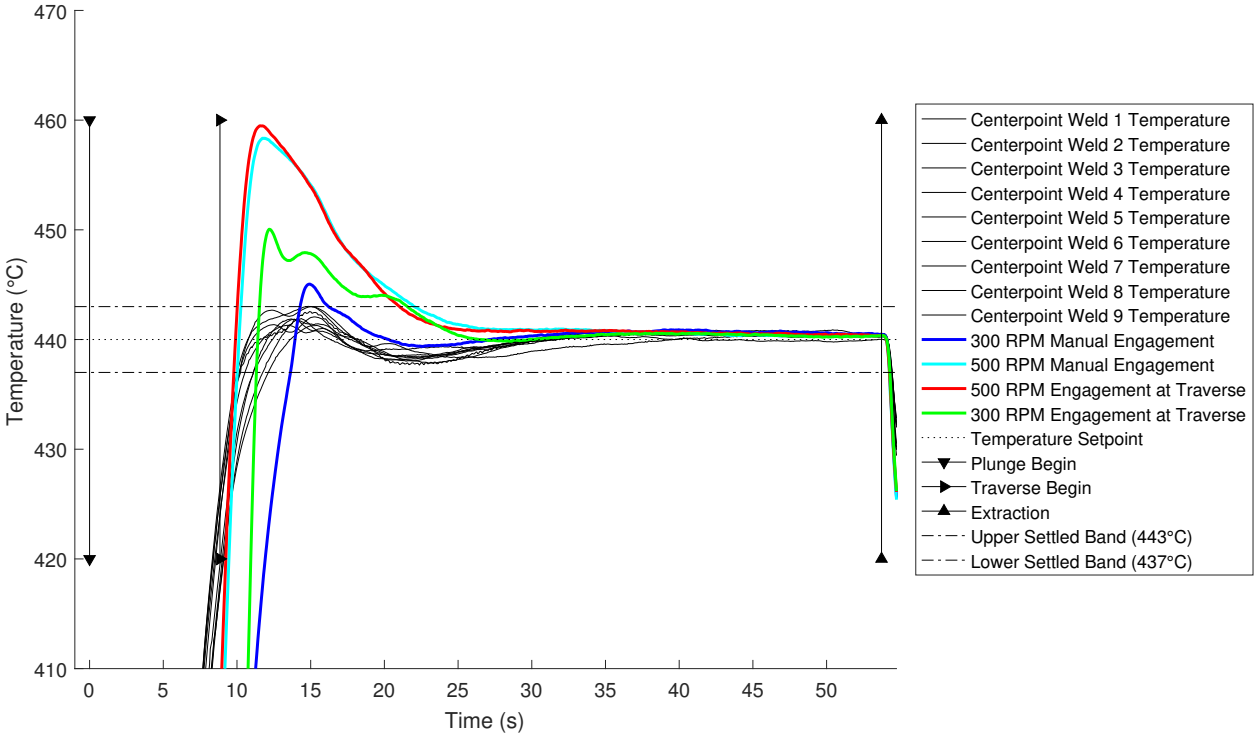

Figure 4.7: Comparison of the 9 demonstration center-point welds to the 4 welds performed without the start-up controller.

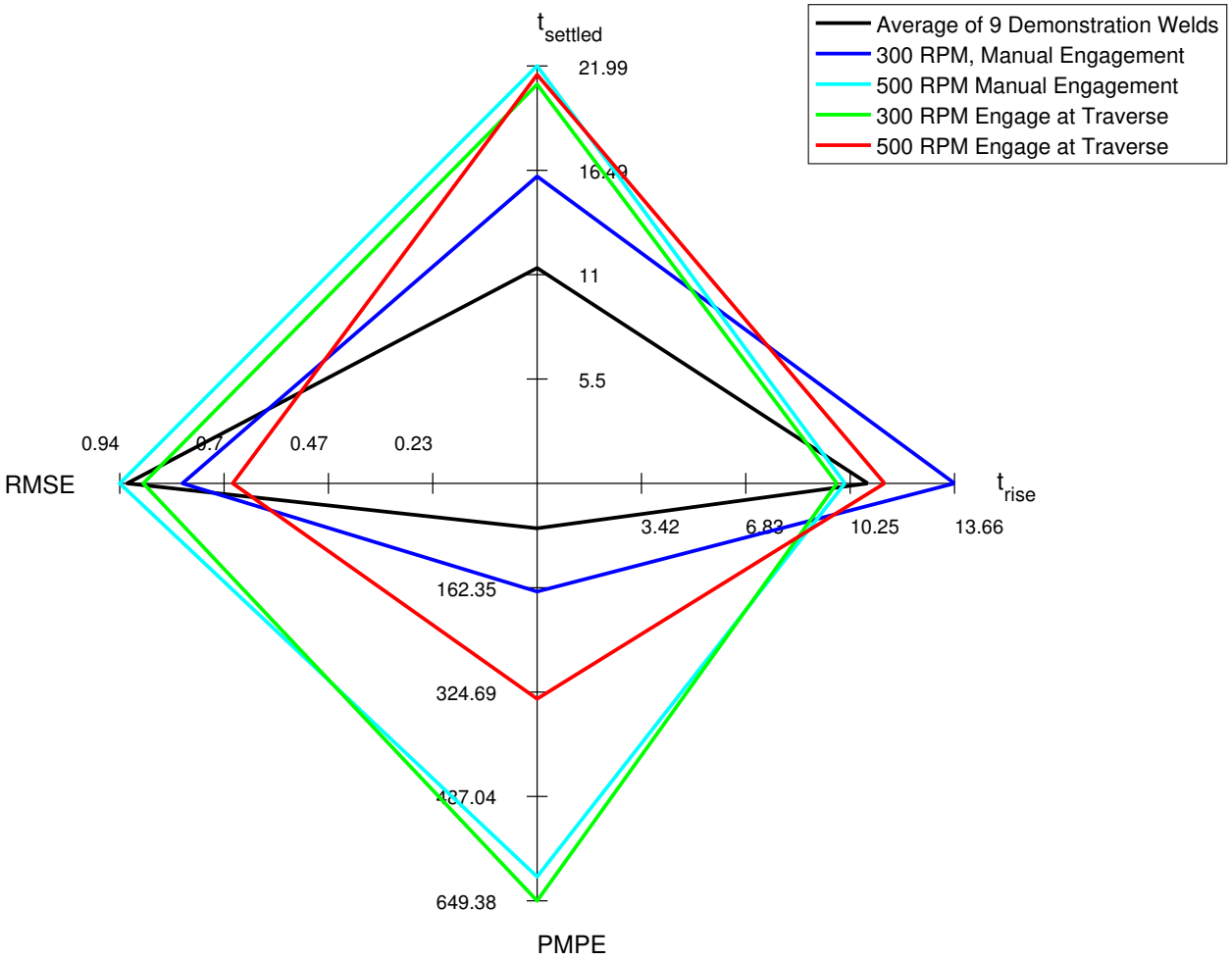

Figure 4.8: Comparison of the performance metrics from the 4 welds performed without the start-up controller to the average metric values of the 9 demonstration welds performed with the start-up controller.

CHAPTER 5. CHARACTERIZATION OF CONTROLLER TUNING PARAMETERS

5.1 Controller Tuning Design of Experiment

The several tuning parameters of the start-up controller presented in Chapter 3 are summarized in Table 5.1. Tuning of the controller may have been guided by a system model, but, as discussed in Appendix B, an acceptable system model of the welding process to predict the weld temperature during start-up conditions could not be constructed. Similarly, the manual tuning procedure presented in Section 3.6 does not result in any form of quantitative characterization of the tuning parameters. This chapter explores the feasibility of constructing multiple regression models to statistically characterize the effects of the PVA tuning parameters. With the aid of accurate models of these parameters, tuning of the temperature controller can be guided to obtain any desired controller behavior without performing additional tuning welds.

The following chapter outlines the experimental method used to characterize the effects of the continuous interval controller gains, $K_{P,o}$, $K_{P,f}$, $K_{V,o}$, and $K_{V,f}$, in terms of the four performance metrics, shown in Table 5.2. Design of experiments (DOE) is a method for collecting experimental data which enables statistical characterization of a system response in terms of the primary and interaction effects [20]. A 2^4 full-factorial design of experiments can be used to obtain data for the

Table 5.1: The tuning parameters of the start-up controller

Tuning Parameter Name	Notation	Explanation
Continuous Interval Half-Width	W_{tran}	Value $\|E\|$ at which control transitions from the saturation interval to the continuous interval
Weighting Function Constant	C	Base of the weighting function
Proportional Gain, Initial	$K_{P,o}$	Proportional gain at $\|E\| = W_{tran}^{\circ}C$
Proportional Gain, Final	$K_{P,f}$	Proportional gain at $\|E\| = 0^{\circ}C$
Velocity Gain, Initial	$K_{V,o}$	Velocity gain at $\|E\| = W_{tran}^{\circ}C$
Velocity Gain, Final	$K_{V,f}$	Velocity gain at $\|E\| = 0^{\circ}C$

construction of regression models which include only linear terms (meaning the primary effects and the interactions between those effects).

There are several controller parameters which are not included in this experiment. As mentioned previously, $K_{A,o}$ and $K_{A,f}$ are set to a value of 0 due to prohibitive noise in the temperature signal. The experiment also does not explore the effects of varying the continuous interval half-width (W_{tran}) or the weighting function constant (C). Additionally, the experimentally identified saturation RPM discussed in Section 2.2 is a constant during the experiment. The weld configuration described in Section 3.1 is used for all welds.

A 2^4 DOE is performed by first selecting high and low values (corresponding to -1 and 1 levels, respectively) for each of the four primary factors. Every possible combination of the high and low levels is generated, resulting in a total of 16 trials. These trials are performed in random order to prevent temporal confounding. In addition to the 16 trials, center-point trials are commonly added to the queue to allow for more complete characterization of the design space [20]. Center-point trails are performed with all factors at the neutral value (corresponding to a 0 level).

Using the controller gains found through the manual tuning process in Section 3.6 as the center-point values, high and low values are selected as $\pm 30\%$ of center-point controller gains. A 30% change is deemed sufficiently large to produce noticeable changes in the system response. The values of the controller gains used in the experiment are shown in Table 5.3. Every possible combination of high and low levels is generated, resulting in a total of 16 combinations. In addition, 2 center-point welds are included in the randomized weld queue, resulting in a total of 18 trials. No replication trials are performed, except for the 2 center-point trials. The implication of not performing replication trials is that a poor estimate of the variation in the design space results.

5.1.1 DOE data

Table 5.4 contains the randomized weld queue (welds 1-18), the input parameters for each weld, and the resultant values of the controller performance metrics. The controller response is plotted as a function of each of the controller gains in Figures 5.1, 5.2, 5.3, and 5.4.

Table 5.2: Controller Performance Metrics

Metric	Notation	Definition
Rise Time	t_{rise}	Time from the beginning of the plunge to the point at which the weld temperature first intersects the settled band
Settling Time	$t_{settled}$	Time after which all temperature error satisfies $\|E\| < 3°$C, prior to $t_{extraction}$
Post-Settled Root-Mean-Square Error	$RMSE$	Calculated as $\sqrt{\sum_{t_{settled}}^{t_{extraction}} E^2}$
Percentage Maximum Post-rise Error	$PMPE$	$\frac{T_{max}-T_{set}}{W_{settled}}$ where $W_{settled}$ is the half-width of the settled band, 3°C.

Table 5.3: Values corresponding to the high, center-point, and low levels of the controller tuning Design of Experiments. The high and low values are $\pm 30\%$ of the center-point values.

Variable	High Value (+1)	Center-point Value (0)	Low Value (-1)
$K_{P,o}$	3.9	3	2.1
$K_{V,o}$	26	20	14
$K_{P,f}$	6.5	5	3.5
$K_{V,f}$	5.85	4.5	3.15

Table 5.4: Design of Experiments data. “1” indicates the high level, “-1”, “0”, and “1” indicate the low, center-point, and high level gains, respectively.

	Controller Gain Levels				Performance Metrics			
Weld	$K_{P,o}$	$K_{P,f}$	$K_{V,o}$	$K_{V,f}$	$t_{settled}$	t_{rise}	PMPE	RMSE
1	-1	-1	-1	1	16.55s	9.47s	430%	0.694°C
2	-1	1	1	-1	24.31s	24.30s	20%	0.882°C
3	1	1	-1	1	29.61s	29.60s	21%	0.858°C
4	-1	1	-1	-1	30.60s	30.60s	15%	0.799°C
5	1	1	1	1	15.46s	15.50s	19%	1.127°C
6	1	-1	1	1	24.25s	8.88s	707%	0.909°C
7	1	-1	1	-1	23.85s	8.86s	905%	0.893°C
8	1	1	-1	-1	21.66s	21.70s	23%	0.93°C
9	-1	1	1	1	24.94s	24.90s	26%	0.938°C
10	0	0	0	0	11.73s	11.70s	64%	0.971°C
11	-1	-1	1	-1	22.19s	9.28s	674%	1.016°C
12	-1	-1	1	1	12.35s	8.56s	724%	0.814°C
13	1	1	1	-1	13.53s	13.50s	22%	0.987°C
14	-1	1	-1	1	32.32s	32.30s	20%	0.829°C
15	0	0	0	0	12.10s	12.10s	43%	0.948°C
16	1	-1	-1	1	16.33s	9.13s	631%	0.785°C
17	-1	-1	-1	-1	14.83s	8.64s	665%	0.766°C
18	1	-1	-1	-1	27.41s	8.98s	835%	0.741°C

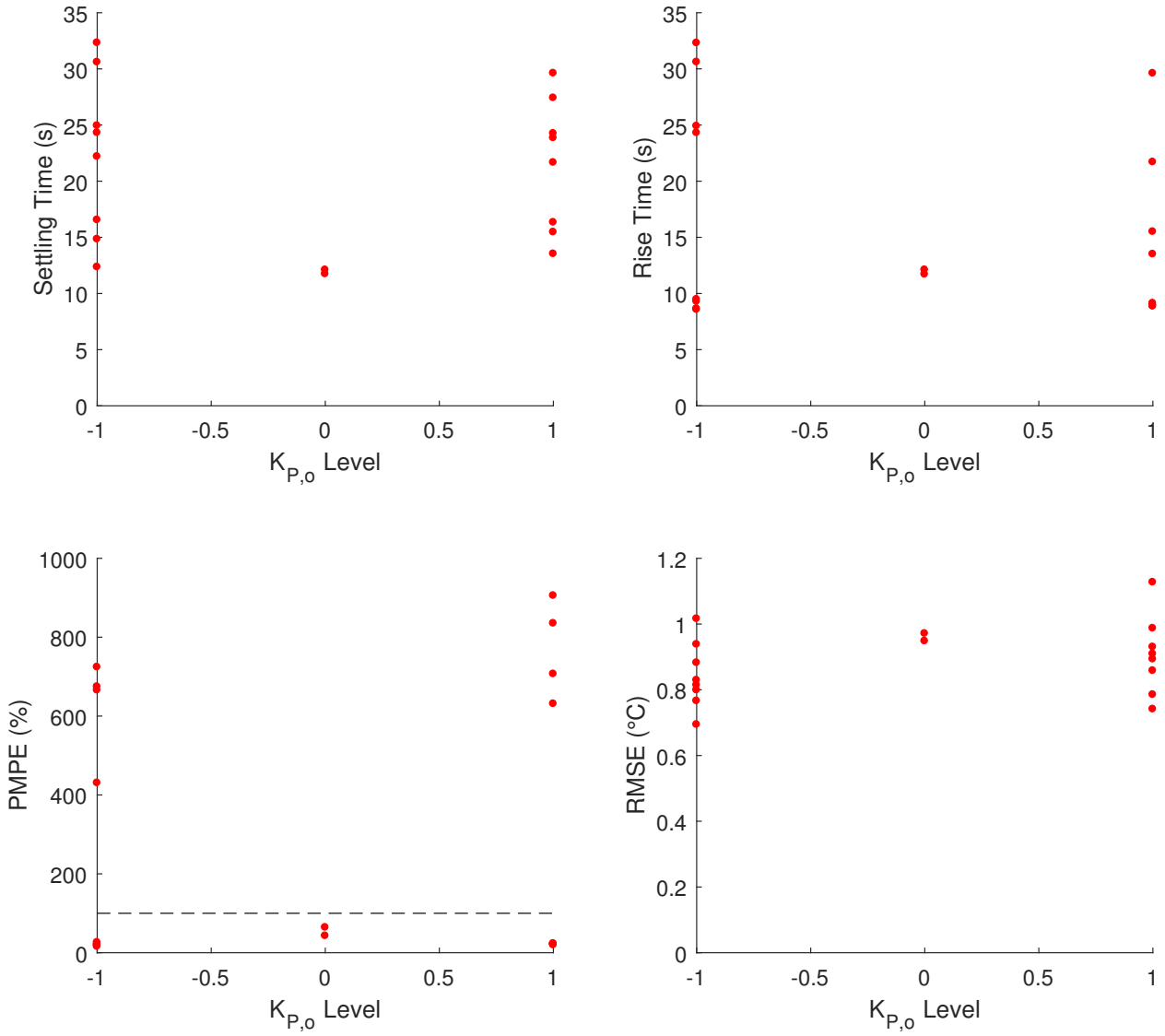

Figure 5.1: Data of the effect of $K_{P,o}$ on the four performance metrics. The dashed line across the PMPE plot indicates 100%.

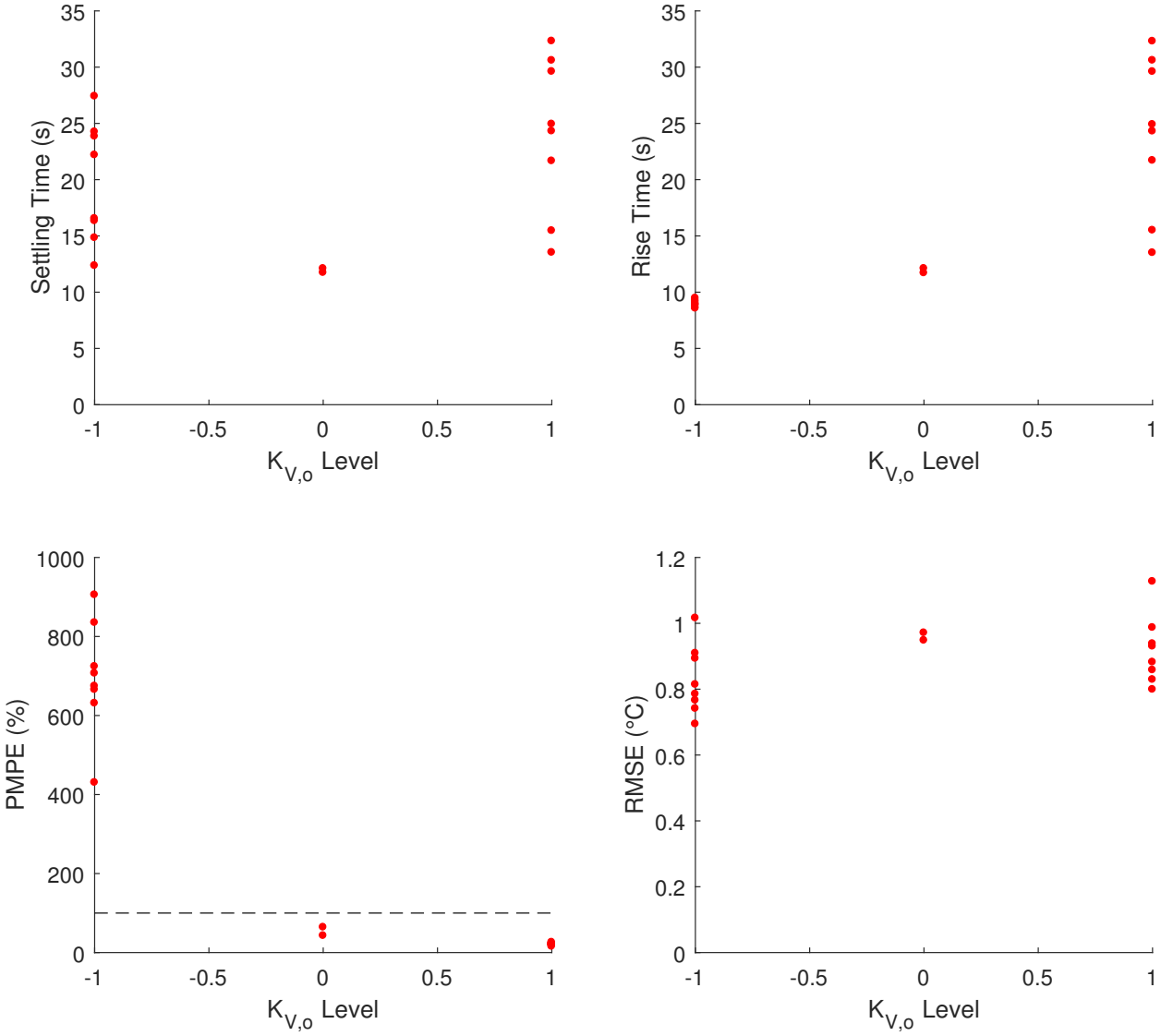

Figure 5.2: Data of the effect of $K_{V,o}$ on the four performance metrics. The dashed line across the PMPE plot indicates 100%.

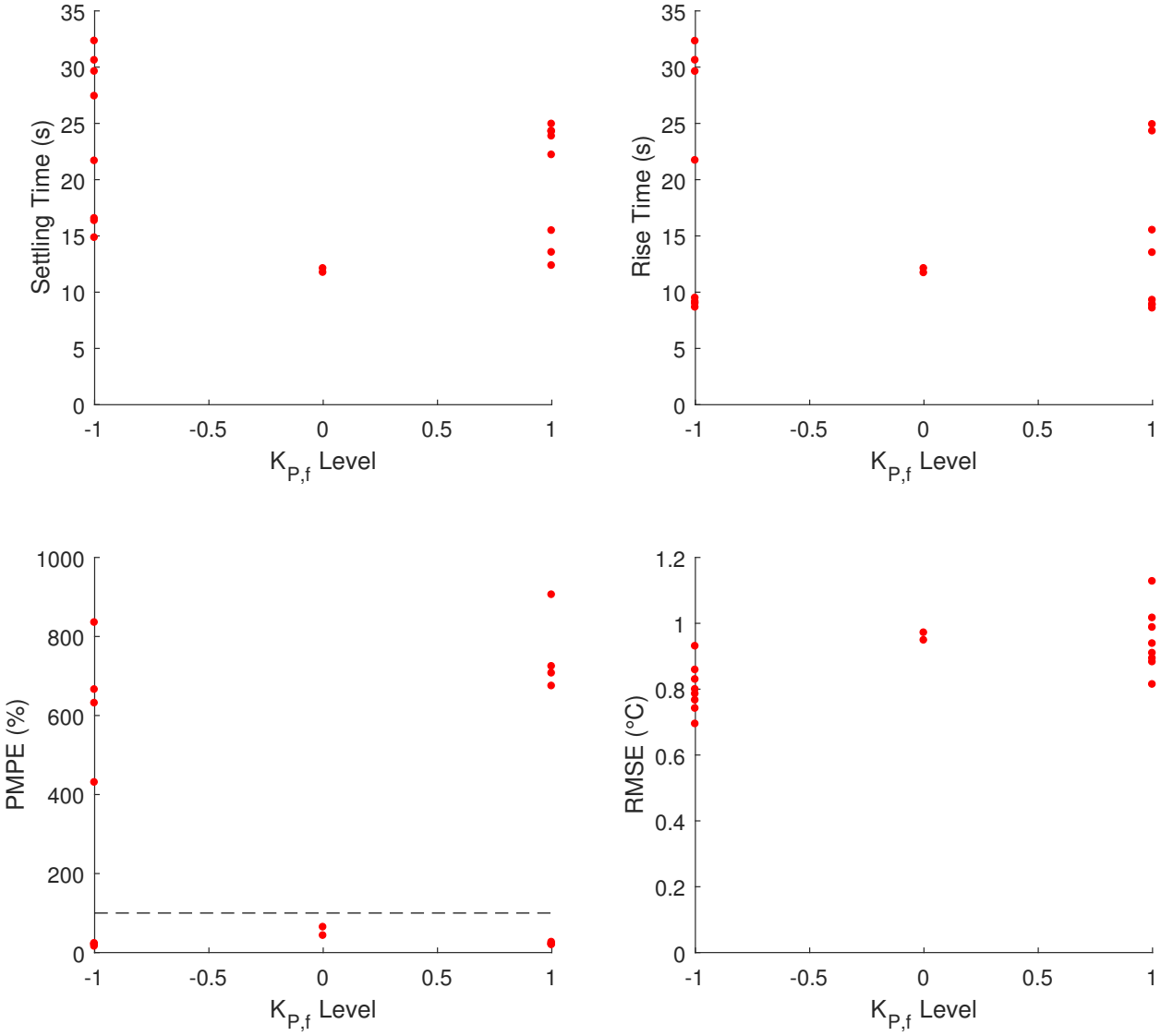

Figure 5.3: Data of the effect of $K_{P,f}$ on the four performance metrics. The dashed line across the PMPE plot indicates 100%.

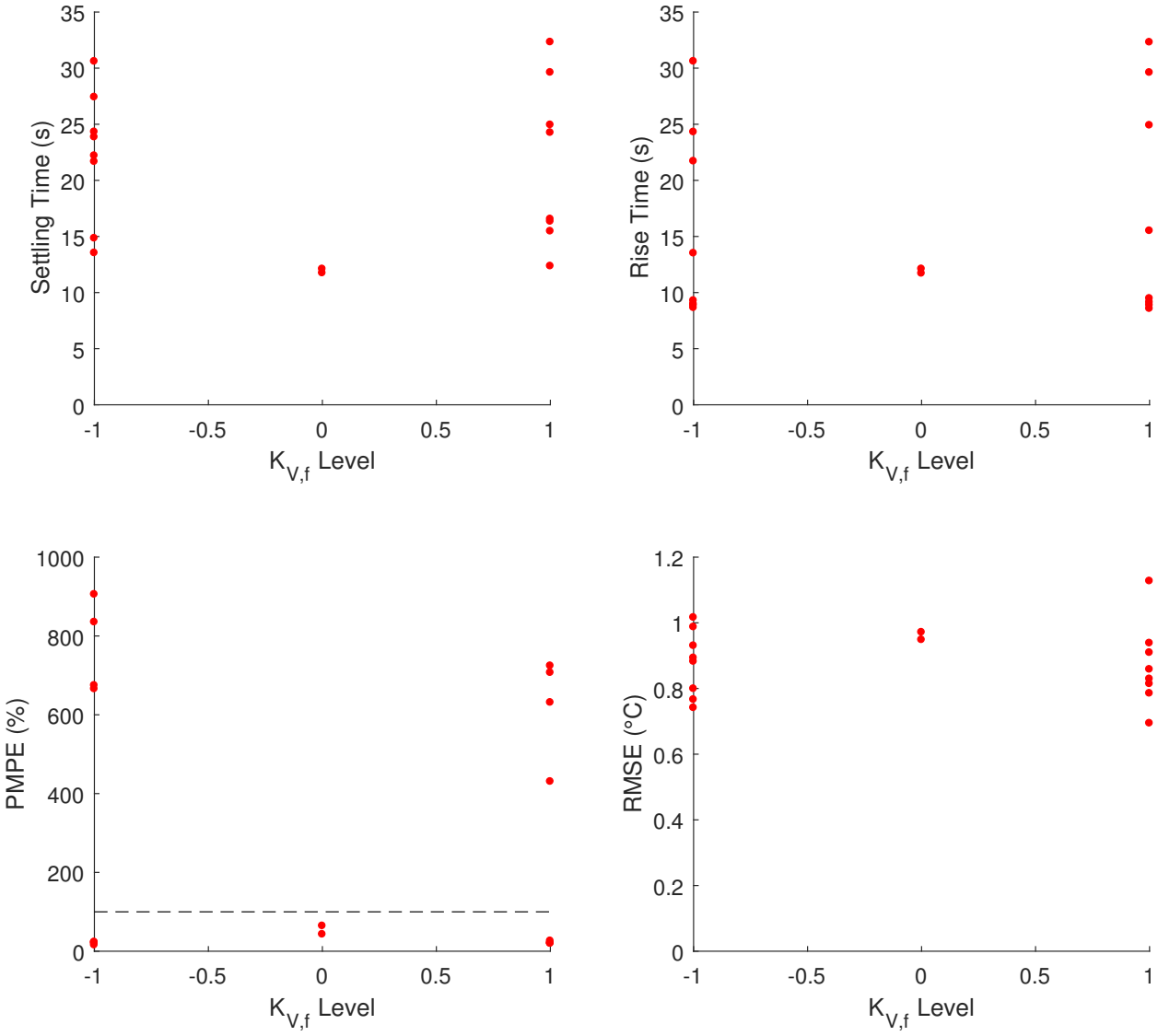

Figure 5.4: Data of the effect of $K_{V,f}$ on the four performance metrics. The dashed line across the PMPE plot indicates 100%.

5.2 Regression Model Construction

Multiple regression models for each of the controller performance metrics can be constructed from the 2^4 DOE data. Multiple regression modeling is a statistical modeling technique used to predict the mean response of a variable as a function of one or more explanatory variables [20]. Given the 2^4 full factorial design performed in this research, the set of possible explanatory variables is limited to the primary effects and the interaction terms. Quadratic or higher order terms must be excluded to avoid over-fitting of the data.

Multiple regression models take the form shown in Equation (5.1), where X_n represents an explanatory variable selected from the full set of possible explanatory variables. The response, Y, is the predicted mean outcome.

$$Y = \beta_0 + \beta_1 * X_1 + \beta_2 * X_2 + ... + \beta_n * X_n \tag{5.1}$$

Models which include interaction terms are required to include the related primary effects. For example, if the interaction $K_{P,o} * K_{V,o}$ is included in a given regression model, the primary effects $K_{P,o}$ and $K_{V,o}$ are required to also be included in the model. Given the four primary effects and their interactions, there exist 112 possible multiple regression models.

In addition to predicting the mean of a system response, multiple regression models estimate the variance of a system about the mean. This estimated range is the individual prediction interval. A 95% confidence individual prediction interval is an estimate of where 95% of future values will fall. Ideally, future values will be normally distributed across the individual prediction interval. If a large percentage of future values fall outside or are heavily skewed across the prediction interval, this may be an indication of an inadequate model [20].

Due to the curvature present in the design space (discussed in several of the model assessments in Section 5.4), the 2 center-point welds from the 2^4 DOE (welds 10 and 15) are excluded in creation of the linear-terms regression models.

5.3 Regression Model Selection and Assessment

To select a linear-terms regression model, all 112 possible models are constructed and compared. The Bayesian Information Criterion (*BIC*) is utilized in this research to compare models. The *BIC* evaluates each model based on how well it fits the data, but penalizes models which rely on large numbers of explanatory variables [20]. The *BIC* is calculated as shown in Equation (5.2), where n is the number of data points, p is the number of parameters estimated by the model, and $\hat{\sigma}^2$ is the estimate of σ^2 from the tentative model.

$$BIC = n * ln(\hat{\sigma}^2) + p * ln(n) \tag{5.2}$$

The model with the lowest *BIC* is selected as the "best" model. Although the *BIC* is a comparative metric, the *BIC* is reported for completeness.

The R^2 statistic, or coefficient of determination, is a statistic which describes the fit of a model to the data on a scale of 0 to 1. Higher R^2 values indicate a better fit to the data [20]. The R^2 statistic is reported to assess the overall fit of each multiple regression model to the data from which the model is contructed.

Aside from the measured DOE data, 19 additional welds are utilized to validate the regression model predictions. The 2 center-point welds from the 2^4 DOE (which were excluded from the linear-terms model construction), the 9 demonstration center-point welds presented in Chapter 4, and 8 additional model validation welds are used to test the predictive accuracy of the regression models. The measured performance metrics of these 19 welds are shown in Table 5.5. In addition, the 16 welds from the 2^4 DOE is included to further validate the models.

In Table 5.5, there is an additional column labeled "Non-vertex Factors". The number of non-vertex factors is a count of the number of factors which are not evaluated at either -1 or 1. This metric seeks to describe where the weld exists in the design space, especially in comparison to the 16 DOE welds. By design, the 16 DOE welds are at the vertices of the hypercube design space. The 19 validation welds in Table 5.5 do not share this characteristic. If curvature is present in the design space, it is presumed that model predictions will deteriorate as the number of non-vertex factors increases because of the increased distance from the data on which the model is based.

The measured values and residuals of the prediction for the 19 validation welds and the 16 DOE welds are plotted in several ways to assess the regression models. The model residuals are calculated as shown in Equation (5.3).

$$Residual = Measured - Predicted \tag{5.3}$$

The first graphical assessment of each model is of the model residuals plotted against the model predictions. This allows for assessment of the overall fit of the model to the data. If the data is not normally distributed about the center-line, it is an indication of a poor model fit.

Second, the measured values are plotted against the predicted values along with the prediction interval to assess the predictive capability of each model.

Table 5.5: Model validation Data. The Source column the data set to which the weld pertains. The two DOE centerpoint welds excluded from the original DOE data set (EX), the 9 demonstration centerpoint welds (CP), and the eight validation welds (VA) comprise the validation data set.

	Controller Gain Levels					Performance Metrics			
Source	$K_{P,o}$	$K_{V,o}$	$K_{P,f}$	$K_{V,f}$	Non-vertex Factors	$t_{settled}$	t_{rise}	PMPE	RMSE
EX	0	0	0	0	4	11.73	11.70	64.0	0.97
EX	0	0	0	0	4	12.10	12.10	42.7	0.95
CP	0	0	0	0	4	11.73	11.70	63.8	0.97
CP	0	0	0	0	4	12.10	12.10	42.6	0.95
CP	0	0	0	0	4	11.12	11.10	62.1	0.87
CP	0	0	0	0	4	11.02	11.00	62.7	0.79
CP	0	0	0	0	4	10.24	10.20	85.0	1.07
CP	0	0	0	0	4	10.12	10.10	68.8	0.84
CP	0	0	0	0	4	10.51	10.50	43.4	0.87
CP	0	0	0	0	4	10.12	10.10	99.6	1.06
CP	0	0	0	0	4	15.16	10.00	100.7	0.86
VA	1	0.09	1	1	1	15.37	9.95	267.3	0.85
VA	1	0.09	1	1	1	15.88	9.85	305.8	1.01
VA	1	0.14	1	-1	1	15.88	9.75	441.5	1.17
VA	1	0.14	1	-1	1	16.01	9.67	444.9	1.19
VA	0.12	0.59	1	-1	2	16.09	11.58	168.9	0.62
VA	0.12	0.59	1	-1	2	21.05	11.04	219.6	1.05
VA	-1	-1	-1	0	1	20.12	9.30	642.2	0.72
VA	-1	-1	-1	0	1	18.97	9.40	593.6	0.67

Third, the residuals normalized by the half-width of the 95% confidence individual prediction interval are plotted against the number of non-vertex factors present in each validation weld. This assessment plot allows for curvature within the design space to be observed. Any dependence on the number of non-vertex factors in a model's predictive accuracy indicates a poor fit.

5.4 Performance Metrics Regression Models

The following subsections present the multiple regression models selected for predicting the 4 temperature controller performance metrics. The presentation and assessment of each regression model is as follows:

- **Tabulated linear-terms model constants**: All models take the form shown in Equation (5.1). The full set of possible explanatory variables is shown. However,only the explanatory variables included in the lowest-BIC regression model have model constants and associated p-values.
- **Model fit assessment statistics**
- **Model fit assessment plots**
- **Linear-terms model discussion**: Discussion of the linear-terms regression models, including assessment of whether higher-order models may be necessary for accurate metric predictions.
- **Exploration of higher-order regression models**: Given poor model predictions from the lowest-BIC linear-terms regression model, regression models which include higher-order terms may be necessary to adequately characterize the design space. If this is the case, models including quadratic terms are explored and assessed with the same methodology used for the linear-terms regression model. This includes the tabulated model constants, the model fit assessment statistics, and the 3 model fit assessment plots.
- **Discussion of quadratic-inclusive settling time model**: This section is included only if a quadratic-terms regression model is explored for the given metric. The predictive accuracy improvements over the linear-terms model is discussed in terms of how tuning of the controller may be enhanced.

5.4.1 Settling Time Model

Table 5.6: Multiple regression model constants for predicting the mean settling time.

Model Constant	Associated Explanatory Variable	Estimate	P-value
β_0	Intercept	21.89	$<$0.0001
β_1	$K_{P,o}$	-0.37	0.6726
β_2	$K_{V,o}$	2.17	0.0347
β_3	$K_{P,f}$	-1.78	0.0706
β_4	$K_{V,f}$	-0.41	0.6425
β_5	$K_{P,o} * K_{V,o}$	-3.61	0.0028
β_6	$K_{P,o} * K_{P,f}$	—	—
β_7	$K_{P,o} * K_{V,f}$	—	—
β_8	$K_{V,o} * K_{P,f}$	-2.72	0.0129
β_9	$K_{V,o} * K_{V,f}$	1.94	0.0524
β_{10}	$K_{P,f} * K_{V,f}$	—	—

Table 5.7: Model assessment statistics for the settling time model.

BIC	R^2
98.52	0.85

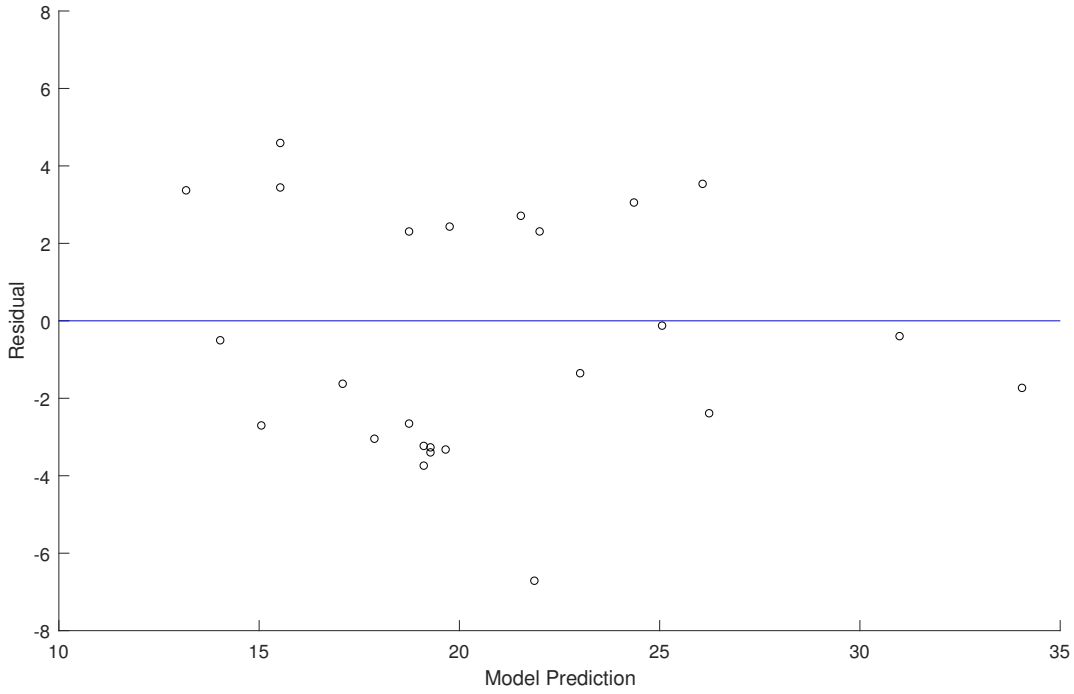

Figure 5.5: Linear-terms settling time model assessment: Residuals vs. predicted values.

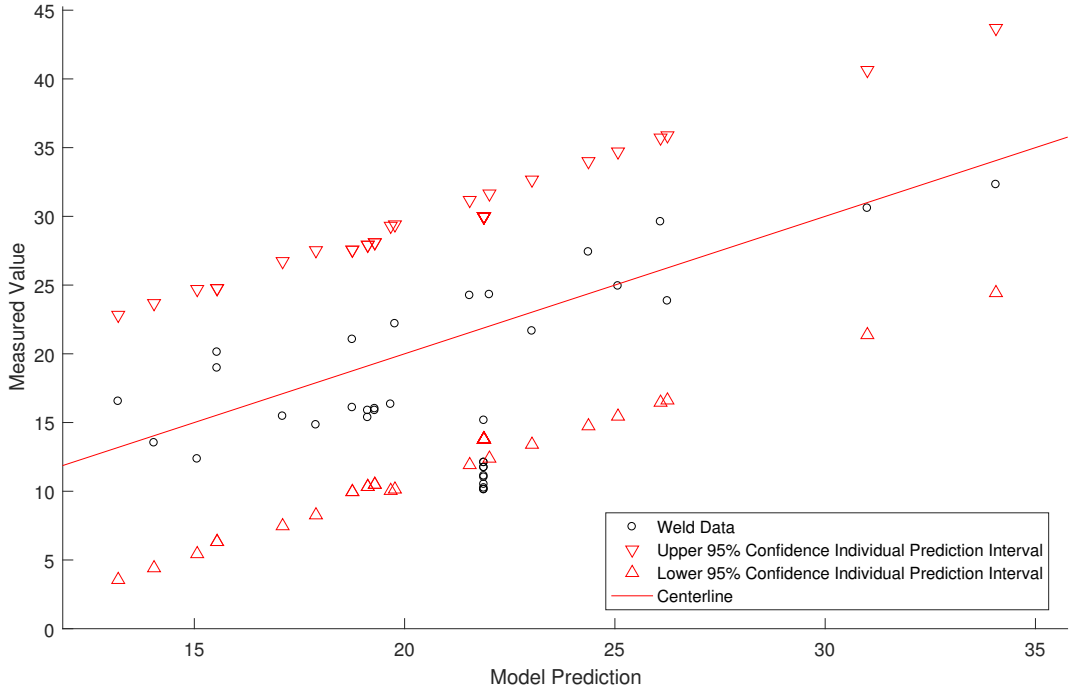

Figure 5.6: Linear-terms settling time model assessment: Measured values vs. predicted values. The center-line bisects the upper and lower prediction interval bounds.

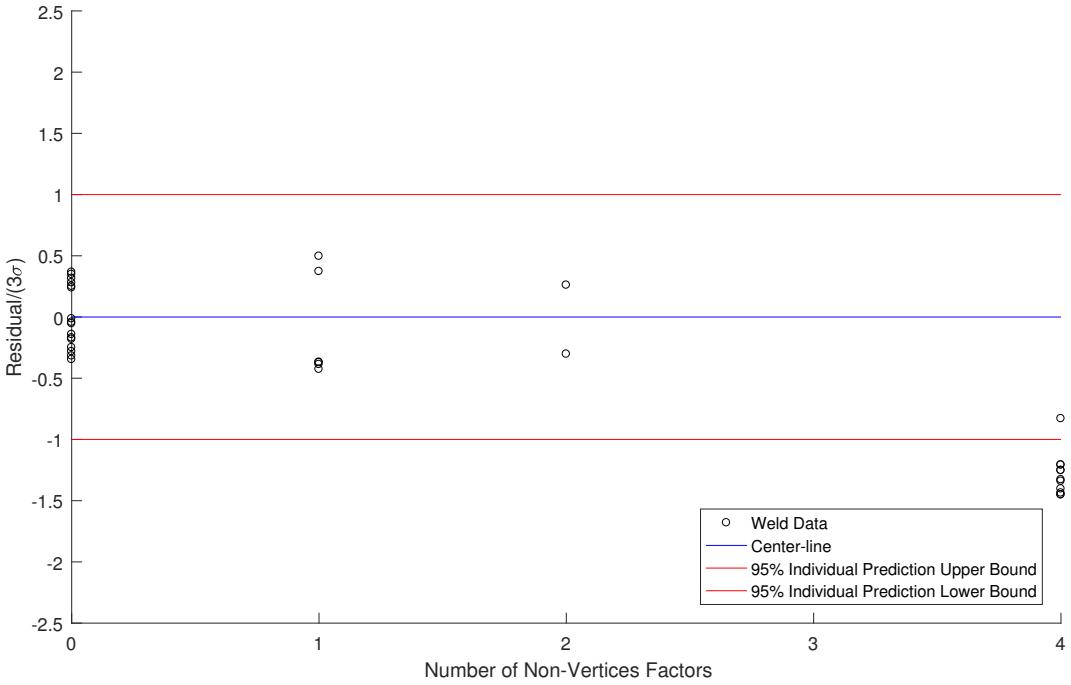

Figure 5.7: Linear-terms settling time model assessment: Residuals divided by the 95% confidence interval half-width vs. number of non-vertex factors.

Discussion of Linear-Terms Settling Time Model

Assessment of the linear-terms settling time regression model indicates deficiencies in its predictive accuracy which would inhibit use of the model for guiding tuning of the controller for desired settling times. The R^2 value of 0.85 in Table 5.7 seems to indicate that the model is well-fit to the model data and Figure 5.6 shows that the majority of the measured settling times are within the 95% individual prediction interval. Both of these assessment tools suggest that this regression model may be adequate.

These positive indications are not supported by the other model assessment plots. The model residuals shown in Figure 5.5 are not normally distributed. In addition, the model predictions appear to rapidly deteriorate as the number of non-vertex factors increases, as shown in Figure 5.7. The model accuracy is acceptable at and near the design space captured by the DOE data, but the decreased accuracy at the center-point of the design space (the welds with 4 non-vertex factors) suggests that there is curvature within the design space which is not adequately captured by the linear-terms settling time model.

The model assessment indicates that additional explanatory variables may be needed for accurate predictions of the settling time of a weld. A linear-terms settling time model may provide preliminary guidance for tuning the temperature controller in some scenarios, but higher-order terms are necessary to allow for more complete guidance of the controller tuning for operator-specified weld settling times.

Exploration of Quadratic-Inclusive Settling Time Model

In order to fit a regression model which describes the curvature of the design space, quadratic terms are introduced. A settling time regression model which allows for quadratic explanatory variables is likely to over-fit data from a 2^4 full-factorial DOE. Therefore, additional data is required to fit regression models which include quadratic terms.

The data collected in the 2^4 DOE is located at the vertices of the hyper-cube design space bounded by the upper and lower levels of each factor. Additional data are needed along the edges or faces of the hyper-cube to avoid over-fitting. For construction of the quadratic-inclusive regression models (for predicting settling time, as well as all other performance metrics), the 2 previously excluded center-point DOE welds and the 8 validation welds (as indicated in Table 5.5) are included in the construction of the regression model. The 8 validations welds provide data along the edges and faces the hypercube space. The 9 demonstration center-point welds are excluded as the high number of replications would bias the regression model.

While a more complete data set is preferable and could be obtained in future research, this exploration is utilized to indicate whether such an experimental design could yield a more accurate characterization of the design space to guide tuning of the controller.

The regression model presented in Table 5.8 is the lowest BIC model of all 1336 possible settling time regressions models which allow for inclusion of quadratic explanatory variables. The associated BIC and R^2 model statistics are shown in Table 5.9. Figures 5.8, 5.9, and 5.10 allow for a comparative assessment to the linear-terms settling time model. These plots include all the validation weld data, including the 9 demonstration welds.

Table 5.8: Multiple regression model constants for predicting the mean settling time, allowing for inclusion of quadratic terms.

Model Constant	Associated Explanatory Variable	Estimate	P-value
β_0	Intercept	11.66652312	<0.0001
β_1	$K_{P,o}$	-0.418219107	0.5444
β_2	$K_{V,o}$	1.312939441	0.0728
β_3	$K_{P,f}$	1.668938258	0.1936
β_4	$K_{V,f}$	0.0177696741	0.9803
β_5	$K_{P,o}^2$	—	—
β_6	$K_{P,o} * K_{V,o}$	-3.61538115	<0.0001
β_7	$K_{P,o} * K_{P,f}$	—	—
β_8	$K_{P,o} * K_{V,f}$	—	—
β_9	$K_{V,o}^2$	3.051032559	0.1059
β_{10}	$K_{V,o} * K_{P,f}$	-2.627757373	0.0014
β_{11}	$K_{V,o} * K_{V,f}$	1.843374201	0.0152
β_{12}	$K_{P,f}^2$	10.89088328	0.0053
β_{13}	$K_{P,f} * K_{V,f}$	—	—
β_{14}	$K_{V,f}^2$	-3.91110292	0.1463

Table 5.9: Model assessment statistics for the settling time model shown in Table 5.9.

BIC	R^2
150.83	0.87

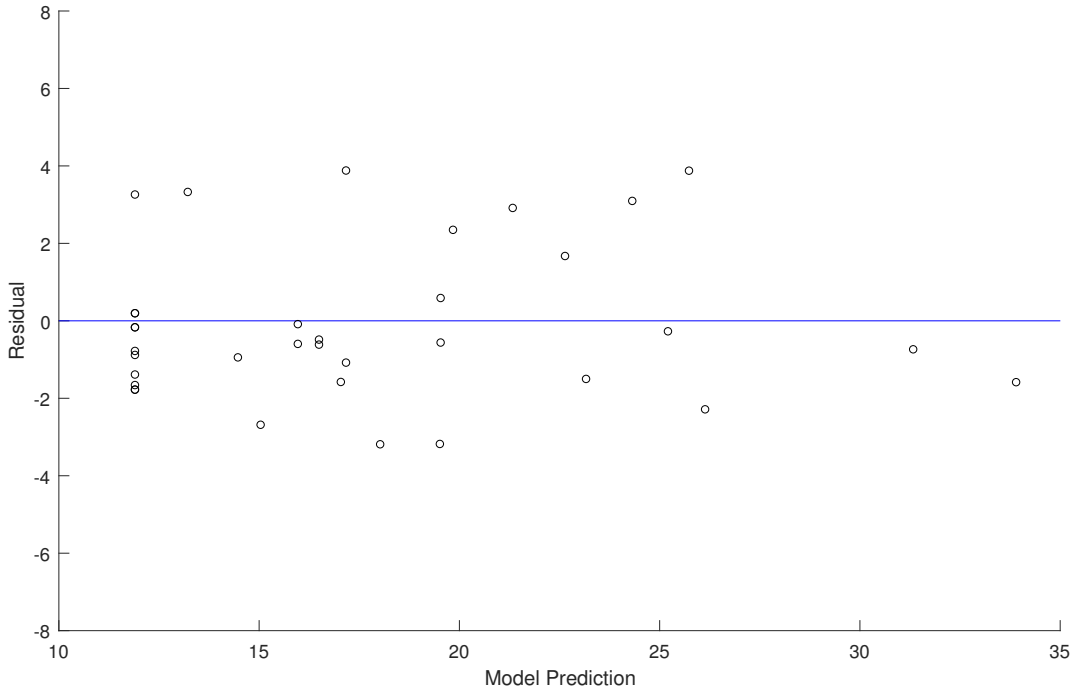

Figure 5.8: Quadratic-terms settling time model assessment: Residuals vs. predicted values.

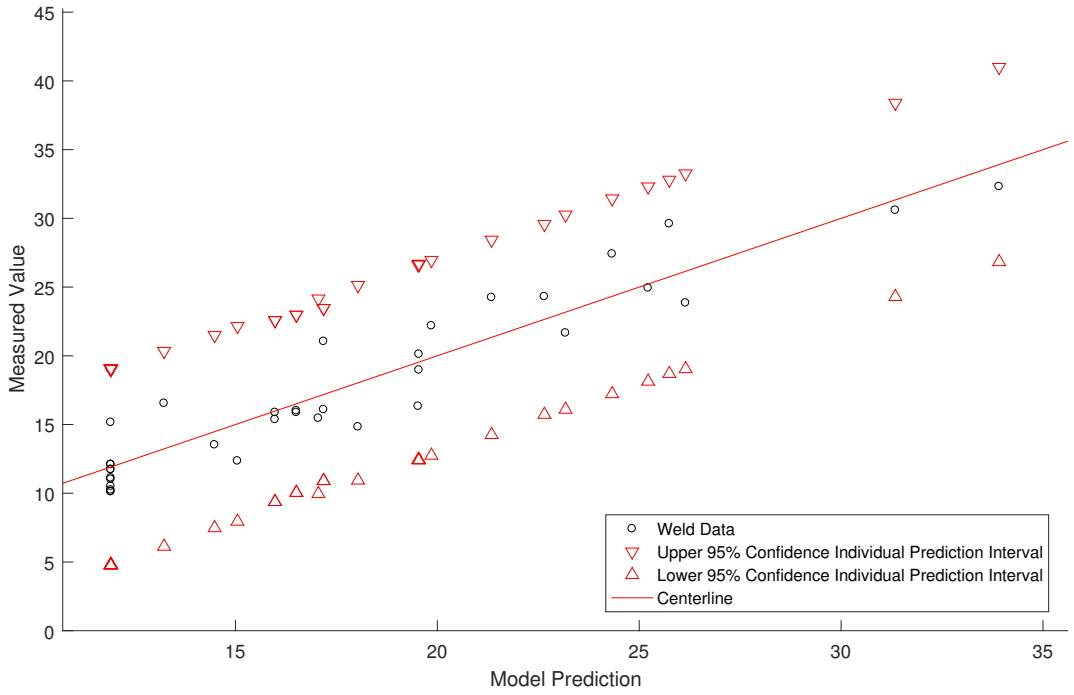

Figure 5.9: Quadratic-terms settling time model assessment: Measured values vs. predicted values. The center-line bisects the upper and lower prediction interval bounds.

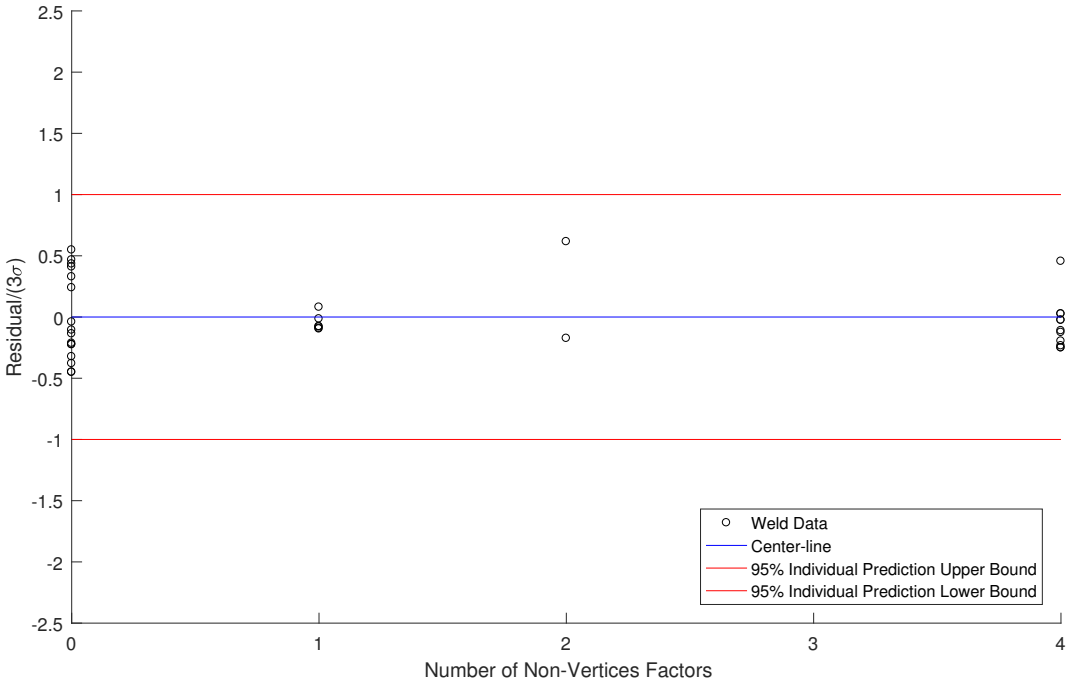

Figure 5.10: Quadratic-terms settling time model assessment: Residuals divided by the 95% confidence interval half-width vs. number of non-vertex factors.

Discussion of Quadratic-Inclusive Settling Time Model

The distribution of the model residuals in Figure 5.8 is an improvement over the model residuals shown in Figure 5.5. The elimination of model outliers is apparent in Figure 5.9, as all data points lie well within the 95% confidence individual prediction interval. Figure 5.10 confirms this improvement, as well as showing that the quadratic-terms regression model reduces any obvious lack-of-fit due to higher-order curvature in the design space.

Allowing quadratic terms to be included in the settling time model improves the settling time model accuracy. Given a more complete set of data from which to construct the regression model, it is clear that a quadratic-inclusive settling time model would more completely characterize the controller tuning design space.

The most noticeable difference between the linear-terms model and quadratic-terms model is that 3 of the 4 possible quadratic model terms are now included in the regression model. Additionally, $K_{P,o}^2$ is estimated to have the single greatest effect on settling time of all the explanatory variables. The p-value associated with this variable indicates a strong statistical significance. The

model indicates that $K^2_{V,f}$ and $K^2_{V,o}$ also have large effects. Given a more complete data set from which to construct the model, insights such as this would provide accurate and helpful tuning guidance of the temperature controller for specified weld settling times.

5.4.2 Rise Time Model

Table 5.10: Multiple regression model constants for predicting the mean rise time.

Model Constant	Associated Explanatory Variable	Estimate	P-value
β_0	Intercept	16.51	<0.0001
β_1	$K_{P,o}$	-2.00	0.0043
β_2	$K_{V,o}$	7.54	<0.0001
β_3	$K_{P,f}$	-2.29	0.0024
β_4	$K_{V,f}$	0.78	0.1119
β_5	$K_{P,o} * K_{V,o}$	-1.99	0.0045
β_6	$K_{P,o} * K_{P,f}$	-0.55	0.2363
β_7	$K_{P,o} * K_{V,f}$	0.47	0.2952
β_8	$K_{V,o} * K_{P,f}$	-2.21	0.0028
β_9	$K_{V,o} * K_{V,f}$	0.75	0.1247
β_{10}	$K_{P,f} * K_{V,f}$	-0.55	0.2342

Table 5.11: Model assessment statistics for the rise time model.

BIC	R^2
75.55	0.99

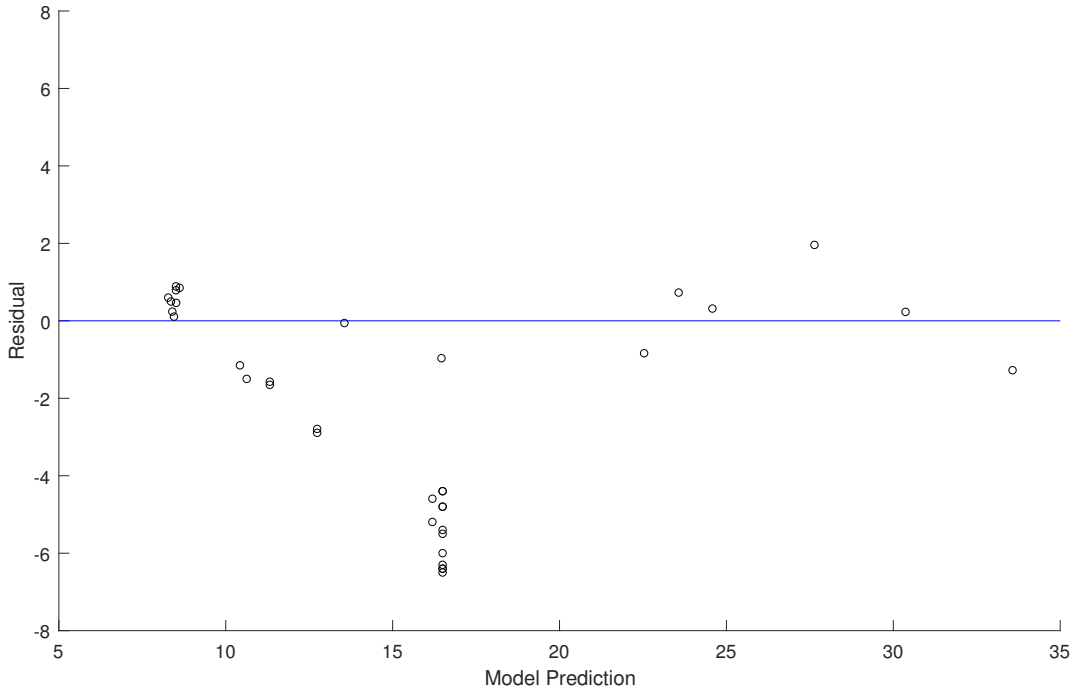

Figure 5.11: Linear-terms rise time model assessment: Residuals vs. predicted values.

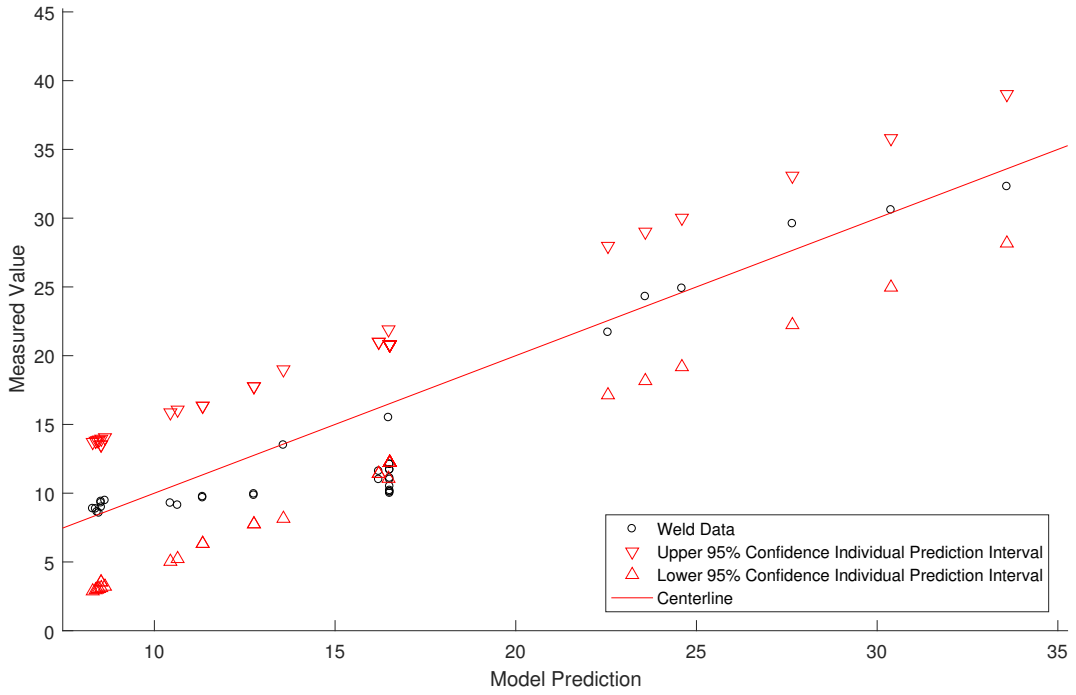

Figure 5.12: Linear-terms rise time model assessment: Measured values vs. predicted values. The center-line bisects the upper and lower prediction interval bounds.

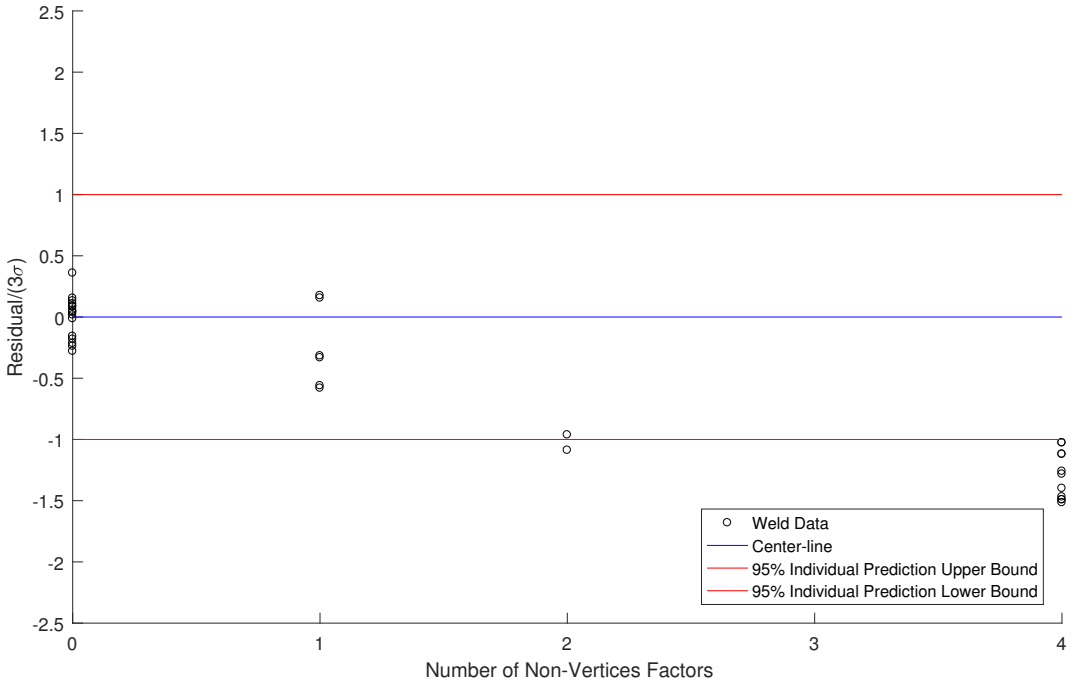

Figure 5.13: Linear-terms rise time model assessment: Residuals divided by the 95% confidence interval half-width vs. number of non-vertex factors.

Discussion of Linear-Terms Rise Time Model

The high R^2 value of 0.99 seems to indicate a very good model fit. However, the results shown in Figures 5.11, 5.12, and 5.13 suggest otherwise. The residuals of the linear-terms rise time model shown in Figure 5.11 are not evenly spread about zero. The skewed spread may indicate that the rise time model tends to over-predict. Figure 5.12 shows that the majority of the measured values lie within the prediction interval. However, the large cluster of points which lie on and near the lower prediction interval suggest inaccuracy in the model prediction. Future values should ideally have normally distributed across the prediction interval, but the cluster of values suggests that the model will not capture this trend. Figure 5.13 shows that the linear-terms rise time model predictions decreases in accuracy as the number of of non-vertex factors increases. As with the linear-terms settling time model, this deterioration is presumed to be due to curvature in the design space which cannot be described by a linear-terms model.

The assessments of the linear-terms rise time regression model suggest that a higher order model will likely improve the model accuracy. Exploration of regression models including

quadratic terms is shown in the following subsection to determine if a more extensive experiment could more accurately characterize the design space and guide tuning of the controller for specified rise time performance.

Exploration of Quadratic-Inclusive Rise Time Model

The procedure for constructing a rise time regression model which allows for quadratic explanatory variables is identical to the method used for constructing the quadratic-terms settling time model in Section 5.4.1. In addition, the same data set is used for construction of the rise time model, as fitting quadratic terms to data from a 2^4 full-factorial DOE will likely result in over-fitting and additional data are therefore required.

A more complete experimental data set would be preferable and could be obtained in future research. As with the quadratic-terms settling time model, this exploratory step is used as an indicator to whether such an experimental design could yield a more accurate characterization of the design space to guide tuning of the controller.

The regression model presented in Table 5.12 is the lowest BIC model of all 1336 possible rise time regression models which allow for inclusion of quadratic explanatory variables. The associated BIC and R^2 model statistics are shown in Table 5.13. Figures 5.14, 5.15, and 5.16 include plots which allow for a comparison to the linear-terms rise time model assessment. These plots include all the validation weld data, including the 9 demonstration welds.

Table 5.12: Multiple regression model constants for predicting the mean rise time, allowing for inclusion of quadratic terms.

Model Constant	Associated Explanatory Variable	Estimate	P-value
β_0	Intercept	11.40949106	<0.0001
β_1	$K_{P,o}$	-1.633110016	<0.0001
β_2	$K_{V,o}$	6.832513592	<0.0001
β_3	$K_{P,f}$	-2.387252258	<0.0001
β_4	$K_{V,f}$	0.6673141083	0.0181
β_5	$K_{P,o}^2$	3.074024802	0.0025
β_6	$K_{P,o} * K_{V,o}$	-1.93890996	<0.0001
β_7	$K_{P,o} * K_{P,f}$	-0.521168851	0.0732
β_8	$K_{P,o} * K_{V,f}$	0.376273071	0.168
β_9	$K_{V,o}^2$	2.031922516	0.0191
β_{10}	$K_{V,o} * K_{P,f}$	-2.190210771	<0.0001
β_{11}	$K_{V,o} * K_{V,f}$	0.7713076357	0.0153
β_{12}	$K_{P,f}^2$	—	—
β_{13}	$K_{P,f} * K_{V,f}$	-0.593005216	0.0367
β_{14}	$K_{V,f}^2$	—	—

Table 5.13: Model assessment statistics for the rise time model shown in Table 5.13.

BIC	R^2
107.01	0.99

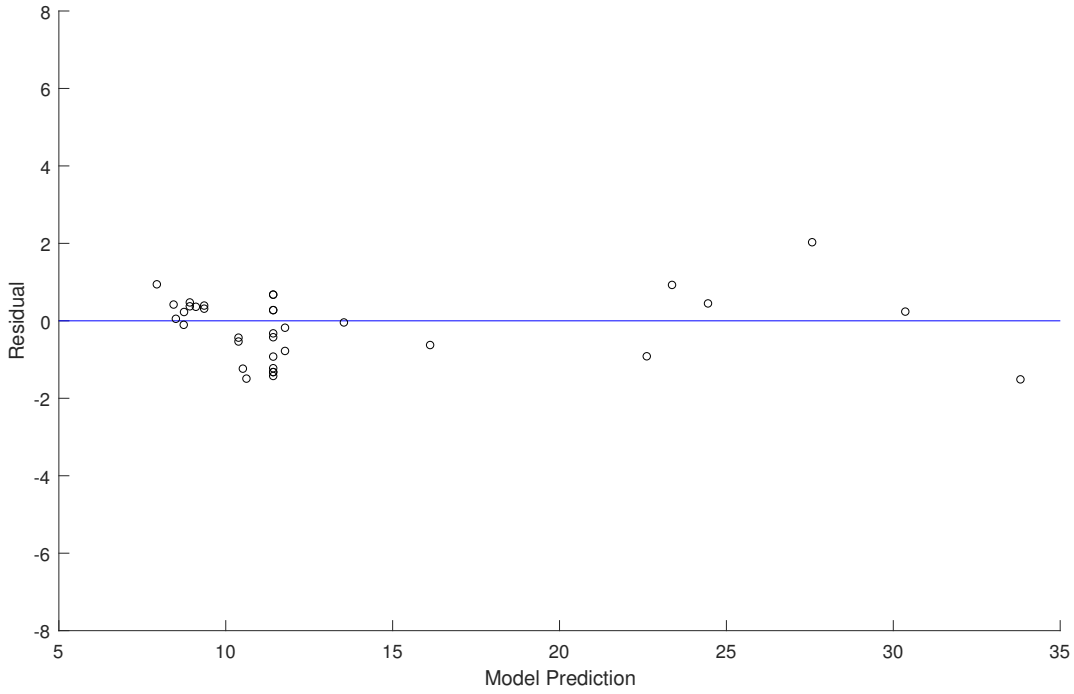

Figure 5.14: Quadratic-terms rise time model assessment: Residuals vs. predicted values.

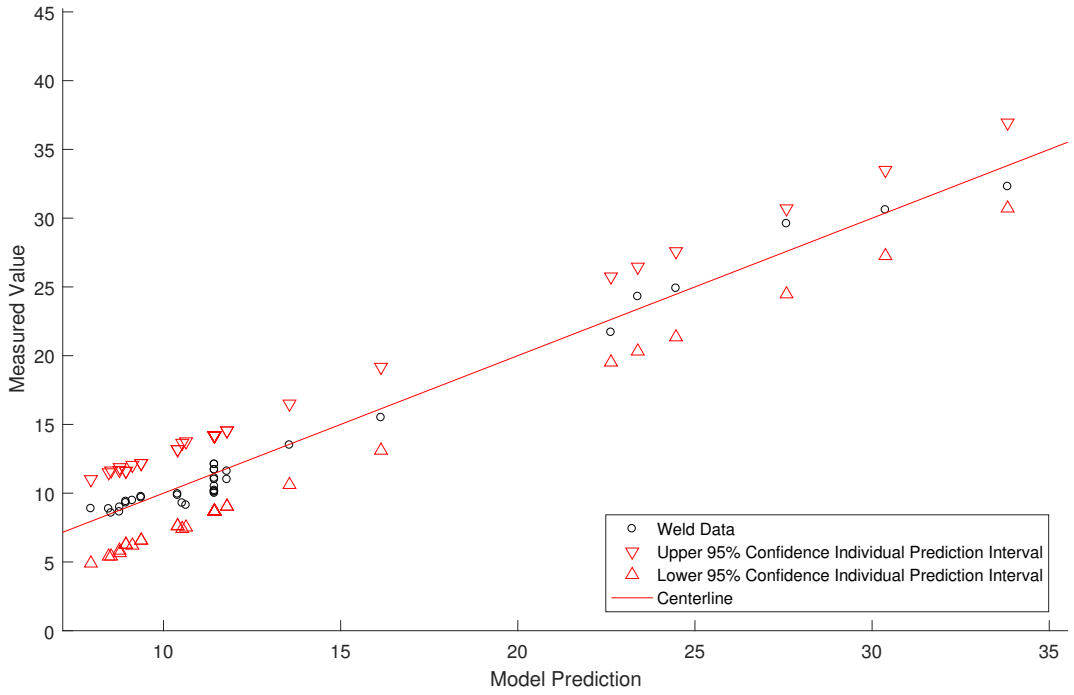

Figure 5.15: Quadratic-terms rise time model assessment: Measured values vs. predicted values. The center-line bisects the upper and lower prediction interval bounds.

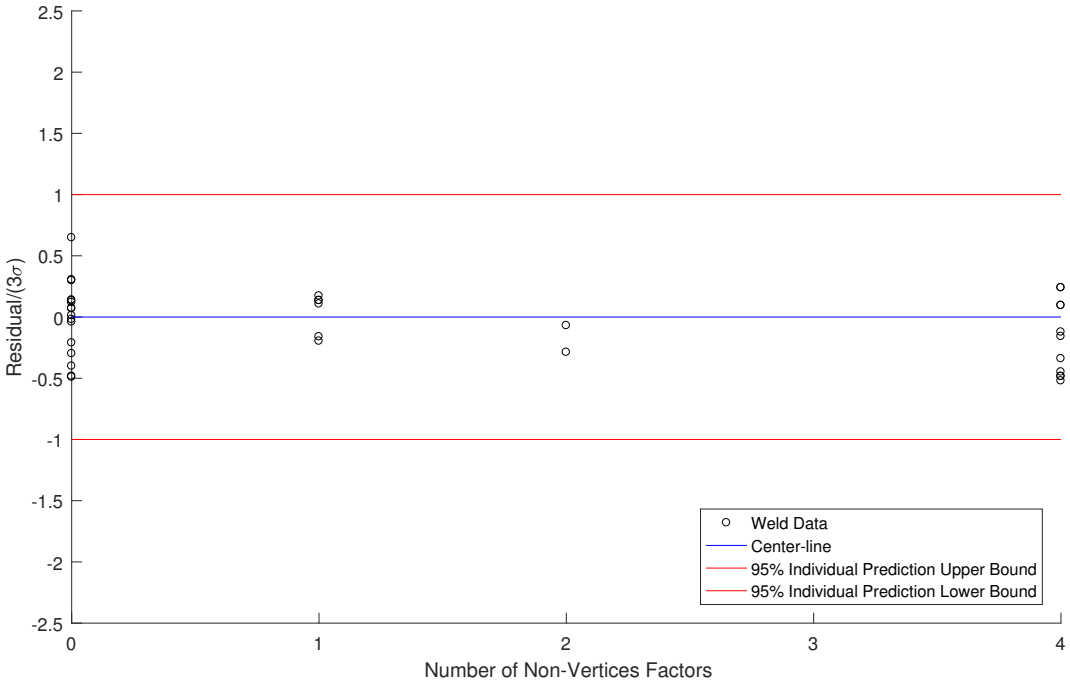

Figure 5.16: Quadratic-terms rise time model assessment: Residuals divided by the 95% confidence interval half-width vs. number of non-vertex factors.

Discussion of Quadratic-Inclusive Rise Time Model

Allowing quadratic terms to be included improves the predictive accuracy of the rise time model. The distribution of the model residuals in Figure 5.14 is a large improvement over the model residuals shown in Figure 5.11. Figure 5.15 shows that no data points lie outside the prediction interval and that there is a relatively even spread of the data across the 95% prediction interval. Figure 5.16 confirms this improvement, as well as showing that the quadratic-terms model reduces the lack-of-fit shown in Figure 5.13.

Given a more complete set of data from which to construct a rise time regression model, this exploration suggests that adding higher order terms would create a significantly superior model. The improved predictive accuracy would enable tuning the temperature controller for a wide range of specified rise times.

All of the linear terms included in the previous rise time model are still included. $K_{P,o}^2$ and $K_{V,o}^2$ are the only terms added to the model. While the linear term $K_{V,o}$ remains the largest effect

with a p-value of <0.0001, the 2 quadratic terms also have large effects and can provide additional insight into how to attain operator-specified rise times.

5.4.3 Percentage Maximum Post-rise Error Model

Table 5.14: Multiple regression model constants for predicting the mean PMPE.

Model Constant	Associated Explanatory Variable	Estimate	P-value
β_0	Intercept	358.67	<0.0001
β_1	$K_{P,o}$	36.80	0.0402
β_2	$K_{V,o}$	-337.83	<0.0001
β_3	$K_{P,f}$	28.58	0.0919
β_4	$K_{V,f}$	-36.42	0.0418
β_5	$K_{P,o} * K_{V,o}$	-36.21	0.0426
β_6	$K_{P,o} * K_{P,f}$	—	—
β_7	$K_{P,o} * K_{V,f}$	—	—
β_8	$K_{V,o} * K_{P,f}$	-27.5	0.1024
β_9	$K_{V,o} * K_{V,f}$	37.08	0.0391
β_{10}	$K_{P,f} * K_{V,f}$	18.17	0.2547

Table 5.15: Model assessment statistics for the PMPE model.

BIC	R^2
190.15	0.99

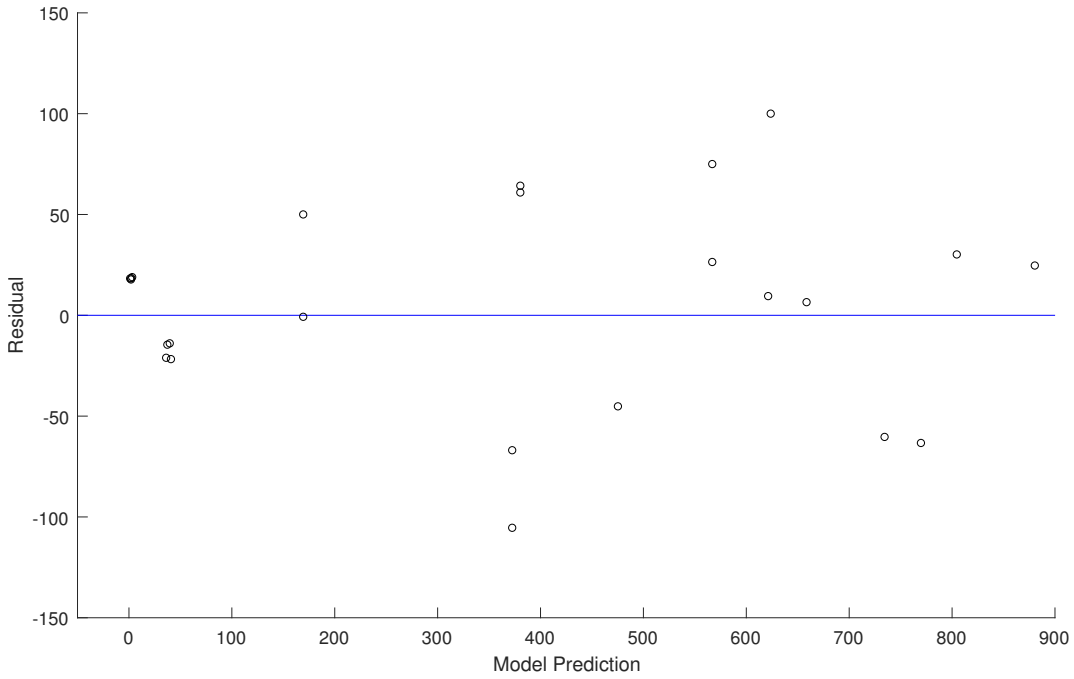

Figure 5.17: Linear-terms PMPE model assessment: Residuals vs. predicted values.

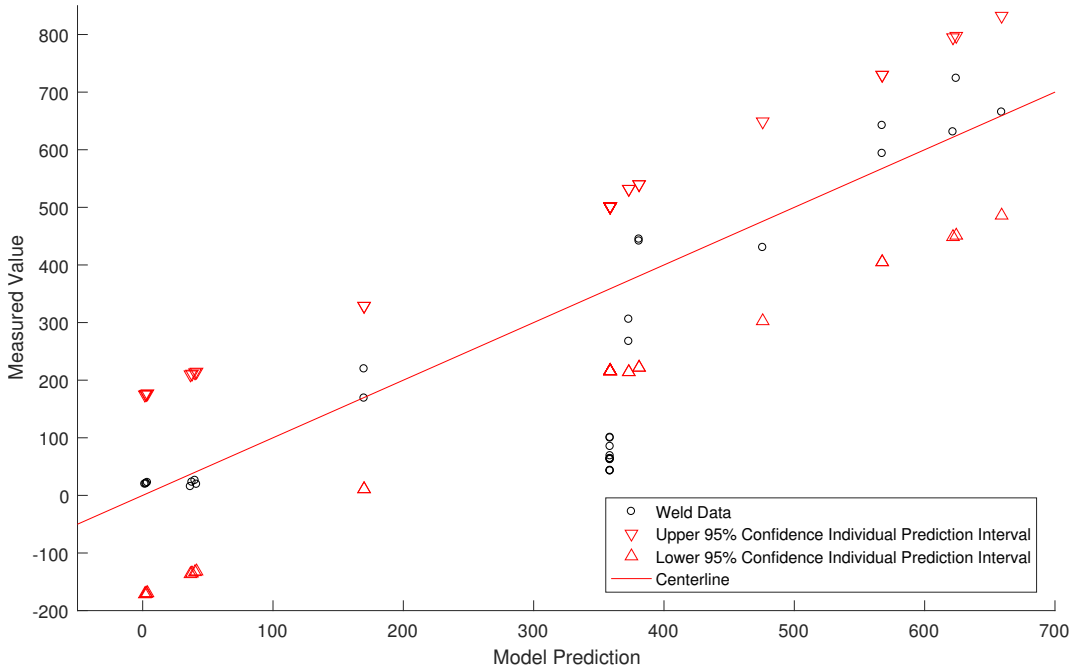

Figure 5.18: Linear-terms PMPE model assessment: Measured values vs. predicted values. The center-line bisects the upper and lower prediction interval bounds.

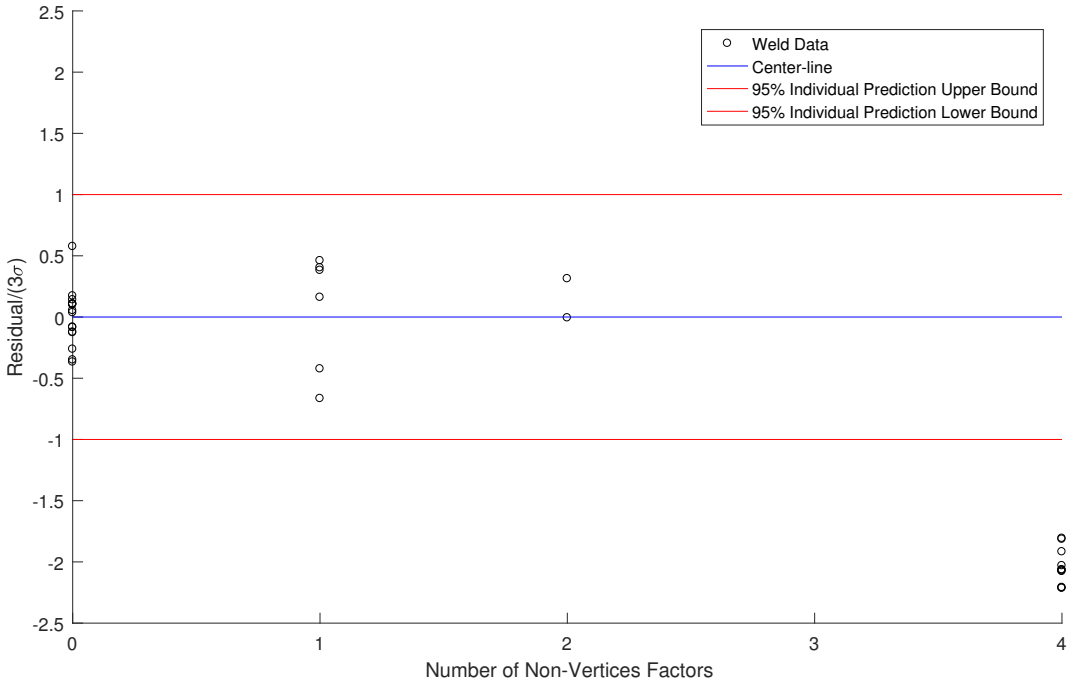

Figure 5.19: Linear-terms PMPE model assessment: Residuals divided by the 95% confidence interval half-width vs. number of non-vertex factors.

Discussion of Linear-Terms Percentage Maximum Post-rise Error Model

The linear-terms PMPE regression model assessment is very similar to the linear-terms rise time regression model assessment. The assessment suggests that the model would be improved by including higher-order terms.

The linear-terms PMPE model has a very high R^2 value of 0.99, which seems to indicate a very good model fit. However, The residuals of the model shown in Figure 5.17 are not normally distributed about zero. The skewed spread seems to indicate that the model tends to under-predict the actual performance. In addition, the variance of the model residuals appears to increase for higher predictions, suggesting this model is not well-fit across the design space.

Figure 5.18 shows that all of the measured values lie within the prediction interval. However, the dense cluster of points at approximately 330% predicted PMPE suggest possible inaccuracy in the model prediction. Future values should ideally have an even spread across the prediction interval, but the cluster of values suggests that the model will not capture this trend.

Figure 5.19 shows that the linear-terms rise time model predictions decrease in accuracy as the number of of non-vertex factors increases. As with the previous linear-terms models, this deterioration is presumed to be due to curvature in the design space which is not characterized by the linear-terms model.

The assessments of the linear-terms PMPE regression model suggest that a higher order model may improve the model accuracy. Exploration of regression models which include allow for inclusion of quadratic terms is shown in the following subsection. This is performed to determine if more extensive experimental data would result in more accurate characterization of the design space, thereby allowing for enhanced tuning of the controller for specified PMPE performance.

Exploration of Quadratic-Inclusive Percentage Maximum Post-rise Error Model

The procedure for constructing a PMPE regression model with quadratic explanatory variables is identical to the method used for constructing the quadratic-terms regression settling time model and rise time model in Sections 5.4.1 and 5.4.2, respectively. In addition, the same data set is used for construction of this model to avoid over-fitting the 2^4 DOE data. This exploratory step is used as an indicator of whether a future experimental design could yield a more accurate characterization of the design space and enhance tuning of the controller for a specified PMPE.

The regression model presented in Table 5.16 is the lowest BIC model of all 1336 possible PMPE regression models which allow for inclusion of quadratic explanatory variables. The associated BIC and R^2 model statistics are shown in Table 5.17. Figures 5.20, 5.21, and 5.22 allow for a comparative assessment to the linear-terms PMPE model. The assessment plots include all the validation weld data, including the 9 demonstration welds.

Table 5.16: Multiple regression model constants for predicting the mean PMPE, allowing for inclusion of quadratic terms.

Model Constant	Associated Explanatory Variable	Estimate	P-value
β_0	Intercept	45.78429344	0.2072
β_1	$K_{P,o}$	34.11742677	0.006
β_2	$K_{V,o}$	-350.6573222	<0.0001
β_3	$K_{P,f}$	118.6929854	<0.0001
β_4	$K_{V,f}$	-45.61949036	0.0005
β_5	$K_{P,o}^2$	—	—
β_6	$K_{P,o} * K_{V,o}$	-32.67264342	0.0122
β_7	$K_{P,o} * K_{P,f}$	—	—
β_8	$K_{P,o} * K_{V,f}$	-21.46203551	0.0683
β_9	$K_{V,o}^2$	—	—
β_{10}	$K_{V,o} * K_{P,f}$	-24.00271615	0.0514
β_{11}	$K_{V,o} * K_{V,f}$	36.36141499	0.0073
β_{12}	$K_{P,f}^2$	307.5148634	<0.0001
β_{13}	$K_{P,f} * K_{V,f}$	—	—
β_{14}	$K_{V,f}^2$	—	—

Table 5.17: Model assessment statistics for the PMPE model shown in Table 5.17.

BIC	R^2
298.43	0.98

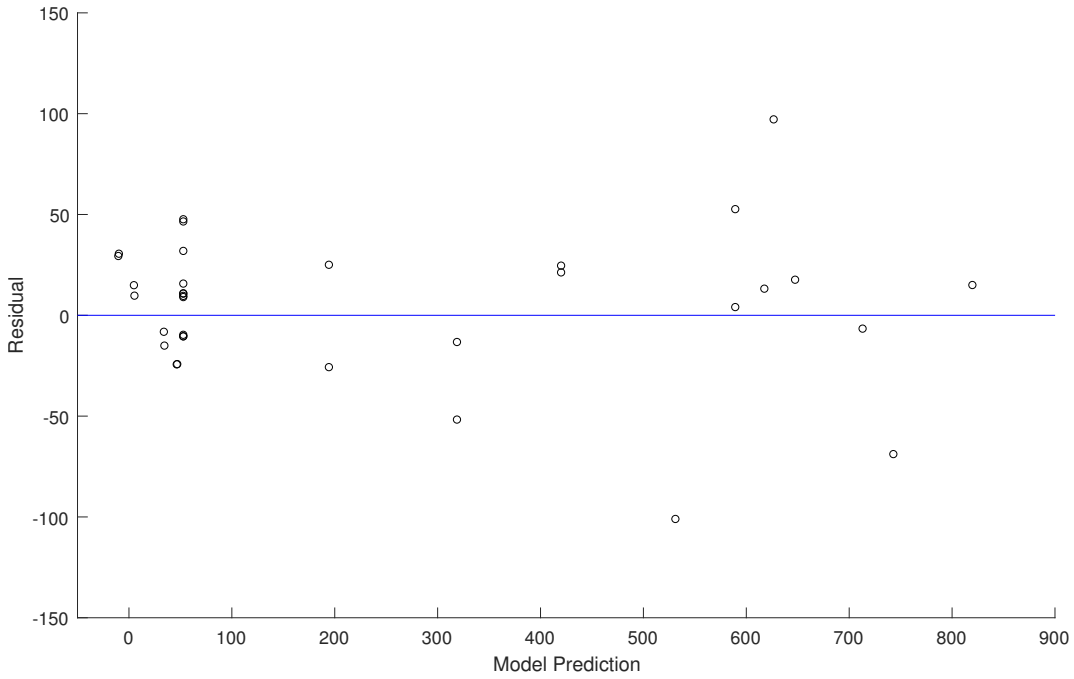

Figure 5.20: Quadratic-terms PMPE model assessment: Residuals vs. predicted values.

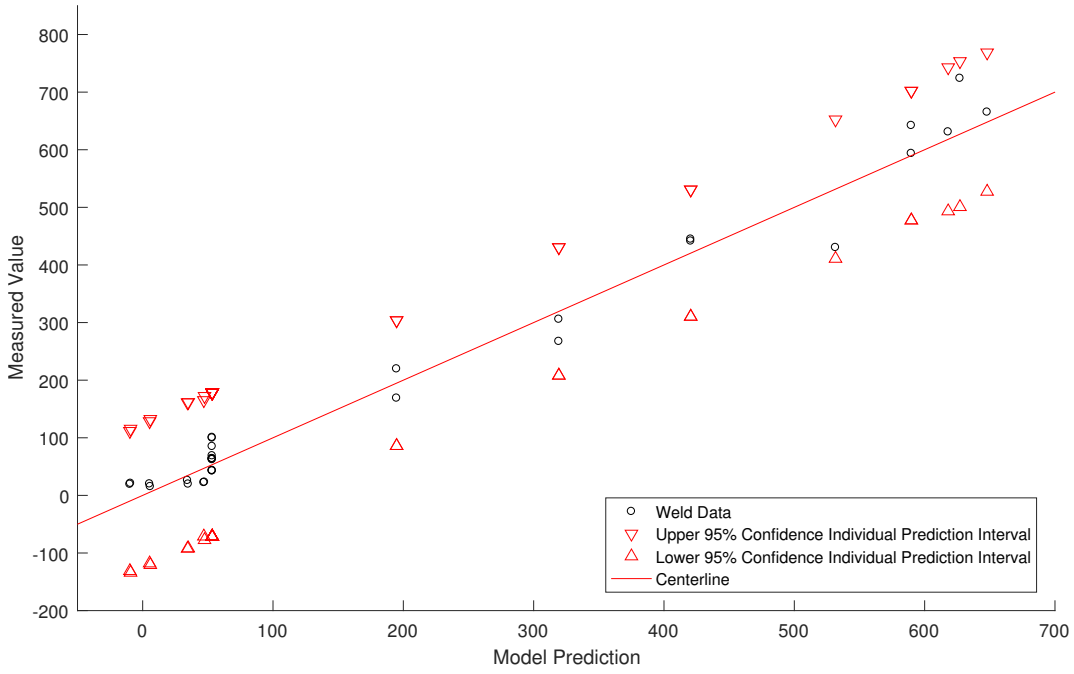

Figure 5.21: Quadratic-terms PMPE model assessment: Measured values vs. predicted values. The center-line bisects the upper and lower prediction interval bounds.

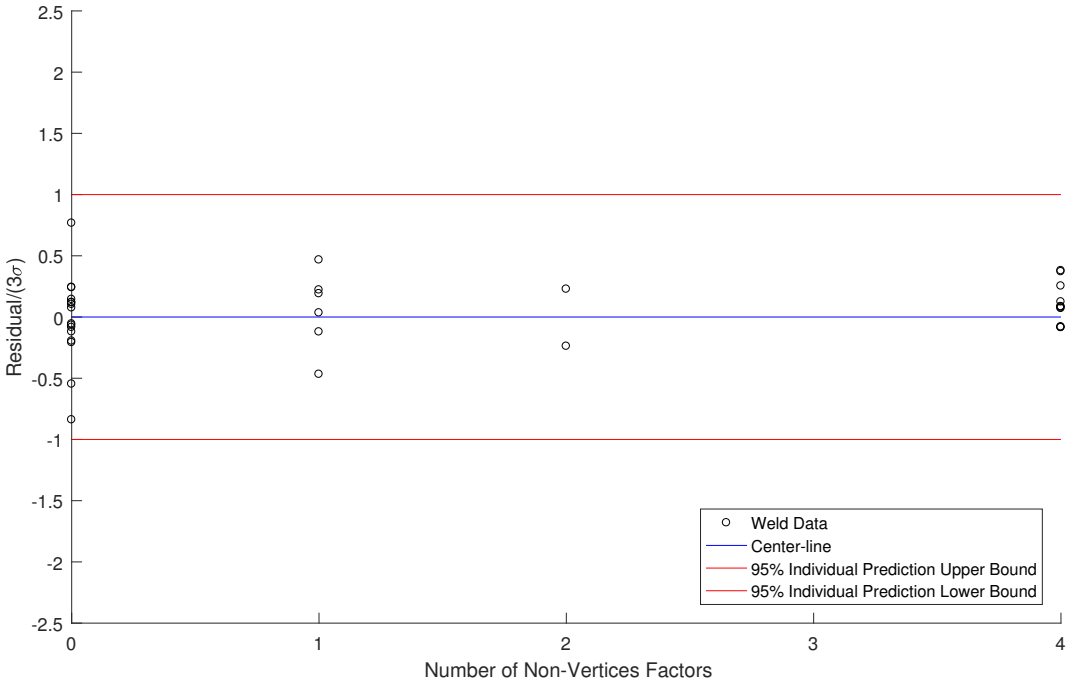

Figure 5.22: Quadratic-terms PMPE model assessment: Residuals divided by the 95% confidence interval half-width vs. number of non-vertex factors.

Discussion of Quadratic-Inclusive Percentage Maximum Post-rise Error Model

Allowing for inclusion of quadratic terms in the PMPE regression model results in a higher accuracy model. The distribution of the model residuals in Figure 5.20 is an improvement over the model residuals shown in Figure 5.17. In addition, the largest magnitude residual from the linear-terms model is -282.1%, which is significantly larger than 101.3% for the quadratic-terms model. Figure 5.21 shows that no data points lie outside the prediction interval and that there is a relatively even spread of the data across the 95% prediction interval. Figure 5.22 confirms this improvement, as well as showing that the quadratic-terms model reduces the model error due to curvature throughout the design space, in contrast to the disparity shown in Figure 5.19.

Allowing quadratic terms to be included improves the predictive accuracy of the PMPE model. Given a more complete set of data from which to construct a PMPE regression model, this exploration suggests that adding higher order terms would create a significantly superior model. The improved predictive accuracy would enable tuning the temperature controller for a wide range of specified rise time performance.

There are 3 terms which are different in the linear-terms model and the quadratic-terms model. $K_{P,o} * K_{V,f}$ and $K_{P,f} * K_{V,f}$ are no longer part of the model and $K_{P,f}^2$ is included. $K_{P,f}^2$ and $K_{V,o}$ are the major effects in the model, both with p-values $<$0.0001. Given a more complete data set from which to build this model, insights such as these would allow for guided tuning of the start-up controller for operator-specified PMPE behavior.

5.4.4 Post-Settled Root Mean Square Error Model

Table 5.18: Multiple regression model constants for predicting the mean post-settled RMSE.

Model Constant	Associated Explanatory Variable	Estimate	P-value
β_0	Intercept	0.873	$<$0.0001
β_1	$K_{P,o}$	0.031	0.0745
β_2	$K_{V,o}$	0.046	0.0137
β_3	$K_{P,f}$	0.073	0.0007
β_4	$K_{V,f}$	—	—
β_5	$K_{P,o} * K_{V,o}$	0.026	0.1239
β_6	$K_{P,o} * K_{P,f}$	—	—
β_7	$K_{P,o} * K_{V,f}$	—	—
β_8	$K_{V,o} * K_{P,f}$	—	—
β_9	$K_{V,o} * K_{V,f}$	—	—
β_{10}	$K_{P,f} * K_{V,f}$	—	—

Table 5.19: Model assessment statistics for the post-settled RMSE model.

BIC	R^2
-32.71	0.77

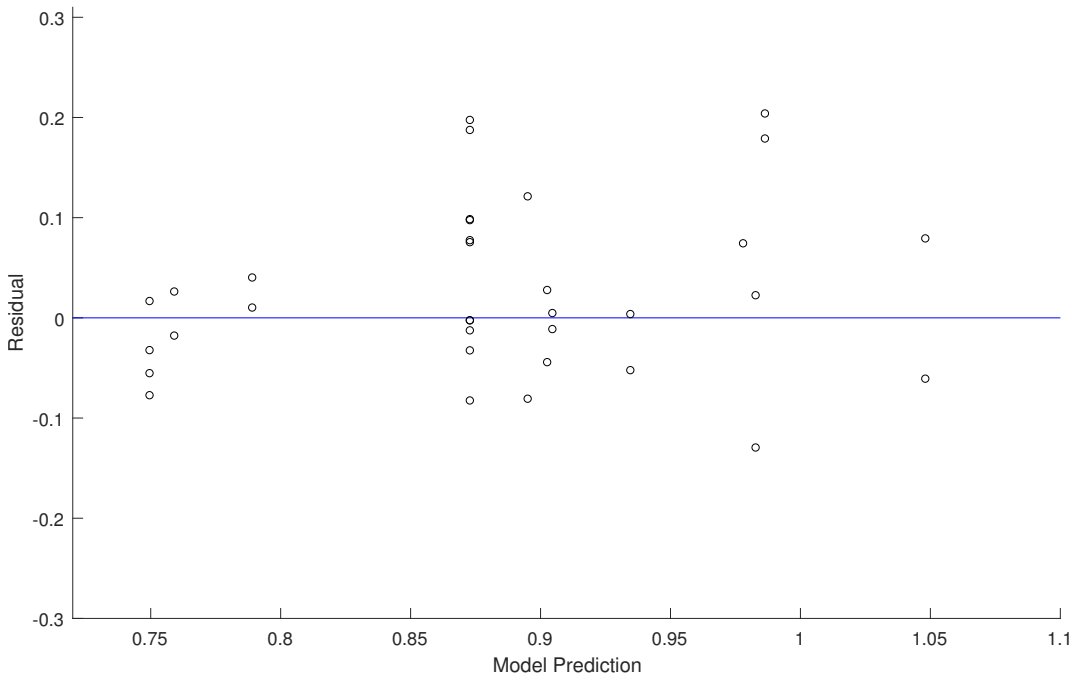

Figure 5.23: Linear-terms post-settled RMSE model assessment: Residuals vs. predicted values.

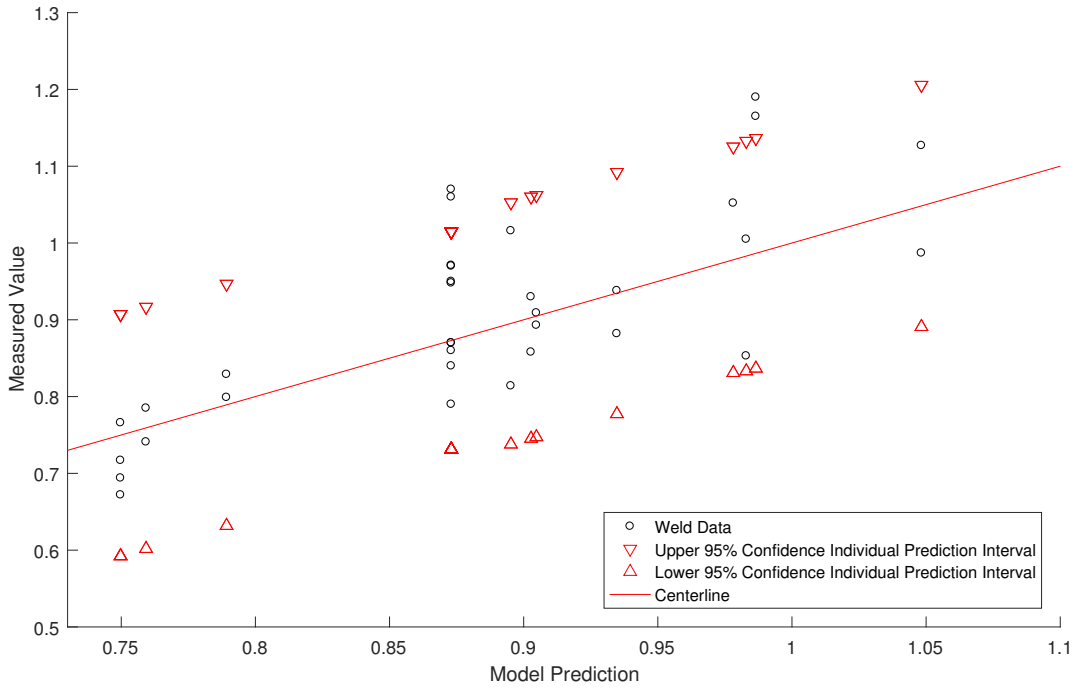

Figure 5.24: Linear-terms post-settled RMSE model assessment: Measured values vs. predicted values. The center-line bisects the upper and lower prediction interval bounds.

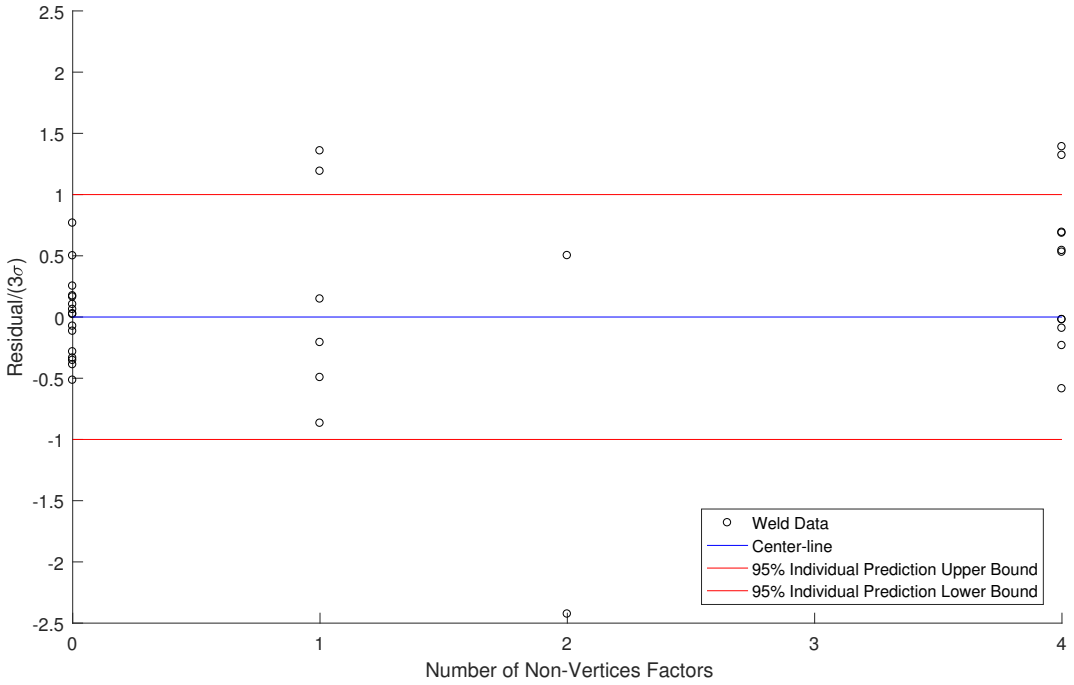

Figure 5.25: Linear-terms post-settled RMSE model assessment: Residuals divided by the 95% confidence interval half-width vs. number of non-vertex factors.

Discussion of Linear-Terms Post-Settled RMS Error Model

Assessment of the post-settled RMSE regression model seems to indicate that a linear-terms regression model is adequate for characterizing the design space and therefore can provide steady-state tuning guidance.

Figure 5.23 shows that the model residuals are relatively normally distributed. While some of the data lies outside the prediction interval shown in Figure 5.24 shows the relatively normally distribution and lack of clustering in the data across the individual prediction interval. This behavior suggests that the model is adequate. However, it can also been seen that the full range of measured values is relatively small. Although the start-up controller may have an effect on the steady-state performance, the effect is small in all cases. This aligns with the design of the controller, in that the steady-state performance is dominated by the steady-state PID controller. Figure 5.25 does not indicate any severe dependence of the residuals on the number of non-vertex factors, suggesting that significant curvature does not exist within the design space.

5.5 Regression Model Discussion

As stated in Section 5.1, the purpose of constructing regression models of the PVA tuning parameters is to enable the operator to obtain a desired controller behavior. The models discussed in the Section 5.4 do this with varying degrees of success.

As stated in Section 5.1, the data collected with the 2^4 DOE full factorial design is theoretically limited to constructing regression models which include only the primary effects or first-order interactions between the primary effects. For predicting the weld settling time, the lowest-BIC linear-terms regression model is inadequate in characterizing the design space. Curvature within the design space is significant, limiting the usefulness of the linear-terms settling time regression model. This is also the case for the rise time and percentage maximum post-rise error linear-terms regression models. The exception is the post-settled RMSE model, which appears to adequately characterize the design space without the need for a model with higher-order terms.

Section 5.4 also explores the potential utility of constructing regression models which include quadratic terms to guide controller tuning. For the settling time, rise time, and percentage maximum post-rise error quadratic-terms regression models, this approach gave promising results. The weld data presented in Table 5.5 allows for construction of these regression models without over-fitting. However, this data set does not completely fill the necessary gaps in the design space to allow for the quadratic-terms models to be utilized with certainty. For possible future work, it is recommended that an alternative experimental design be selected which is capable of fitting quadratic or higher-order term regression models. A 3^4 full-factorial DOE or a central composite DOE would allow for robust construction of quadratic-terms models.

CHAPTER 6. CONCLUSIONS

The following conclusions are made about the design and characterization of the plunge-capable FSW temperature controller. Conclusions about the performance of the temperature controller are made in Section 6.1 and pertain to the results presented in Chapter 4. Conclusions about the characterization of the controller tuning are stated in Section 6.2 and pertain to the work presented in Section 5.

6.1 FSW Temperature Controller

- The start-up temperature controller engaged at the beginning of the plunge and succeeded in rapidly reaching and maintaining the temperature set-point for all of the 9 demonstration welds. This performance demonstrates that the proposed controller is a viable method for attaining fully-automated active temperature control during the entire plunge and traverse of the weld with no operator input.

- The temperature controller achieved the mean performance metrics shown in Table 6.1. This level of performance indicates that the temperature controller is able to attain excellent temperature control during the entirety of the weld.

- The coefficients of variation of the performance metrics from the 9 demonstration welds are shown in Table 6.1. The consistency of the controller's performance indicates that the proposed temperature controller is a viable method for attaining acceptable FSW temperature control.

Table 6.1: Mean and coefficients of variation of each the performance metrics for the 9 demonstration welds.

Performance Metric	$\bar{x}$	Coefficient of Variation
t_{rise}	10.82s	5.9%
$t_{settled}$	11.35s	13.5%
PMPE	69.86%	24.2%
RMSE	0.92°C	8.9%

- 4 comparisons welds were performed with the methodology used in previous work: engaging the steady-state controller at the beginning of the traverse (2 welds) or at the operator's discretion (2 welds). The average settling time and percentage maximum post-rise error achieved by the start-up controller improve on the performance metrics achieved by the 4 comparison welds. The average rise time and post-settled RMS error of the start-up controller are equivalent to the performance of the 4 comparison welds. Maintaining the post-settled RMS error performance is a significant achievement as it shows that the start-up controller does not negatively impact the steady-state tracking performance. Although it is not a direct comparison due to the difference in welding scenarios, the start-up controller improves the set-point tracking performance of previous work during the initial traverse by reducing the set-point tracking range from ± 5°C [11] to ± 3°C. In addition to these improvements, the start-up controller reduces inconsistencies in the temperature control of a weld potentially caused by differences in operator input.

6.2 Characterization of the FSW Temperature Controller

- Regression models were constructed of the settling time, rise time, and percentage maximum post-rise error from data obtained through a 2^4 full-factorial DOE. The the set of possible explanatory variables for these regression models are the four PVA controller gains ($K_{P,o}$, $K_{V,o}$, $K_{P,f}$, and $K_{V,f}$) and the interaction effects. The lowest-BIC regression model was selected

from the set of all possible models. These linear-terms regression models did not characterize the design space with sufficient accuracy to guide tuning of the start-up controller.

- Exploration of quadratic-inclusive regression models of the settling time, rise time, and percentage maximum post-rise error were performed. To avoid over-fitting, an additional data set was utilized (obtained outside the 2^4 full-factorial DOE). The incompleteness of this data set is an area of possible future work, but the quadratic-inclusive regression models showed significant improvements over their linear-terms model counterparts. It is recommended that an alternative experimental design be selected which allows for fitting of quadratic or higher-order term regression models. A 3^4 full-factorial DOE or a central composite DOE would allow for robust construction of quadratic-terms models.

- The quadratic-inclusive settling time regression model indicates that $K_{P,o}^2$ has the single greatest effect on settling time of all the explanatory variables. The p-value associated with this variable indicates a strong statistical significance. This model indicates that $K_{V,f}^2$ and $K_{V,o}^2$ also have large effects.

- The lowest BIC quadratic-inclusive rise time model adds $K_{P,o}^2$ and $K_{V,o}^2$ to the set of terms included in the linear-terms model. $K_{V,o}$ has the largest effect (with a p-value of <0.0001), but the second-order terms have large effects as well.

- The quadratic-inclusive percentage maximum post-rise error model indicates that 3 of the terms in the linear-terms model should not be included: $K_{P,o} * K_{V,f}$ and $K_{P,f} * K_{V,f}$. $K_{P,f}^2$ is the only quadratic term added to the model. $K_{P,f}^2$ and $K_{V,o}$ are estimated to have the largest effects on percentage maximum post-rise error (both with p-values <0.0001).

- A linear-terms regression model of the post-settled RMS error was constructed from the data obtained through the 2^4 full-factorial DOE and the lowest-BIC model was selected from the set of all possible models. This linear-terms regression model characterizes the design space with sufficient accuracy to guide tuning of the controller for operator-specified steady-state tracking performance. There is no evidence that higher-order regression models are necessary. $K_{P,f}$ is estimated to have the largest effect on post-settled RMS error (p-value of 0.0007).

Bibliography

[1] Peel, M., Steuwer, A., Preuss, M., and Withers, P., 2003. "Microstructure, mechanical properties and residual stresses as a function of welding speed in aluminium AA5083 friction stir welds." *Acta Materialia,* **51**(16), pp. 4791–4801. viii, 1, 2

[2] Bussu, G., and Irving, P., 2003. "The role of residual stress and heat affected zone properties on fatigue crack propagation in friction stir welded 2024-T351 aluminium joints." *International Journal of Fatigue,* **25**(1), pp. 77–88. 1

[3] Cavaliere, P., Squillace, a., and Panella, F., 2008. "Effect of welding parameters on mechanical and microstructural properties of aa6082 joints produced by friction stir welding." *Journal of Materials Processing Technology,* **200**(1–3), pp. 364–372. 1

[4] Sato, Y. S., Urata, M., and Kukowa, H., 2002. "Parameters controlling microstructure and hardness during friction-stir welding of precipitation-hardenable aluminum alloy 6063." *Metallurgical and Materials Transactions,* **33**, pp. 625–635. 1

[5] Ross, K., Sutton, B., Grant, G., Cannell, G., Frederick, G., and Couch, R., 2017. "Development of friction stir processing for repair of nuclear dry cask storage system canisters." *The Minerals, Metals and Materials Society,* **1**, pp. 39–46. 1

[6] Taysom, S., 2015. "Temperature control in friction stir welding using model predictive control." PhD thesis, Brigham Young University. 1, 15, 34, 81

[7] Ross, K., 2012,. "Investigation and implementation of a robust temperature control algorithm for friction stir welding." Master's thesis, Brigham Young University. 1, 15

[8] Marshall, D., 2013,. "An alternative system identification method for friction stir processing." Master's thesis, Brigham Young University. 1, 10, 11

[9] Cederqvist, L., Garpinger, O., Hagglund, T., and Robertsson, A., 2011. "Reliable sealing of copper canisters through cascaded control of power input and tool temperature." *Friction Stir Welding and Processing VI - Held During the TMS 2011 Annual Meeting and Exhibition*, pp. 51–58. 1

[10] Ross, K., 2014. "Temperature control in friction stir welding for industrial and research applications." *The Welding Institute*. 1

[11] Taysom, B. S., Sorensen, C. D., and D.Hedengren, J., 2017. "A comparison of model predictive control and pid temperature control in friction stir welding." *Journal of Manufacturing Processes,* **29**, pp. 232–241. 2, 34, 75

[12] Seborg, D., Edgar, T., and Mellichamp, D., 2004. *Process Dynamics and Control*. International series of monographs on physics. Wiley. 4, 6, 8

[13] Hermes, H., and Lasalle, J. P., 1969. *Functional Analysis and Time Optimal Control*., Vol. 56 of *Mathematics in Science and Engineering* Academic Press, Inc., 111 Fifth Avenue, New York, New York 10003. 6

[14] Tan Kok Kiong, Wang Qing-Guo, H. C. C., 1999. *Advances in PID Control*. Advances in Industrial Control. Springer. 8

[15] O'Dwyer, A., 2006. *Handbook of PI and PID Controller Tuning Rules: Aidan O'Dwyer*. Imperial College Press. 11

[16] Tang, W., Guo, X., McClure, J., Murr, L., and Nunes, A., 1998. "Heat input and temperature distribution in friction stir welding." *Journal of Materials Processing and Manufacturing Science,* **7**(2), pp. 163–172. 14

[17] Longhurst, W., Strauss, A., Cook, G., and Fleming, P., 2010. "Torque control of friction stir welding for manufacturing and automation." *International Journal of Advanced Manufacturing Technology,* **51**(9-12), pp. 905–913. 15

[18] FitzSimons, P. M., and Palazzolo, J. J., 1994. "Part ii: Control of a one-degree-of-freedom active hydraulic mount." *Journal of Dynamic Systems, Measurement, and Control*, pp. 443–448. 18

[19] Hozo, S. P., Djulbegovic, B., and Hozo, I., 2005. "Estimating the mean and variance from the median, range, and the size of a sample." *BMC Medical Research Methodology,* **5**(13), April. 32

[20] Ramsey, F. L., and Schafer, D. W., 2002. *The Statistical Sleuth: A Course in Methods of Data Analysis*., 2 ed. Brooks/Cole, Cengage Learning, 10 David Drive, Belmont, CA 94002, USA. 37, 38, 44, 45, 46

[21] Hou, Z., and Komanduri, R., 2000. "General solutions for stationary/moving plane heat source problems in manufacturing and tribology." *International Journal of Heat and Mass Transfer,* **43**(10), pp. 1679–1698. 81

APPENDIX A. CS4 TOOL GEOMETRY

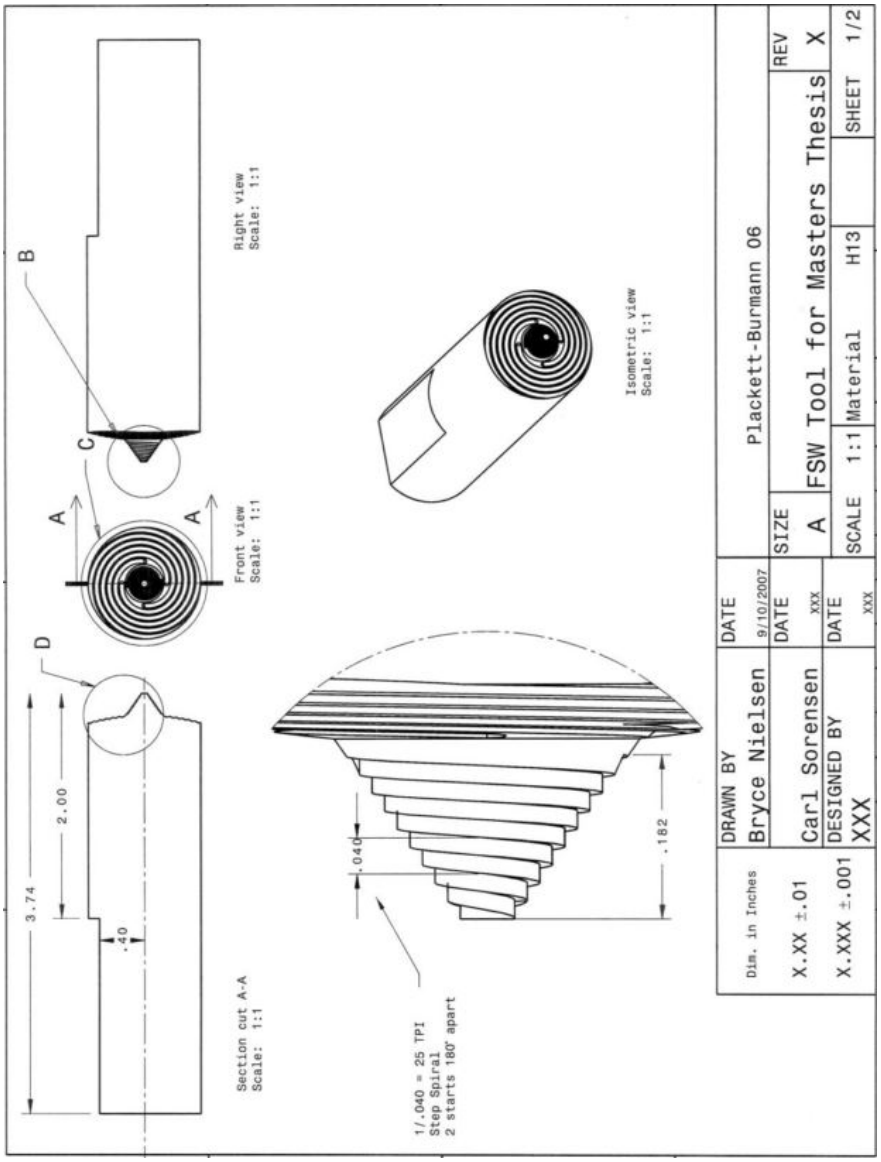

Figure A.1: CS4 tool geometry. Used for welding 7075 Aluminum.

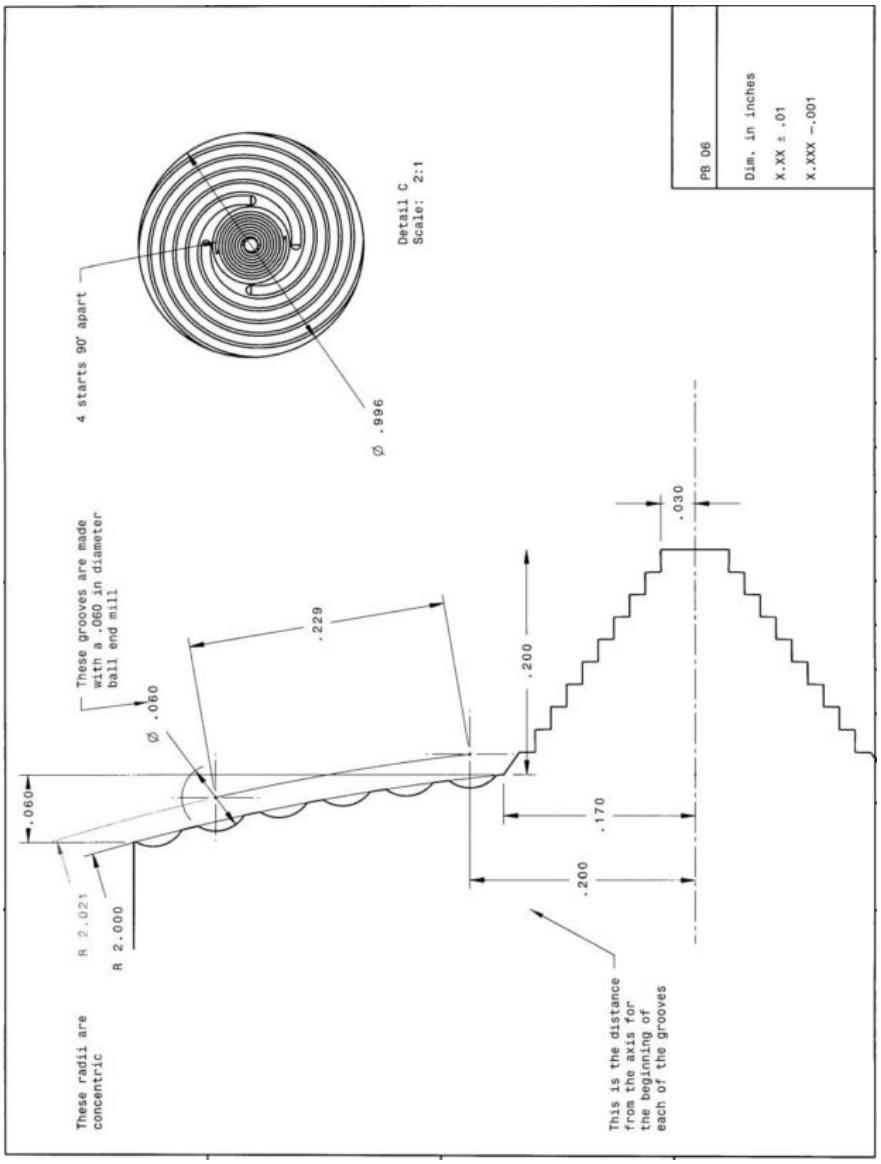

Figure A.2: CS4 tool geometry. Used for welding 7075 Aluminum.

APPENDIX B. SYSTEM MODEL DEVELOPMENT

B.1 System Model Development

When possible, active feedback controllers are designed and tuned based on information gleaned from a system model. A system model can serve one or both of 2 purposes: (1) To provide insights into a system's behavior and the effectiveness a controller may have and (2) to establish approximate controller gains prior to real-world use of the controller. In order to be useful, a system model must be capable of predicting the output of the real-world system within a reasonable tolerance.

Several models were pursued to aid in the design of the transient-capable controller, including the Moving Planar Heat Source model [21], the Moving Point Heat Source model [21], and a First-Order Plus Dead Time model [6]. Comparison of the magnitude, 1^{st} derivative, and 2^{nd} derivative of the model output to actual weld temperature was used to gauge model viability. Due to the complex and rapidly changing nature of the transient portion of the weld, a sufficiently representative system model could not be constructed.

APPENDIX C. RELAY FEEDBACK TEST DATA

The system parameters shown in C.1 were calculated from relay feedback test data, a portion of which is shown in Figure C.1. The measured values necessary for the PID gain calculations are average measurements from several relay tests. Tables C.2 and C.3 display the calculated servo and regulator PID controller gains.

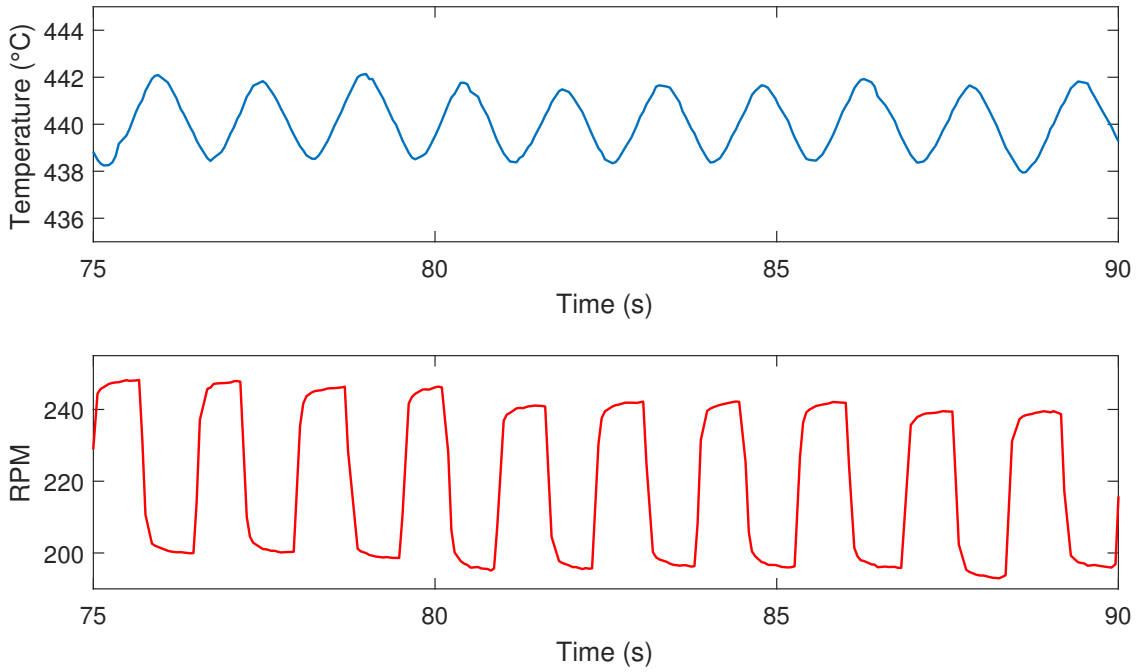

Figure C.1: Sample of the RPM (input) and weld temperature (output) data collected during the relay feedback test. This data was collected about 440C at 100 mm/min.

Table C.1: System parameters calculated from the data shown in Figure C.1.

Parameter	Value
ω_u	2.618
K_u	7.640
K_m	1.707
τ	6.560
θ	0.480

Table C.2: Servo PID controller gains.

Controller Gain	Value
K_P	4.81
K_I	0.73
K_D	1.15

Table C.3: Regulator PID controller gains.

Controller Gain	Value
K_P	9.46
K_I	8.37
K_D	4.60

APPENDIX D. TEMPERATURE CONTROLLER PERFORMANCE DATA

The following sections display the complete temperature profiles and performance metrics for each of the 9 demonstrative welds discussed in Chapter 4. The format of each section is the following:

1. Table of the measured performance metrics
2. Figure of the full weld temperature profile of the weld
3. Figure of the weld temperature profile, but with the Temperature axis limited to $\pm 20^{\circ}C$ about the set-point to demonstrate the performance of the controller near the set-point.

D.1 Weld 1 Temperature Profile

Table D.1: Performance metrics for Weld 1.

Weld No.	$t_{settled}$	t_{rise}	RMSE	PMPE
1	11.79s	11.79s	0.97°C	63.8%

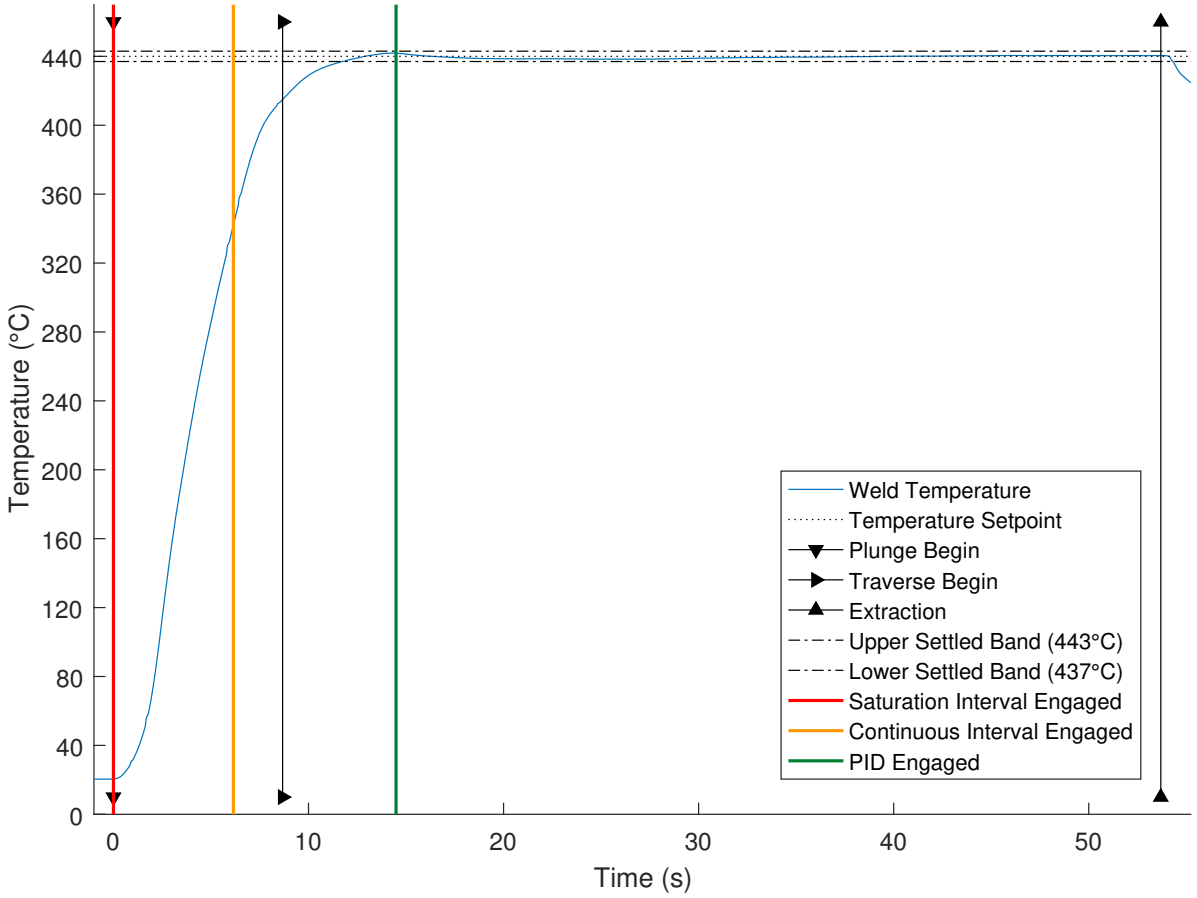

Figure D.1: Temperature profile of Weld 1, zoomed out.

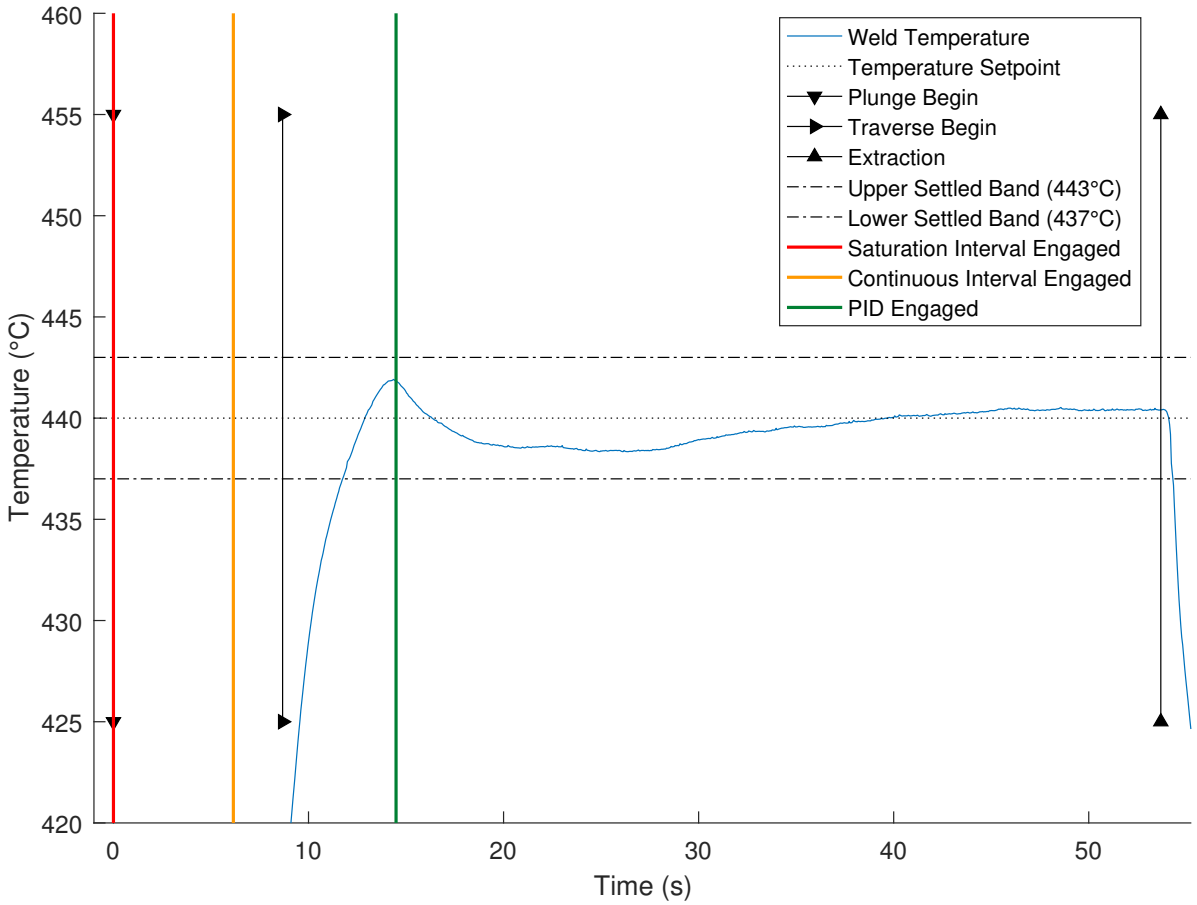

Figure D.2: Temperature profile of Weld 1, zoomed in.

D.2 Weld 2 Temperature Profile

Table D.2: Performance metrics for Weld 2.

Weld No.	$t_{settled}$	t_{rise}	RMSE	PMPE
2	12.14s	12.14s	0.95°C	42.6%

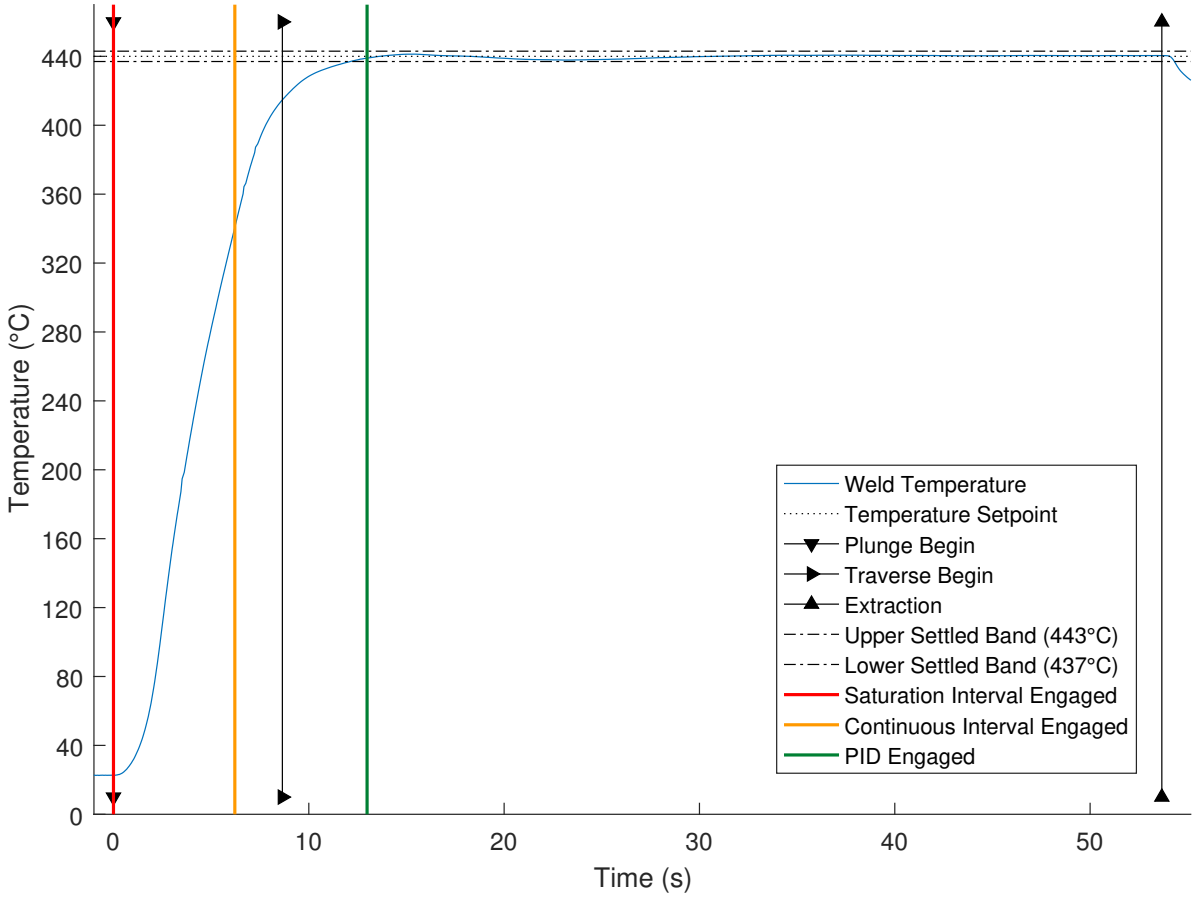

Figure D.3: Temperature profile of Weld 2, zoomed out.

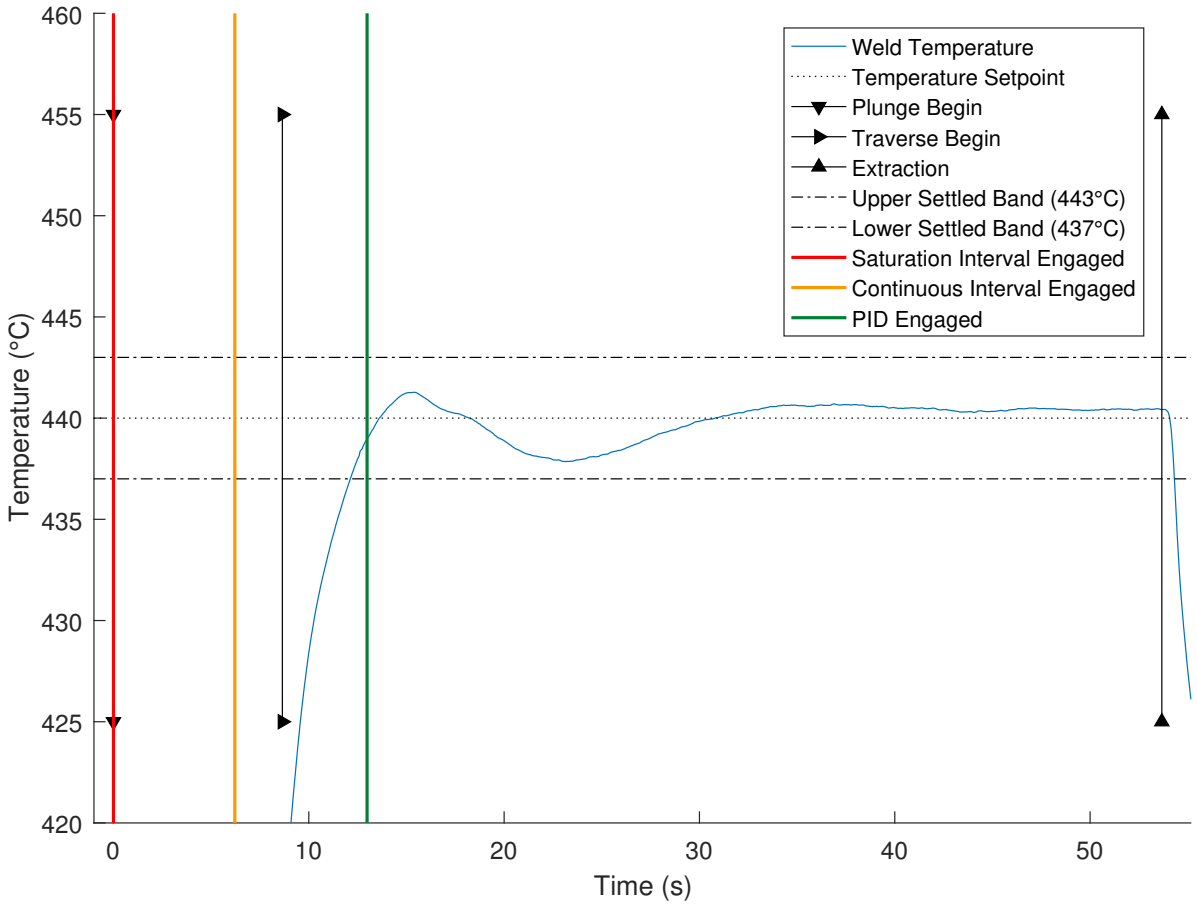

Figure D.4: Temperature profile of Weld 2, zoomed in.

D.3 Weld 3 Temperature Profile

Table D.3: Performance metrics for Weld 3.

Weld No.	$t_{settled}$	t_{rise}	RMSE	PMPE
3	11.12s	11.12s	0.87°C	62.1%

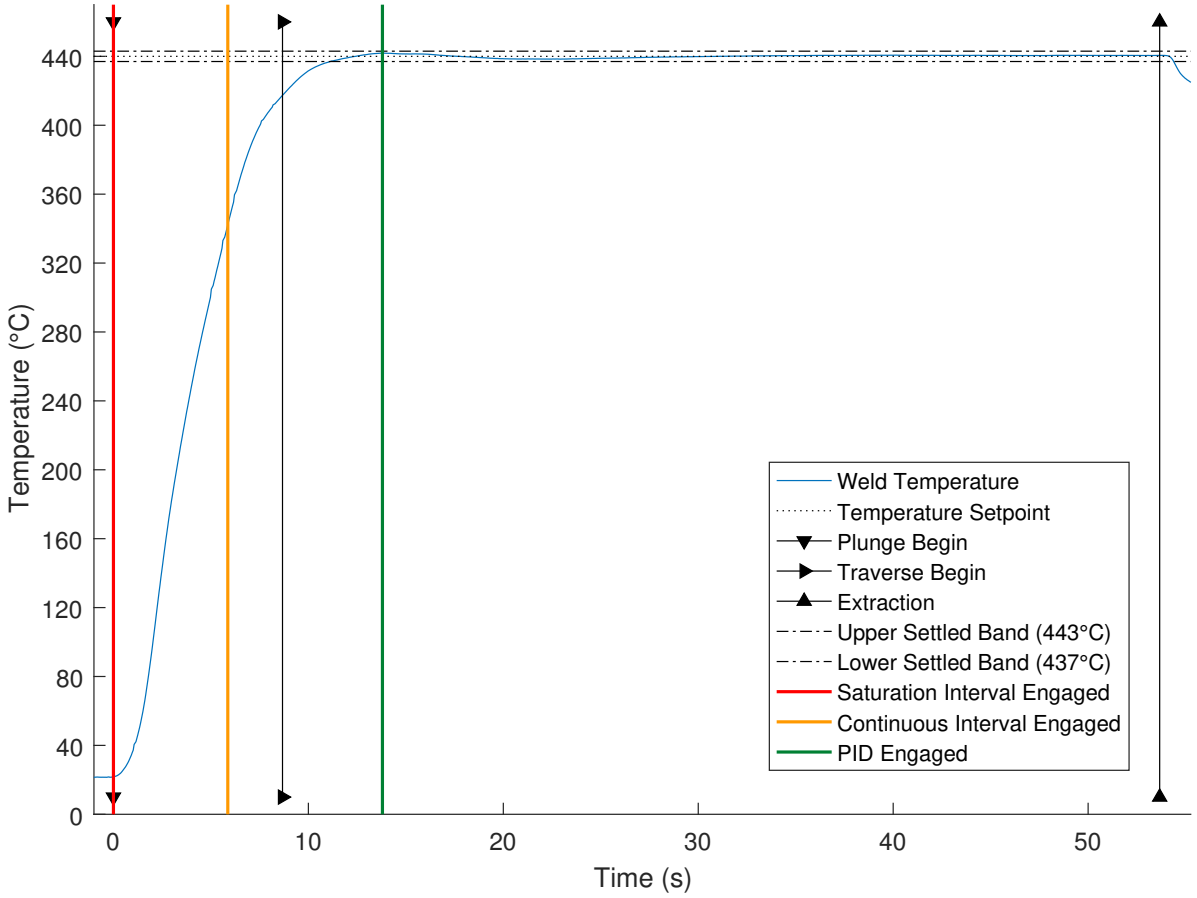

Figure D.5: Temperature profile of Weld 3, zoomed out.

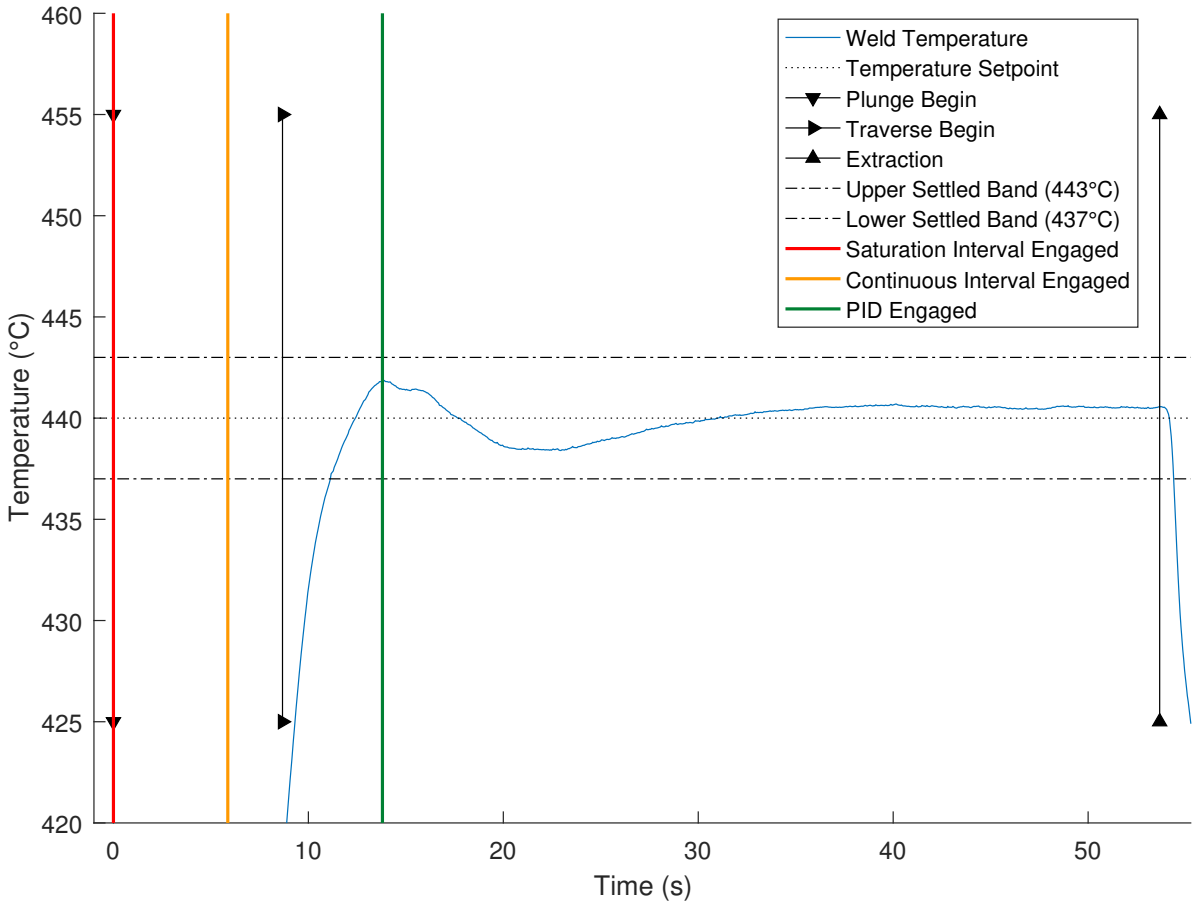

Figure D.6: Temperature profile of Weld 3, zoomed in.

D.4 Weld 4 Temperature Profile

Table D.4: Performance metrics for Weld 4.

Weld No.	$t_{settled}$	t_{rise}	RMSE	PMPE
4	11.02s	11.02s	0.79°C	62.7%

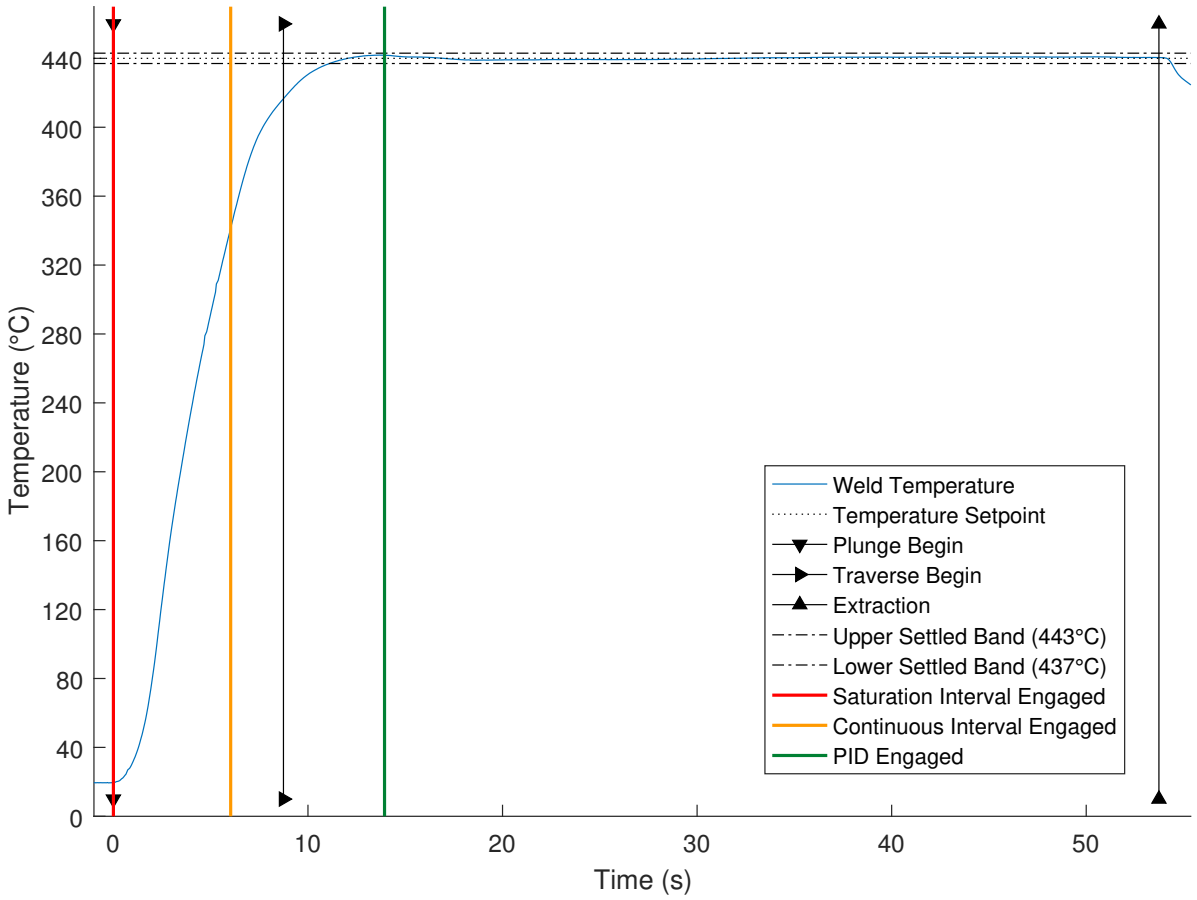

Figure D.7: Temperature profile of Weld 4, zoomed out.

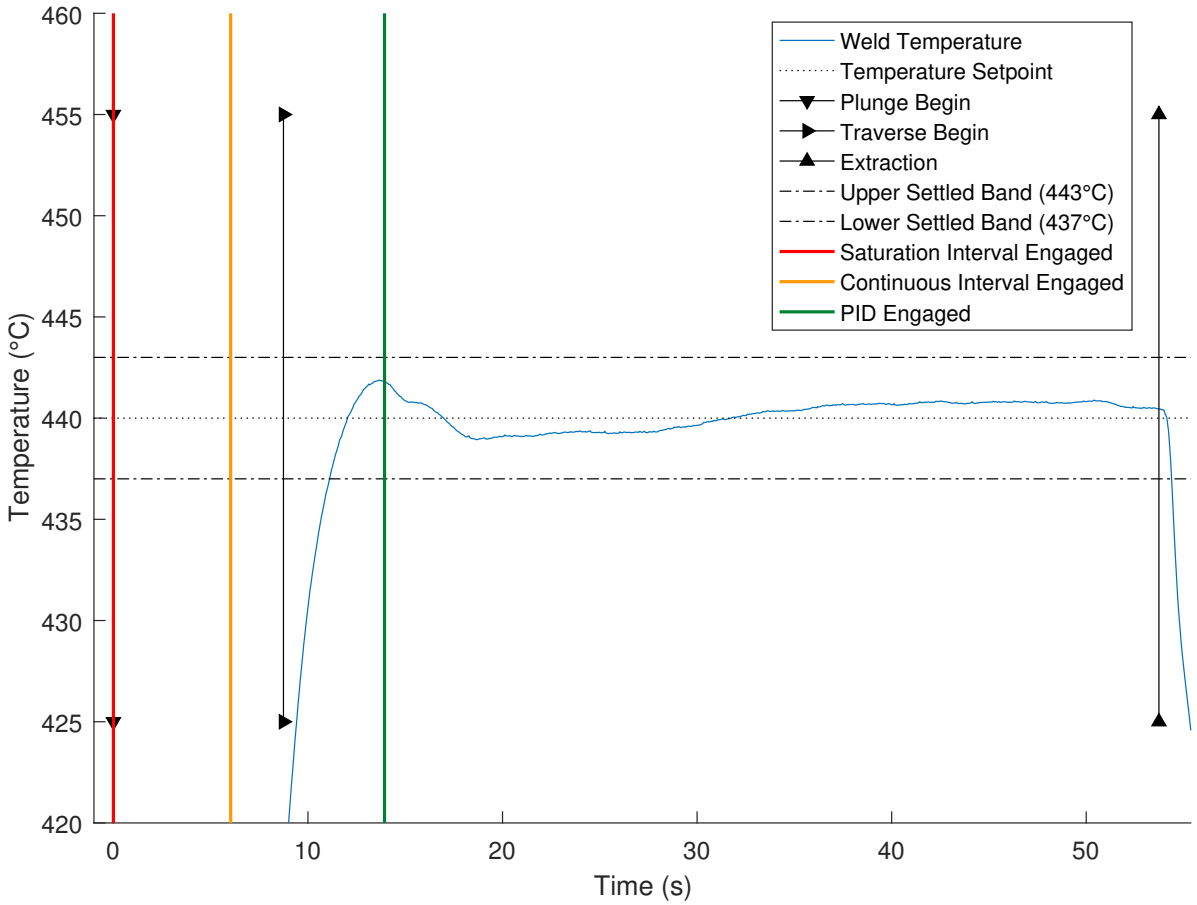

Figure D.8: Temperature profile of Weld 4, zoomed in.

D.5 Weld 5 Temperature Profile

Table D.5: Performance metrics for Weld 5.

Weld No.	$t_{settled}$	t_{rise}	RMSE	PMPE
5	10.24s	10.24s	1.07°C	85.0%

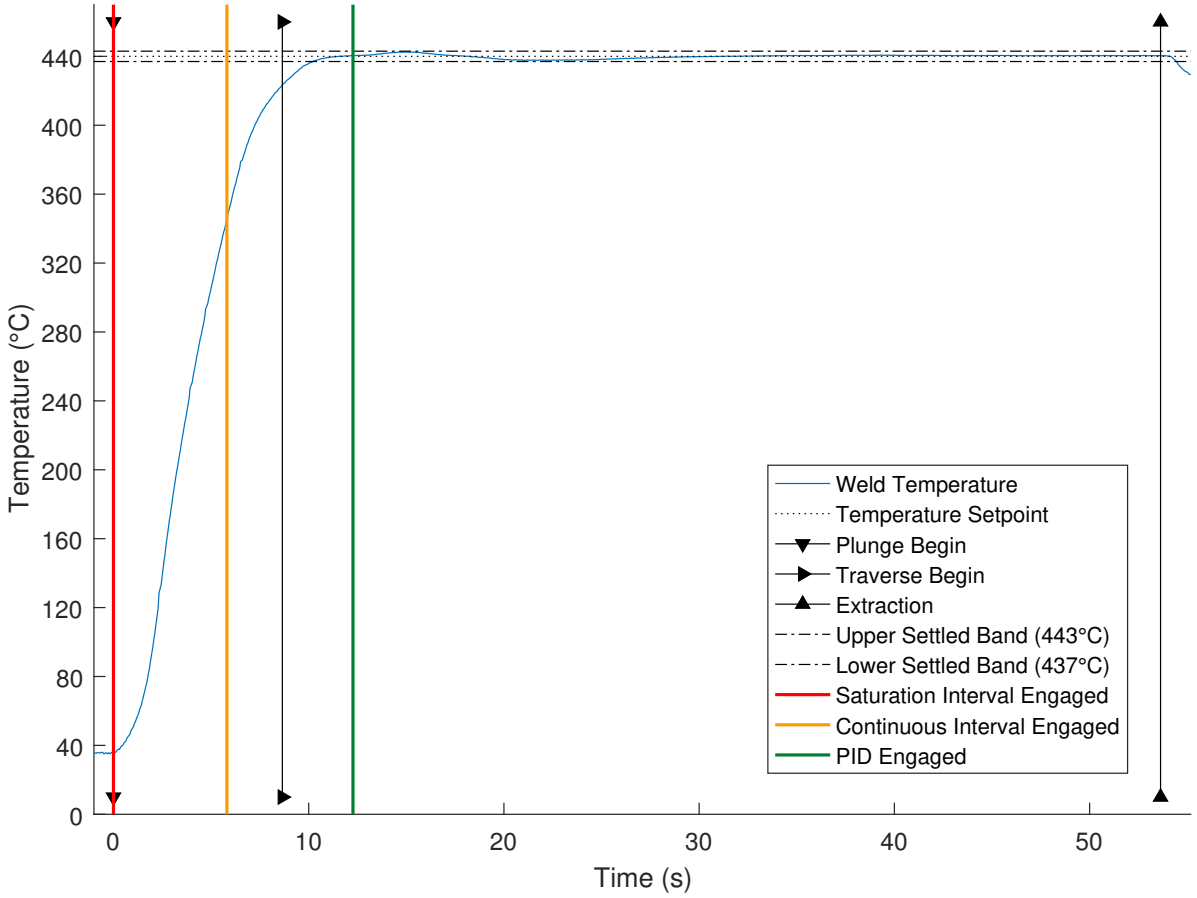

Figure D.9: Temperature profile of Weld 5, zoomed out.

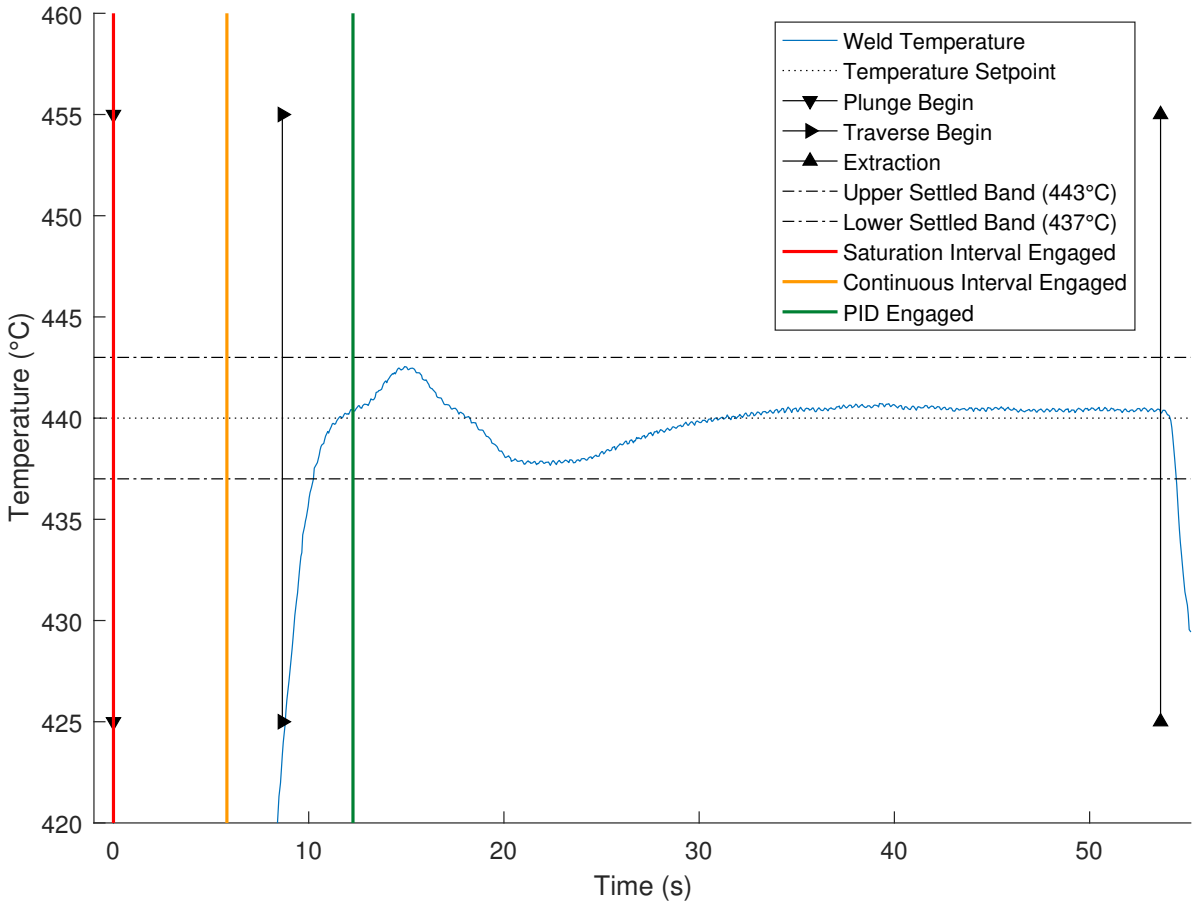

Figure D.10: Temperature profile of Weld 5, zoomed in.

D.6 Weld 6 Temperature Profile

Table D.6: Performance metrics for Weld 6.

Weld No.	$t_{settled}$	t_{rise}	RMSE	PMPE
6	10.12s	10.12s	0.84°C	68.8%

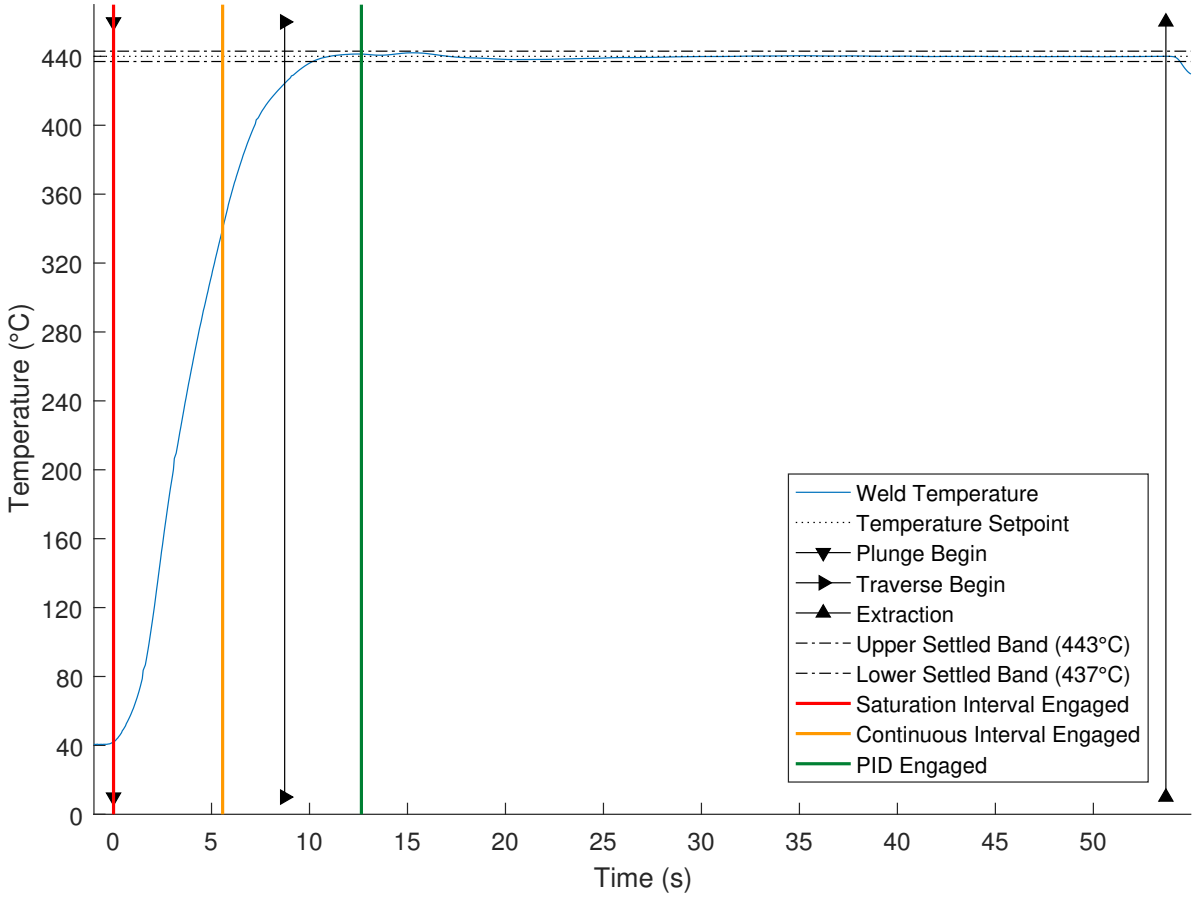

Figure D.11: Temperature profile of Weld 6, zoomed out.

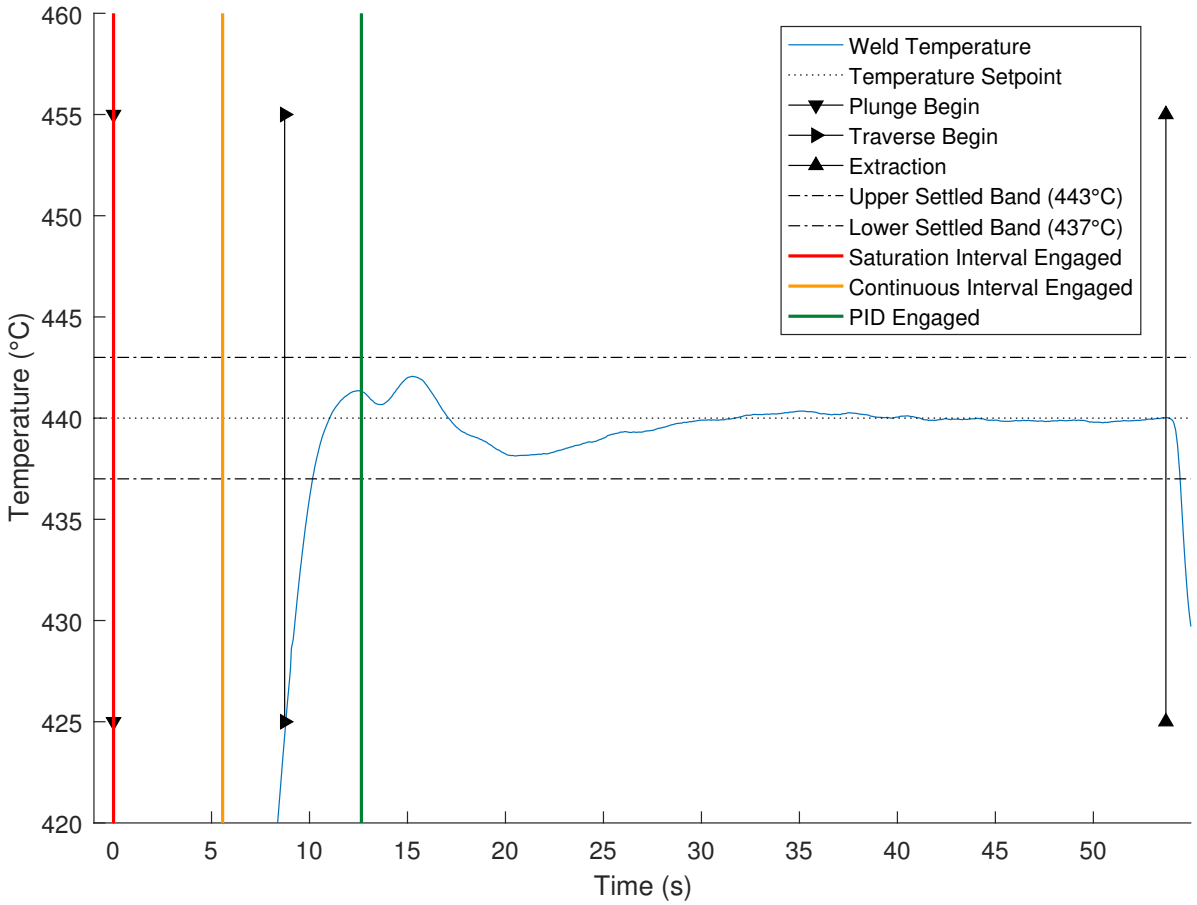

Figure D.12: Temperature profile of Weld 6, zoomed in.

D.7 Weld 7 Temperature Profile

Table D.7: Performance metrics for Weld 7.

Weld No.	$t_{settled}$	t_{rise}	RMSE	PMPE
7	10.51s	10.51s	0.87°C	43.4%

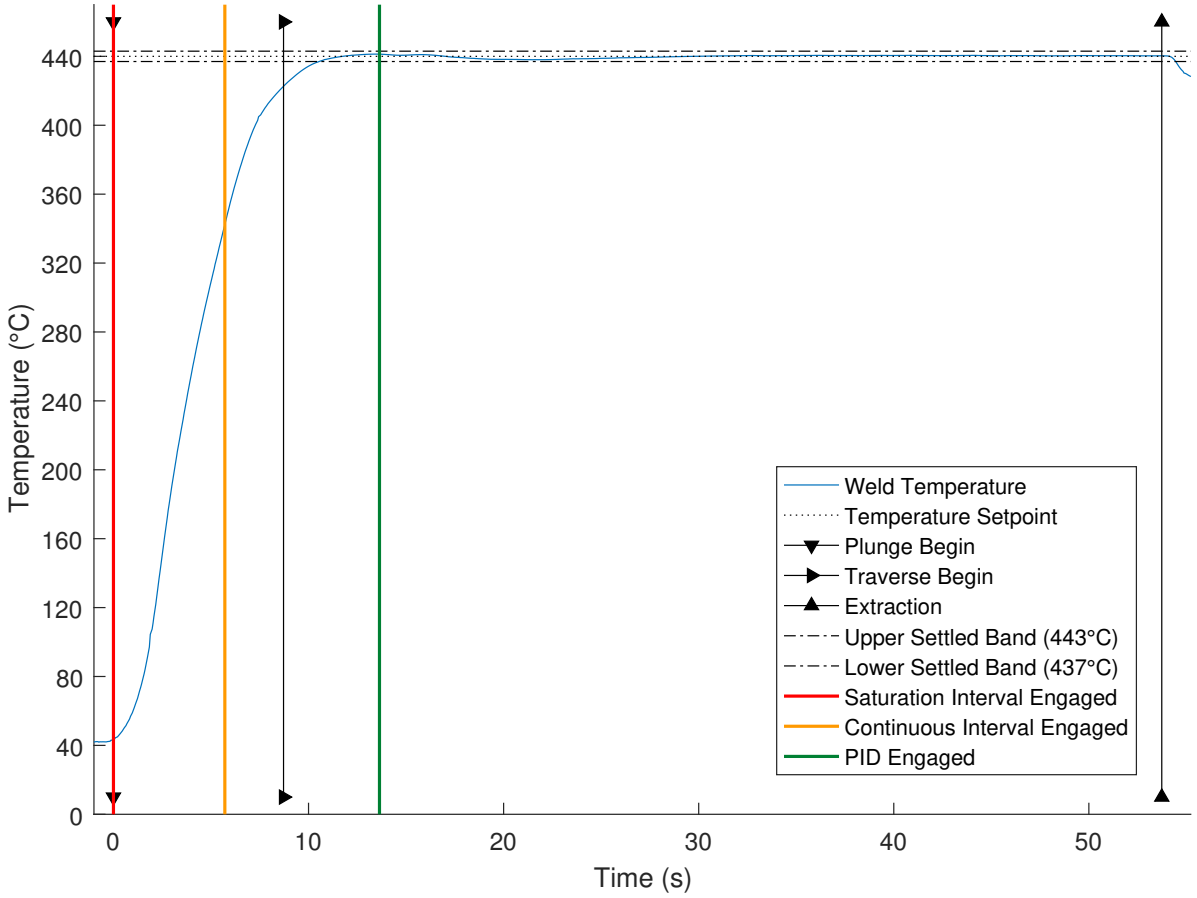

Figure D.13: Temperature profile of Weld 7, zoomed out.

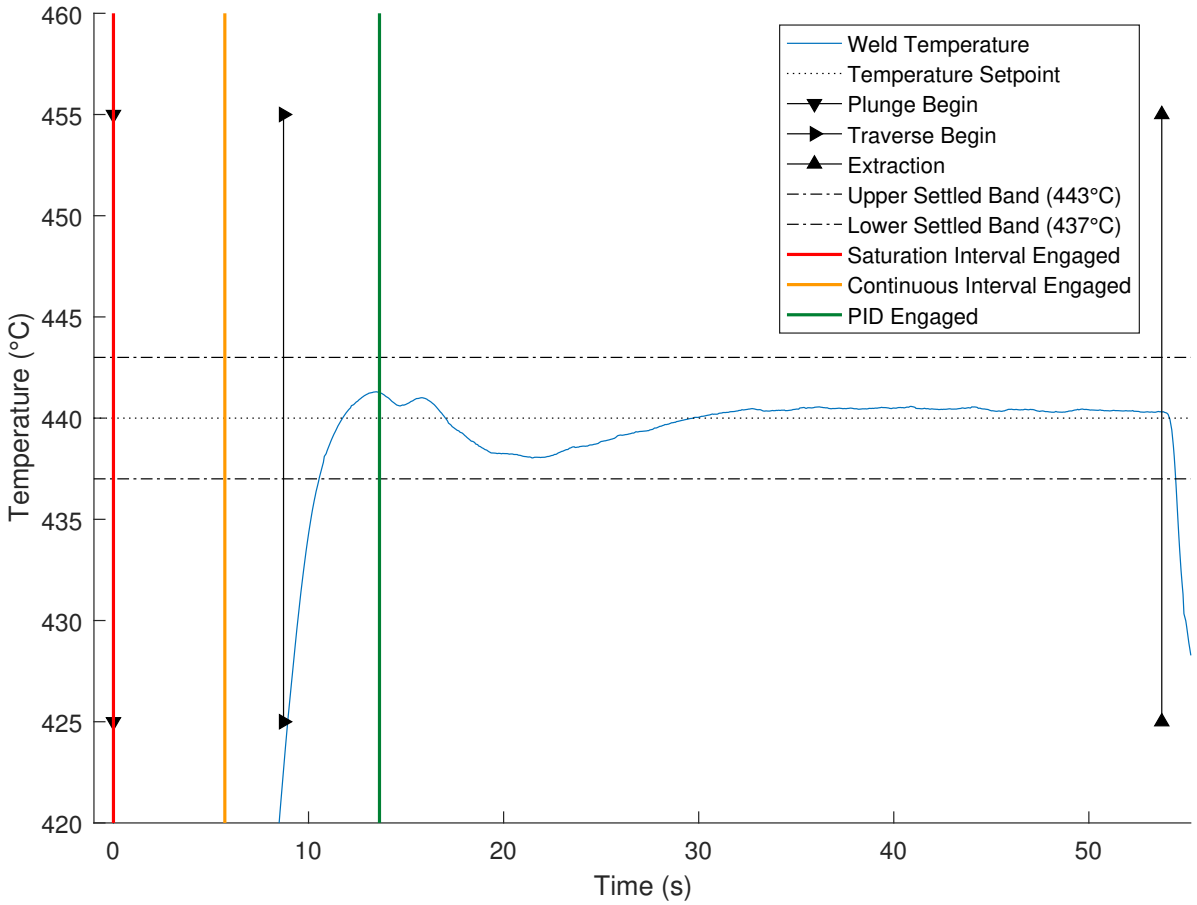

Figure D.14: Temperature profile of Weld 7, zoomed in.

D.8 Weld 8 Temperature Profile

Table D.8: Performance metrics for Weld 8.

Weld No.	$t_{settled}$	t_{rise}	RMSE	PMPE
8	10.14s	10.14s	1.06°C	99.6%

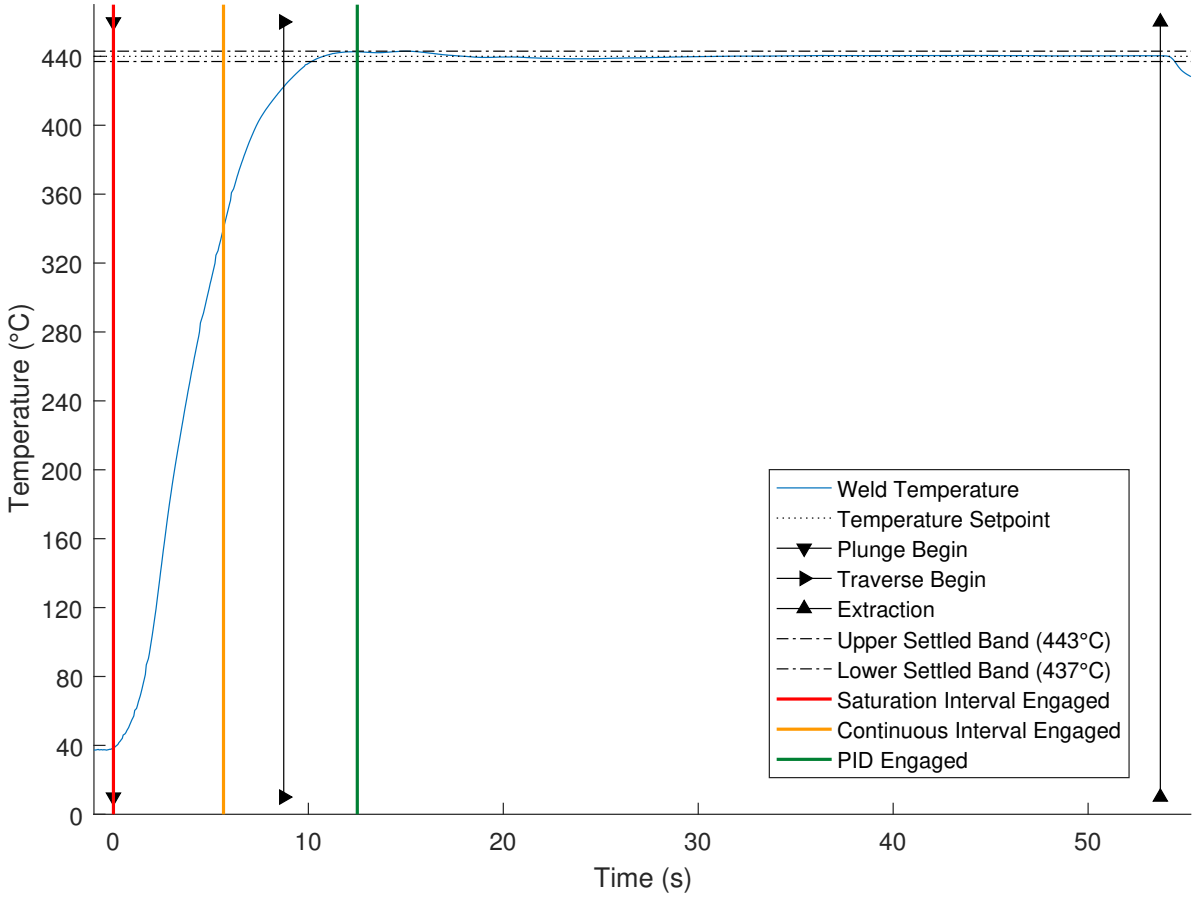

Figure D.15: Temperature profile of Weld 8, zoomed out.

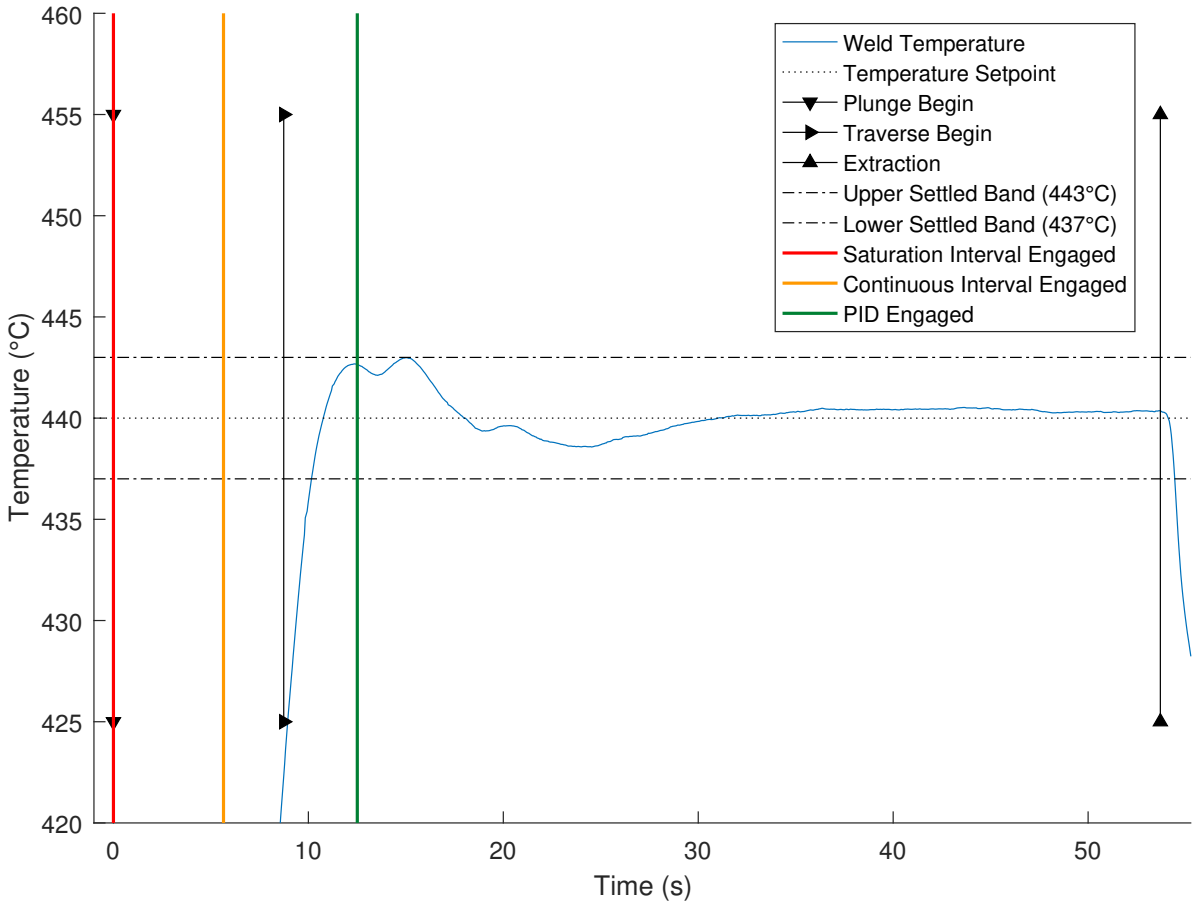

Figure D.16: Temperature profile of Weld 8, zoomed in.

D.9 Weld 9 Temperature Profile

Table D.9: Performance metrics for Weld 9.

Weld No.	$t_{settled}$	t_{rise}	RMSE	PMPE
9	15.16s	10.00s	0.86°C	100.7%

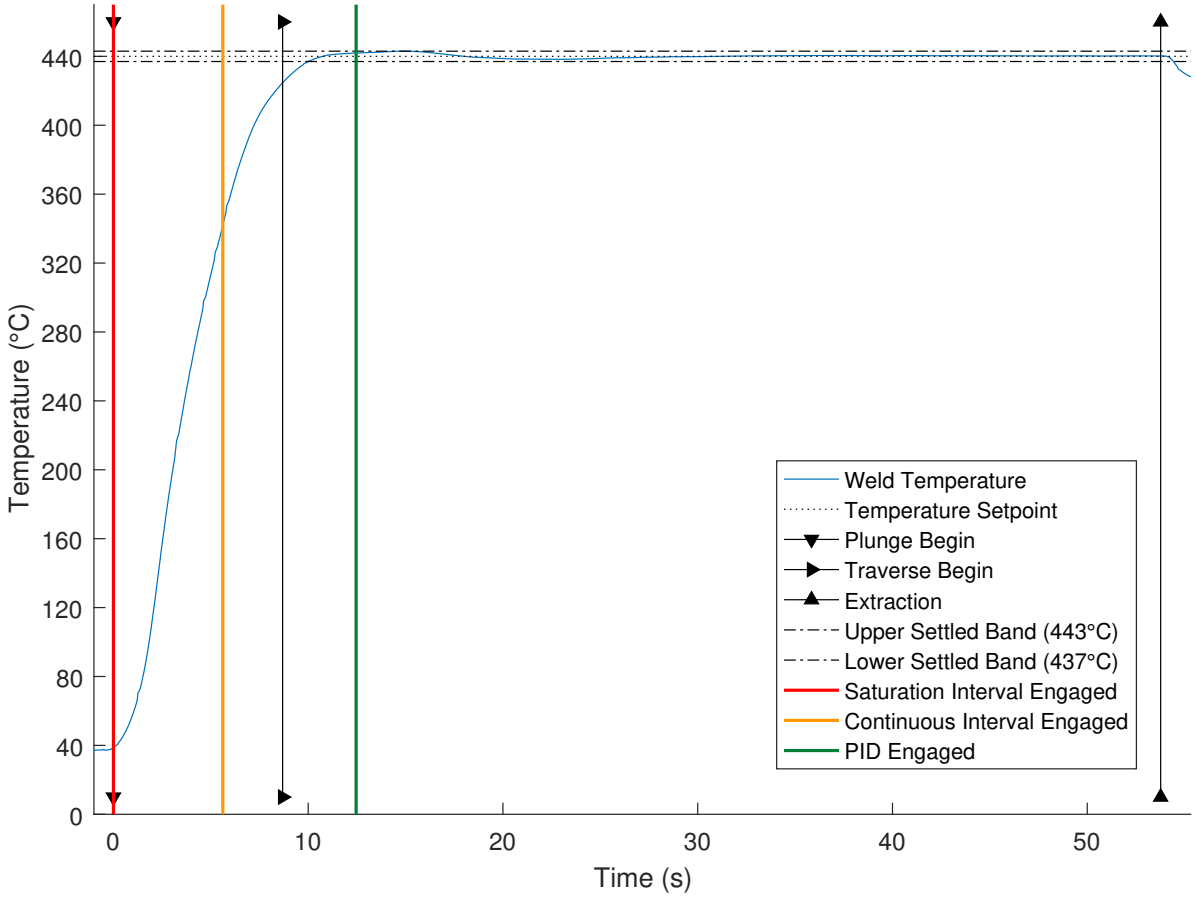

Figure D.17: Temperature profile of Weld 9, zoomed out.

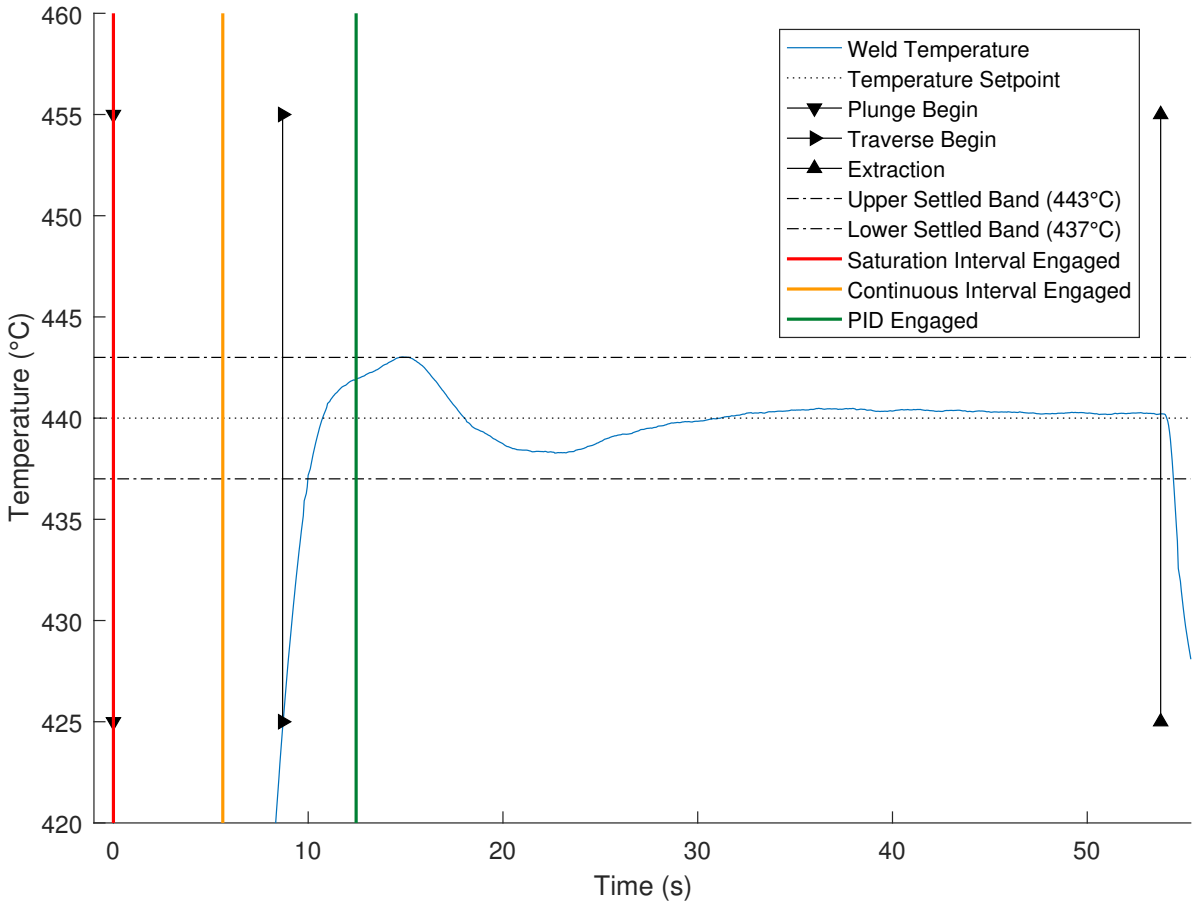

Figure D.18: Temperature profile of Weld 9, zoomed in.